Probing self-association of CetZ1 cytoskeletal protein from *Haloferax volcanii*

by Vinaya Devidas Shinde

Thesis submitted in fulfilment of the requirements for the degree of

Master of Science by Research

under the supervision of A. Prof. Iain Duggin

University of Technology Sydney

Faculty of Science

March 2021

CERTIFICATE OF ORIGINAL AUTHORSHIP

I, Vinaya Devidas Shinde, declare that this thesis, is submitted in fulfilment of the requirement for the award of Master of Science by Research degree, in the School of Life Sciences/Faculty of Science at the University of Technology Sydney.

This thesis is wholly my own work unless otherwise referenced or acknowledged. In addition, I certify that all information sources and literature used are indicated in the thesis.

This document has not been submitted for qualification at any other academic institution.

This research is supported by an Australian Government Research Training Program.

Production Note:
Signature removed prior to publication.

Signature

Date: 29/03/2021

ACKNOWLEGMENT

There are many people who helped me along the way on this journey. I want to thank all of them. First and foremost, special thanks to my supervisor, A/Prof. Iain Duggin for providing me with the opportunity to undertake a Master of Science by Research under his guidance and supervision. Without your support, significant advice, I would not be able to complete this project. I am very grateful for your time and patience throughout my journey.

To my co-supervisor and dear friend Yan Liao, she always provided constant support, availability and constructive suggestions which helped in completing the research. Thank you Yan for everything, I have learned a lot on how to be a good scientist.

A big thank you to my past and present lab mates Dora, Hannah, Tamika, Solenne, Tayla and Carly for your friendship and for creating a wonderful vibe to work in. Special thanks to Hannah for reading my thesis and her constant support throughout the thesis writing process. I am so grateful to have met you.

I am thankful to Mark Lockrey from MAU for training me on the electron microscope. Thank you to Rodrigues lab for attending our lab meetings and for the insightful discussions about my project. Thank you to Chris from the MIF for training me on the microscopes, and finally, thank you to everyone at ithree institute.

Finally, I must express my profound gratitude to my husband, Vishal for providing me with unfailing support and continuous encouragement throughout the degree. Also, to my family, even though they are not in Sydney, I still appreciated all the support they have shown, which gave me strength to be better each day. This accomplishment would not have been possible without them. Thank you.

CONFERENCE PROCEEDINGS

2020

Lorne Conference on Protein Structure and Function, Cumberland, Lorne, Australia. Presented poster titled, **“Structure function studies of CetZ tubulin like cytoskeletal proteins from haloarchaea”. Shinde V,** De Silva R.T. Liao Y, Duggin I.

2019

Foster, Sydney, Australia. Presented poster titled, **“Study of a divergent cytoskeletal protein from haloarchaea”. Vinaya Shinde**, Roshali De Silva, Yan Liao, Iain Duggin

ABBREVIATIONS

AMP	Ampicillin
BSA	Bovine Serum Albumin
CetZ	Cell-structure-related Euryarchaeota tubulin/FtsZ
DNA	deoxyribonucleic acid
g	Gram
GTP	Guanosine triphosphate
GDP	Guanosine diphosphate
h	Hour(s)
IPTG	Isopropyl β-D-1-thiogalactopyranoside
kDa	Kilo base pair(s)
min	Minute(s)
mL	Millilitre(s)
MQW	Milli-Q-water
OD	Optical Density
PBS	Phosphate Buffered Saline
PIPES	1,4-Piperazinediethanesulfonic acid
PIPES Buffer	800 mM PIPES, 3M KCl, 10 mM $MgCl_2$, pH 7.3
M	Molar concentration
mM	Millimolar concentration
MW	Molecular Weight
MWCO	Molecular weight cut-off
n	Nano
ROW	Reverse osmosis water
RT	Room Temperature
rpm	Revolution per minute
SDS-PAGE	Sodium dodecyl sulphate polyacrylamide gel electrophoresis
sec	Seconds
TEM	Transmission electron microscope

TEMED	N,N,N′,N′-Tetramethylethane-1,3 diamine
Tris	Tris (hydroxymethyl) methylamine
v	Volume
w	Weight
W	Wild-type
µ	Micro
Δ	Delta (change in)

TABLE OF CONTENTS

LIST OF FIGURES

LIST OF TABLES

ABSTRACT

The cytoskeleton is a dynamic network of proteins, which are required by all cells for cell division, growth, and maintenance of cell shape. A major group of cytoskeleton proteins present in nearly all cells are the tubulin superfamily proteins. Archaea, the third domain of life, encode a great diversity of tubulin superfamily proteins, including FtsZ and the tubulins that are more similar to those in eukaryotes. Recently a new group of cytoskeletal proteins was found in archaea, named "CetZ", which show characteristics in common with both tubulin and FtsZ and are involved in cell shape regulation. They form dynamic cytoplasmic filaments at or near the cell envelope, which are required for cell shape determination (Duggin et al., 2015). However, the mechanisms by which CetZ proteins lead to remodelling of the cell envelope to modulate cell shape remain unknown.

Based on crystal structures of CetZ proteins and their likely manner of self-association, we have initiated a structure-function analysis of CetZ interactions *in vivo* (De Silva, 2019 PhD Thesis) and, in the present study, *in vitro*. Point mutations were introduced into the *Haloferax volcanii* CetZ1 protein, designed to target putative functional interactions in self-association and putative membrane association. In the present study, mutations that disrupt the longitudinal and lateral interactions were selected for the *in vitro* analysis. Light scattering and TEM were used as an approach to analyse the polymerization cycle and structural features of CetZ polymers, correlating these to the *in vivo* structures observed by high- and super-resolution fluorescence microscopy.

The *in vitro* studies demonstrated that CetZ1 forms GTP-dependent single-stranded filaments and polymer stability was clearly altered in predicted self-association mutants. The longitudinal interface mutants demonstrated that the GTP binding site and GTPase activity controls the longitudinal interaction of CetZ1 polymer formation by GTP hydrolysis. Lateral interaction mutants showed decreased polymerization ability. The mutation in the M-loop region, revealed that it is crucial for polymer formation. Preliminary investigation into possible CetZ1 lipid membrane binding suggests that CetZ1 can bind to the lipid membrane and modify shape changes in them, dependent on the polymerization ability of CetZ1.

These findings have contributed to the understanding of tubulin-like cytoskeleton proteins in archaea, which, by comparison to the cytoskeletons of bacteria and eukaryotes, are

expected to provide future insights into cytoskeleton evolution and help reveal fundamental principles of cytoskeletal function across the three domains of life.

Chapter I
General introduction

1.1 Introduction to Archaea

Cellular life is divided into three major evolutionary lines called the three domains of life: the Eukarya, the Bacteria and the Archaea (Woese, Kandler, & Wheelis, 1990). Archaea are a diverse group of microorganisms which are known for their unique traits and capacity to thrive in harsh environments. Archaea share some traits that are common with both Eukarya and Bacteria. For example, their metabolism is bacteria-like and the information processing system that include DNA replication, transcription and translation are similar to Eukarya (Gribaldo, Poole, Daubin, Forterre, & Brochier-Armanet, 2010). Secondly, like bacteria, archaea are single-celled organisms containing a circular chromosome. Some Archaea have multiple replication origins per chromosome, analogous to eukaryotic chromosome with multi-origin arrangement (O'Donnell, Langston, & Stillman, 2013; Samson & Bell, 2011). However, Archaea also have several distinguishing traits from Eukarya and Bacteria. They have glycerol-1-phosphate as the backbone of the phospholipids and their branched hydrocarbon chains are bound by ether linkages, whereas in Bacteria and Eukarya, glycerol-3-phosphate is used to build their membrane phospholipids and linked by ester bonds. Moreover, they are the only life forms that are known to produce biological methane via methanogenesis (Cavicchioli, 2011). The unique and shared traits of Archaea have stimulated a broad range of evolutionary studies to investigate the course of evolution on Earth.

Archaea display considerable phylogenetic diversity. They consist of two main archaeal phyla: Crenarchaeota and Euryarchaeota (Woese et al., 1990). However, advances in DNA sequencing technologies and approaches in cultivation independent genomics have provided data for new archaeal lineages including Korarchaeota, Thaumarachaeota, Aigarchaeota, Geoarchaeota and Nanoarchaeota (Eme, Spang, Lombard, Stairs, & Ettema, 2017). Thaumarachaeota, Aigarchaeota, Crenarchaeota and Korarchaeota constitute a monophyletic group known as TACK superphylum (Guy, Saw, & Ettema, 2014). Other archaeal lineages which include small cells and small genomes form the DPANN (Diapherotrites, Parvarchaeota, Aenigmarchaeota, Nanoarchaeota and Nanohaloarchaeota) superphylum (Baker et al., 2010). Another new proposed superphylum is the Asgard that consist of Lokiarchaeota, Odinarchaeota, Thorarchaeota and Heimdallarchaeota. They are thought to be the closest relatives of eukaryotes (Imachi et al., 2020; Zaremba-Niedzwiedzka et al., 2017).

Archaea have been found in a broad range of habitats, including harsh environmental conditions such as hypersaline lakes, and a variety of temperate and cold environments. Archaea are classified into four main groups: Methanogens, Halophiles, Thermophiles and Psychrophiles. Methanogens are methane-producing anaerobic archaea. They can be found in sewage treatment plants, bogs, and ruminant digestive tracts. Thermophiles are bacteria that thrive in hot environments, such as hydrothermal vents and hot springs. Many thermophiles are chemosynthetic, meaning they get their energy from dissolved sulphur or other elements as their energy source and iron as a means of respiration. Psychrophilic archaea are cold-loving organisms that inhabit areas below 15^{o}C and often thrive at temperatures near the freezing point of water. Halophilic archaea (haloarchaea) are salt-loving organisms, and some haloarchaeal species have served as excellent model organisms to study archaeal molecular and cellular biology.

The present study uses the halophilic archaeal species *Haloferax volcanii,* a widely studied archaeal species, thus availing its genomic and primary biochemical data. One of the notable characteristics of haloarchaea is their diverse range of cell shapes such as plates, rods (Mormile et al., 2003), triangles (Oren, 1999), disks and squares (Burns et al., 2007). They are highly pleiomorphic, and these changes to cell shape are regulated and important for their adaptation to changing environments. Specifically, *H. volcanii* grow as plate shaped cells but can develop into rods conditionally (Duggin et al., 2015). For instance, the flattened plate-shaped cells improve solute exchange as they have higher surface area to volume ratio; whereas rod shaped cells have more streamlined bodies which give them a motility advantage. Typically, archaea have a myriad of cell shapes in nature, and why these cell shapes are developed or how they are regulated is largely unclear.

Archaea have unique and interesting characteristics, including archaeal-specific families of cytoskeletal proteins (Duggin et al., 2015). These specific cytoskeletal proteins can reveal new insights into diversity, function and evolution of cytoskeletal systems, as archaea encode proteins homologous to known bacterial and eukaryotic cytoskeletal proteins. Exploring cytoskeletal proteins in Archaea may shed light on the underlying mechanisms responsible for the pleomorphism of many archaeal species.

1.2 Cytoskeletal proteins

The cytoskeleton is defined as a complex, dynamic network of protein structures which perform a multitude of functions within the cell. They represent the basic structural framework of the cell. The highly dynamic protein filaments of the cytoskeleton coordinate together to maintain the structure and the internal organization of the cell. The proteins perform various activities such as cell motility, cytokinesis, cell polarity, movement of vesicles and organelles through the cytoplasm, and many other functions that are necessary for cell survival and homeostasis (Erickson, 2007). Unique cytoskeletal components are spread across all domains of life, each contributing to their own active and dynamic cytoskeletal system.

The eukaryotic cytoskeleton is primarily made of three types of filaments: microtubules, intermediate filaments and microfilaments (Wickstead & Gull, 2011). These three cytoskeleton components are involved in diverse cellular functions. Microtubules are the structure made up of tubulins and their function involves intracellular transport and chromosome segregation (Löwe & Amos, 2009). The intermediate filaments are composed of different proteins which provide mechanical strength to the cell (Fuchs & Weber, 1994). Microfilaments consist of actin polymers and they control the locomotion, cell shape and cytokinesis (Dominguez & Holmes, 2011). The protein filaments, with the help of motor proteins such as kinesin and dynein, come together to maintain the integrity of the cell (Erickson, 2007; Wagstaff & Löwe, 2018; Wickstead & Gull, 2011).

Although bacteria and archaea are generally much smaller than eukaryotes, they still have dynamic cytoskeletal systems which are responsible for important cellular processes. The prokaryotic cytoskeleton is analogous to the eukaryotic cytoskeleton and contains counterparts such as FtsZ, the homolog to the eukaryotic tubulin which is found in bacteria and archaea. In addition, MreB is the most common prokaryotic homolog to the eukaryotic actin (Erickson, 1995; Esue, Cordero, Wirtz, & Tseng, 2005; Romberg, Simon, & Erickson, 2001). Some bacteria such as the *Prosthecobacter* species have microtubule forming homologues of tubulin called the BtuA and B, however they are restricted to *Prosthecobacter* species and they have high sequence similarity to eukaryotic tubulin rather than FtsZ therefore, suggesting that they might have acquired the genes for microtubules via horizontal gene transfer from eukaryotes (Pilhofer, 2008; Schlieper, Oliva, Andreu, & Löwe, 2005).

Crescentin are the bacterial cytoskeletal proteins resembling the eukaryotic intermediate filaments (Charbon, Cabeen, & Jacobs-Wagner, 2009). Entirely new classes of filaments that are specific to bacteria have also been discovered, broadening our concept of the cytoskeleton as we know it (Löwe, van den Ent, & Amos, 2004; Michie & Löwe, 2006).

Archaea are a diverse group of microorganisms having specific cytoskeletal proteins. They have great potential to disclose new insights into the evolution of cytoskeletal proteins (Duggin et al., 2015). The present study focuses on the tubulin-like, CetZ proteins which are found in, and are specific to archaea. CetZ1 has been found to be essential for rod development in *Haloferax volcanii* (Duggin et al., 2015). Understanding the role and mechanism of CetZ tubulin–like proteins is crucial for answering questions about the evolution of cytoskeletal proteins across all three domains of life - Archaea, Bacteria and Eukarya. These various protein filaments of the cytoskeleton have been preserved during evolution, and yet are utilised in different cellular processes throughout the cell. The following sections will review and summarize the knowledge of tubulin superfamily protein, their structures and the biological process driven by these proteins in eukaryotes, bacteria and archaea.

1.3 Tubulin superfamily proteins

A superfamily is defined as a wide group of proteins sharing a common ancestor. The tubulin superfamily is one such group that is comprised of proteins belonging to the boarder P loop GTPases, which perform cytoskeletal, motility and cell division functions (Makarova & Koonin, 2010). These GTPases are found in archaea, bacteria, eukaryotes, plasmids and viruses (Leipe, Wolf, Koonin, & Aravind, 2002). The common and essential feature among tubulin superfamily proteins is their conserved signature nucleotide binding motif, which is responsible for their GTPase activity, polymerization, and their subsequent function in cellular activities (Mukherjee & Lutkenhaus, 1998). Tubulin superfamily proteins are mainly used for cytomotive functions i.e., to pull or push molecules in the cytoplasm (Mukherjee & Lutkenhaus, 1998; Nogales, 2001; Wagstaff & Löwe, 2018).

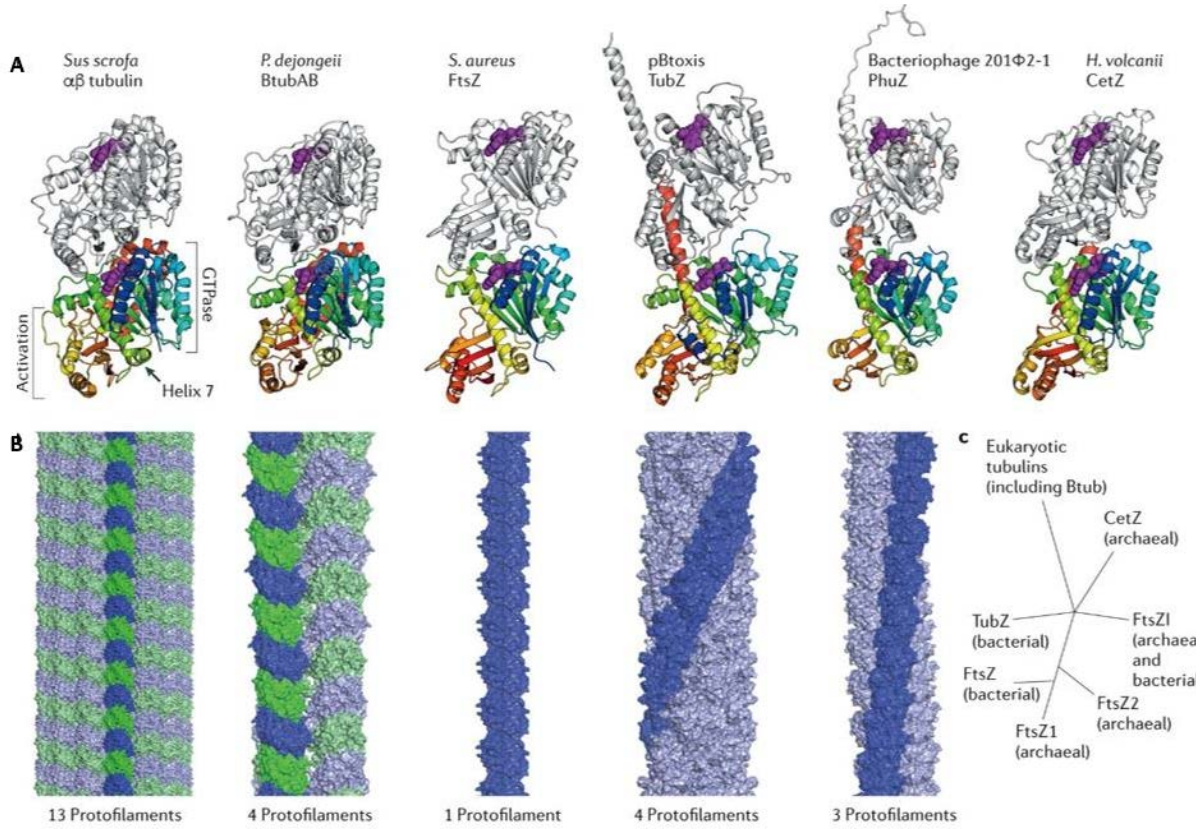

Figure 1.1: Tubulin superfamily proteins

(A) Monomeric structures of tubulin superfamily proteins are shown in cartoon representation, where the upper subunit is grey and the purple spheres represent the nucleotides. The lower subunits of all the proteins are coloured from the N-terminal in red, to C-terminal in blue. (B) Filament structure of the tubulin superfamily proteins are shown as surface representations. Darker colour represents a single protofilament of the larger polymer structure. The α subunits of the heterodimers are represented in blue and the β subunits in green. The number of protofilaments which assemble to form the full polymer are given below each schematic. (C) Inferred phylogeny of tubulin superfamily proteins is represented in the form of a Phylogenetic tree based on two sequence analyses. Adapted from (Wagstaff & Löwe, 2018).

Although tubulin superfamily proteins have low sequence identity among one another, they are structural homologues, sharing a common three-dimensional core structure. The structure comprises of an N-terminal GTP binding domain made up of alpha helices and beta sheets, together forming the modified Rossmann fold that is connected by an alpha helix to

the carboxyl terminal GTPase activating domain. They also have a divergent C-terminal tail region (Downing & Nogales, 1998; McKean, Vaughan, & Gull, 2001). For example, FtsZ proteins have two beta sheets which extend in a variable tail of different lengths depending on the species of bacteria, whereas tubulin have a short acidic C-terminal tail (Downing & Nogales, 1998; Nogales, 2001; Oliva & Andreu, 2001; Yutin & Koonin, 2012). It is speculated that the alpha and beta domains of tubulin have evolved from two independent proteins. The N-terminal domain is equivalent to small GTPases, and the second domain, GAP, is the GTPase activating domain. The two tubulin subunits are predicted to have fused into one single ancestor molecule which had the ability to self-associate and form linear polymers through a GTP-dependent polymerisation mechanism. This single common ancestor is later thought to have evolved to possess the variety of protein structures we know of today (Oliva, C. Cordell, & J. Löwe, 2004).

The tubulin-like proteins typically associate in a head to tail manner, forming a polar protofilament which subsequently assemble into polymers of different types and structures, and have characteristic functions. Tubulins are comprised of a globular domain with a conserved fold containing two subdomains: the amino terminal GTP-binding domain and the carboxyl terminal GTPase activation domain (P. Buske & Levin, 2013; Gardner, Moore, & Erickson, 2013). The polymerization occurs through the association of a GTP-bound GTPase domain from one monomer with the activation domain of the next monomer; this polymerization is an important function of the tubulin superfamily proteins, and is essential for the stability of the cytoskeleton (Scheffers & Driessen, 2001) (*Figure 1.1)*.

Although the proteins in the tubulin superfamily are structural homologs, there are still a few differences in their protein structure which contribute to their differences in cellular function. For instance, FtsZ has an N-terminal extension to the core of the GTP binding domain, which is not present in microtubules. Moreover, dissimilarities are seen in the overall polymeric structure, which is consistent with the individual functions of each protein (Löwe & Amos, 1998).

1.4 Eukaryotic Microtubules

Microtubules are a major component of the eukaryotic cytoskeleton. They help cells to divide by forming the spindle apparatus that segregates the chromosomes into the daughter cells. They also form the internal transport network for the vesicles, which transports cargo with the help of kinesin and dynein motor proteins (Kapitein et al., 2010). Microtubules provide the tracks for organelle localization when the cell is in interphase and maintains and establishes the cell polarity (Müsch, 2004; Siegrist & Doe, 2007). They are also found in the flagella, basal bodies, cilia and centrioles of the eukaryotic cells (Satir & Christensen, 2007). All of these functions of microtubules involve their interaction with microtubule-associated proteins (MAPs). MAPs are essential for the distribution and regulation of microtubules throughout the cell (Amos & Schlieper, 2005).

Microtubules have polarity, which is important for the biological function of microtubules themselves, and for MAPS. For example, the polarity of microtubules provides motor proteins with directionality, and antiparallel spindles are formed by microtubules that protrude from each pole of the cell, in order to facilitate the separation of spindles (Heald & Nogales, 2002; Walker et al., 1988). Microtubules have dynamic instability, which means they can regulate between the phases of polymerization and depolymerization (Mitchison & Kirschner, 1984). Dynamic instability is based on the binding and hydrolysis of the GTP by the subunits of tubulin (Carlier & Pantaloni, 1981; Hill, 1985). The interconversion between the phases is stochastic and seen both *in vivo* and *in vitro.* This process is essential to bring the microtubules into the contact with vesicles and chromosomes, that require active transport and can quickly adapt to the changes in the cell shape (Gregoretti, 2007; Hill, 1985).

1.4.1 Microtubule structure, dynamics and regulation

A) Structure: Microtubules are made of αβ tubulin heterodimers. The assembled heterodimers form long, hollow polymers that are 25 nm wide and range in length from 1 to 100 nm. The tubulin subunits are approximately 35% identical in sequence but have very similar protein structures. Both subunits have the ability to bind to GTP (Nogales, 2001). The binding site in the α-subunit is called the N-site which is non-exchangeable. The binding site in the β-subunit is known as the E-site, which is exchangeable and has intrinsic GTPase activity

and is required for the polymerization. GTP hydrolysis to GDP occurs upon the addition of α/β heterodimers, resulting in polymerisation. GDP can be exchanged for a new GTP molecule when the heterodimer is detached and released, resulting in depolymerisation (Nogales & Wang, 2006). The C-terminal tail of the tubulins consists of acidic amino acids and is not resolved in the crystal structure due to its intrinsically disordered nature. However, this region participates in the binding of MAPs and motor proteins. The walls of microtubules contain holes large enough to allow diffusion of small molecules and water (Goodson & Jonasson, 2018). The luminal structure inside the microtubule is an intriguing space, that is unexplored in the terms of interactions with other molecules. But studies have shown that enzymes involved in post translational modification of tubulin subunits, such as acetylation, function inside the microtubules (Perdiz, Mackeh, Poüs, & Baillet, 2011). They also have larger surface loops as compared to FtsZ, and many of these loops form contacts with neighbouring subunits (Oliva & Andreu, 2001).

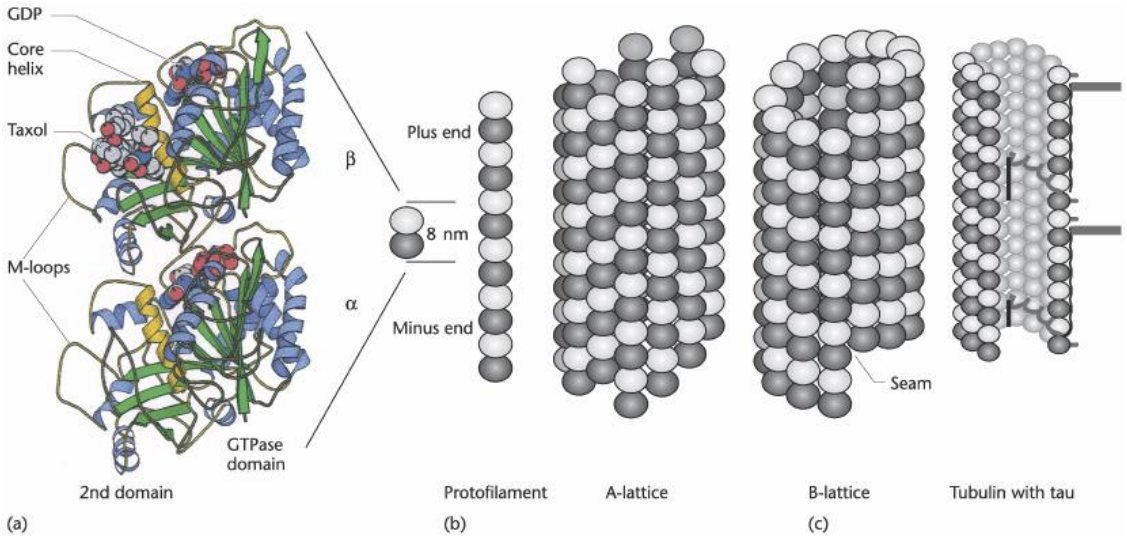

Figure 1.2: Microtubule structure

(A) Atomic structure of the microtubule showing the α/β subunits as a ribbon representation. GTP, GDP and Taxol bound to the structure, α-helices are shown in blue and β sheets in green. (B) Protofilament arrangement of the microtubules. A-lattice arrangement of symmetrical 13 protofilaments and B-lattice with a seam. (C) Microtubule associated protein (MAPS) stabilize the polymer structure. As an example, Tau contains sequence repeats that bind to the

microtubule filament at a similar site to Taxol. The C-terminal of microtubule interact with the MAPs. Adapted from (Amos, 2001).

Cryoelectron microscopy shows that microtubules assemble in a tubular arrangement of parallel protofilaments (Li, DeRosier, Nicholson, Nogales, & Downing, 2002). The stacking of αβ tubulin heterodimers provides microtubules with directionality. The exposed β tubulin subunit constitutes the plus end of the microtubule, while the exposed α tubulin subunit constitutes the minus end, as shown in *Figure 1.2*. (Wiese & Zheng, 2000). While assembling into a protofilaments, GTP on β tubulin is hydrolysed due to the interaction with α tubulin in the adjacent dimer. The GTP bound to α tubulin is not hydrolysed because of differences in co-catalytic residues involved in GTP hydrolysis (Nogales, 2001).

In vivo microtubules have 13 protofilaments, although *in vitro* self-assembled microtubules can vary from 11 to 15 protofilaments. Lateral interactions between the protofilaments form a lattice structure of tubulin monomers. Lateral interactions are controlled by the flexible M-loop of the αβ heterodimer. Most of the dominated lateral interactions are between the M-loop and the H1-S2 loop and H3 helix. The M-loop has the capability to hinge without disrupting its interaction with the adjacent subunits, therefore a variation between 11-15 tubulin protofilaments is evident in different types of cells, and despite this variation, lateral contacts are conserved. The M-loop conformation indicates that destabilisation of the lateral interaction triggers the catastrophe of the compact lattice into a low energy state curved lattice structure. H3 helix interaction with the M-loop and the adjacent subunit are located near to the GTP γ-phosphate contact site. Therefore, depolymerization is seen when a conformational change in the H3 helix destabilises the lateral interaction (Nogales, Whittaker, Milligan, & Downing, 1999). The unique feature of the 13 protofilament structure is that they have a seam as shown in *Figure 1.2*. Over this seam, the α-monomer is in lateral contact with the β-monomer of its neighbour while the β monomer is in contact with its α-tubulin neighbour. This distinct seam interaction does not exist in the rest of the microtubule, in which α-monomers are laterally adjacent to another α-monomer, and similarly for β-monomers which interact laterally with other β monomers. Two possible arrangements are seen for each pair of protofilaments depending on whether the nearest neighbours are alike or different. A-lattice is the arrangement of protofilaments where nearest neighbour is a different subunit, giving perfect helical symmetry. Another important feature of the seam is

that there is a shift of 1.5 heterodimers that results from the non-orthogonal arrangement of the subunits in the lattice. In a B-lattice, the main lateral contact between protofilaments is between the subunits of same type. Therefore, the common microtubule is not helical. Studies suggest that intra-protofilament contacts are stronger than inter-protofilament contacts (Amos, 2001). Atomic models of microtubules show that both the monomers have similar structures but they are different in nucleotide-bound states. Research has shown that tubulin exists in two conformations: the straight conformation with GTP bound at the E-site, and the curved conformation containing GDP bound tubulin (Nogales & Wang, 2006). Electron microscopy studies have shown that when the GTP cap is lost, protofilaments curl and peel off, forming closed rings and revealing its curved conformation.

B) Dynamics and regulation: Microtubule dynamics are very energy consuming. The polymerization of αβ dimers utilises the energy stored in the GTP molecules. The polymerization process takes place in three phases: nucleation, elongation, and steady state. They are well studied both *in vivo* and *in vitro*. Nucleation is the process where tubulin dimers assemble into new microtubules. They can nucleate and grow from specialized templates called the γ-tubulin containing microtubule organizing centres (Bornens, Bailly, Gosti, & Keryer, 2012). Y-tubulin along with other associated proteins form a γ-tubulin ring complex (γ-TuRC). The complex behaves as a template for the αβ dimer to begin the polymerization, it also acts as a cap at the minus end when the microtubules are growing continuously away from the microtubule organizing centres, towards the positive end. However, microtubules can nucleate from other sites as well. For instance, the Golgi apparatus is an important platform for the microtubule nucleation (Sanders & Kaverina, 2015). Other examples of microtubule nucleation platforms include the basal bodies of cilia and flagella in eukaryotes. Microtubules can also nucleate from existing microtubule lattices and generate microtubules with identical polarity. This process is not seen *in vitro,* as specialized proteins such as TPX2, Ran and Augmin are required for this process (Petry, Groen, Ishihara, Mitchison, & Vale, 2013).

The second phase of assembly is the elongation, during which tubulin dimers add at the end of the microtubules. The last stage of the assembly is the steady-state phase, in which a fixed proportion of tubulin heterodimers are in the assembled form whereas other tubulins are

soluble. Microtubules can continuously grow as long as the free tubulin concentration is above critical level. At steady-state microtubules are in equilibrium. GTP is hydrolysed continuously and therefore the energy is consumed to maintain the steady state. The energy generates the active exchanges between constitutive subunits with the tubulin molecules of the soluble pool. Two mechanisms are responsible for tubulin exchanges: treadmilling and dynamic instability. During treadmilling, the plus end continuously incorporates new tubulin subunits, while the minus end continuously loses them. This asymmetric behaviour requires energy consumption (Margolis & Wilson, 1998).Dynamic instability is where microtubules switch between growing and shrinking phases, originating from the delay of GTP hydrolysis at the E-site after the heterodimer is polymerized (Erickson & O'Brien, 1992). The GTP cap model is the most commonly accepted model for dynamic instability. According to this model, a GTP cap is formed at the polymerizing tip of growing microtubules. The hydrolysis of GTP in the growing microtubules causes the tip to lose its stability, resulting in shortening of the microtubules and leads to catastrophe - a change in polymerization phases from growth to shortening. However the depolymerization of microtubules restores the GTP cap by polymerization of new subunits and this activates a change where growth phase resumes. This event is called as rescue (Drechsel & Kirschner, 1994; Heald & Nogales, 2002) as shown in *Figure 1.3*. Dynamic instability is predominantly controlled by nucleotide cycling and conformational cycling.

GTP binding to β tubulin plays an important role in the dynamic instability of microtubules. GTP bound dimers are allowed to enter the growing and dynamic plus end. The newly bound tubulin initially forms a longitudinal contact and then lateral contacts. Then, another new tubulin dimer binds directly on the top of the first, and GTP hydrolysis occurs. During the course of growth, tubulins in the lattice undergo GTP hydrolysis at the E-site to create a highly unstable GDP microtubule core. The stabilizing GTP cap, formed by the layer of GTP bound tubulins that have not undergone hydrolysis, prevents the microtubules from disassembling, but loss of the cap results in catastrophe leading to disassembly. This disassembly releases the now GDP bound tubulin dimers back into the solution to exchange the nucleotides for GTP. The tubulin dimers that have exchanged the nucleotides for GTP can then re-enter the cycle of polymerization. Recent research has shown that tubulin changes conformation as it

enters and exits the microtubule lattice, from straight to curved and vice versa (Brouhard & Rice, 2018).

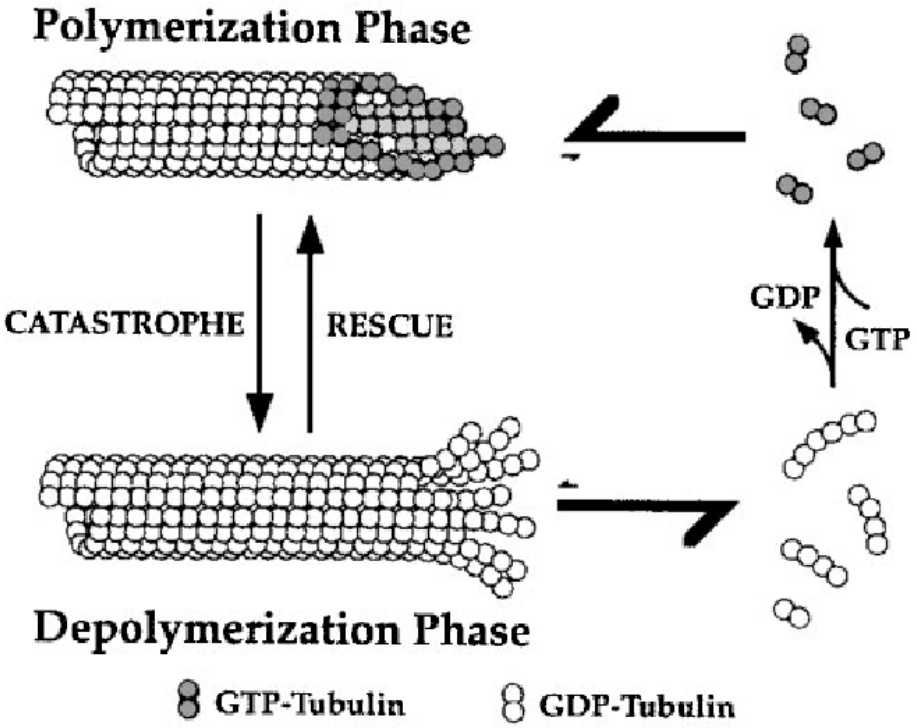

Figure 1.3**: **Microtubule dynamic instability

Dynamic instability consists of polymerization and depolymerization of microtubules. GTP shown in grey and GDP in white. GTP-tubulin is incorporated at the polymerising end, GTP is hydrolysed during the polymerization. Polymerising microtubule transitions to the depolymerization phase (catastrophe). Depolymerising microtubules also can transition back to the polymerization phase (rescue). The GTP cap stabilizes the structure at the polymerising ends. Taken from (Desai & Mitchison, 1997)

The tubulin dimers in the cap pass through three mechanical states during microtubule growth and shrinkage. These states are curved, expanded, and compacted, and they store and release strain energy throughout these cycles. The free GTP bound heterodimers start in a curved conformation, which has a 12° kink at the intradimer surface. Upon polymerization

and binding to the microtubule ends, the tubulin dimers adapt a straight and expanded conformation which establishes a strain energy into the microtubule lattice. This is followed by GTP hydrolysis and phosphate release that leads to a subsequent conformational change in the tubulin dimer to the compact conformation, shortening the lattice. The strain energy stored in dimers during the conformation changes is used to perform work by the microtubules (Brouhard & Rice, 2018; H.-W. Wang & Nogales, 2005).

Dynamic instability depends on the functional GTPase cycle of the tubulin, as well as the ability of the tubulin dimers to transition through the conformational changes as they enter and exit the microtubule polymer. Tubulin polymerization with nucleotide analogues has helped to establish GTP hydrolysis significantly. Microtubules assembled from the slowly hydrolysing analogue of GTP-GMPCPP form polymers as normal but depolymerize much slower in comparison to microtubules assembled with GTP. Hence, the energy of GTP is used not to build it but to destroy the microtubule. It is not yet clear whether it is the GTP hydrolysis or the presence of the inorganic phosphate that induces bending of the heterodimers and depolymerization, although conformational changes are mostly related to phosphate release (Goodson & Jonasson, 2018).

Recent studies conducted by Geyer et al. show that structural changes associated with GTP hydrolysis cause microtubule instability. They studied polymerization dynamics of yeast purified protein with a mutation in the H7 helix of β-tubulin- T238A. This mutation blocked the H7 movement upon GTP hydrolysis. While the GTPase activity of the microtubule was not affected, the T238A mutation appears to prevent structural changes that occur with hydrolysis. The microtubule assembly from the mutation was seen to be hyper stable, indicating that GTP hydrolysis has some allosteric effect rather than effecting microtubule instability by hydrolysis (Geyer et al., 2015). Studying additional tubulin mutants will likely provide a better understanding between tubulin structure and microtubule dynamics.

Several microtubules associated proteins (MAPs) also play and important role in microtubule dynamics by controlling the assembly and organisation in the cells. For instance, MAPs such TPX2 and DCX bind to the subunits in the curved conformation and stabilise the dimers by accelerating nucleation. Contrary to that, MAPs such as MCAK creates lag time during nucleation by preferring the curved conformation of tubulin subunits (W. Wang et al., 2017). Different MAPs regulate the catastrophe event of microtubules by identifying different

conformations of the dynamic state of microtubules. Mal3, a yeast EB protein (EB proteins are highly conserved groups of proteins that localize to cytoplasmic microtubules and spindles at the distal tips) has shown that increase in the EB proteins have high changes of catastrophe by reducing the size of the stabilising cap. EB proteins have high affinity for GTPγS, an analogue of GTP, wherein the EB proteins bind to the compact conformation, thus promoting the catastrophe by increasing GTPase activity (Maurer, Fourniol, Bohner, Moores, & Surrey, 2012). These microtubule binding proteins are essential to microtubule cellular functions.

Constant turnover of microtubules is necessary for the cell physiology, as it allows the cells to adapt to changes in cell shape and environment. The probing generated by the dynamic instability permits individual microtubules to transverse cellular spaces and come into contact with cargo such as organelles and chromosomes, which cannot diffuse in the crowded environment of the cytoplasm due to their larger size. Microtubules assemble from pure tubulins that are unstable at the edge of catastrophe. In this situation tubulins respond quickly to the changing environment and influence the regulatory proteins. Microtubule regulatory proteins include stabilizers, destabilisers, capping proteins, and bundle/cross-linkers and microtubule associated proteins (MAPs). These proteins play an important conformation-specific regulatory role in tubulin dynamics.

1.5 FtsZ

Bacteria have cytoskeleton elements that are related to eukaryotic actin and tubulin components and evidence has shown that like eukaryotes, they have a dynamic cytoskeleton system. FtsZ is the prokaryotic homolog to tubulin and is fundamental to regulating bacterial cell division. It is conserved in bacteria and archaea and also exists in certain eukaryotic mitochondria and chloroplasts (Gilson & Beech, 2001; Romberg & Levin, 2003). Like tubulin, FtsZ polymerises into protofilaments, however FtsZ protofilaments assemble into a ring called the Z ring, which provides the framework for a larger division complex, and determines the division plane. FtsZ, along with help of other proteins, forms a functional division complex that modulates the cell division of bacteria (Szwedziak, Wang, Bharat, Tsim, & Löwe, 2014). FtsZ forms polymers in the presence of GTP and depolymerizes as GTP hydrolyses. *In vivo,* the FtsZ assembly is transitory, the subunits continually exchange. The balance between assembly and disassembly in the polymers is able to trigger changes in the FtsZ structures in the cell to

help the timing and location of cytokinesis. *In vitro*, the stability of FtsZ polymers, like that of tubulins, is fine-tuned (Romberg & Levin, 2003).

1.5.1 FtsZ structure

The first crystal structure of FtsZ was obtained from the thermophilic archaea *Methanococcus jannaschaii*. Although FtsZ shares ~10% to 18% sequence homology with tubulin, both share similar structure in respect to GTP binding interaction and protein folds (Löwe & Amos, 1998; Nogales, Downing, Amos, & Löwe, 1998). The structure contains two domains: The N-terminal domain which is nucleotide binding, and the C- terminal globular domain. Both the domains are separated by a central α-helix (*Figure 1.4*). The GTP/GDP nucleotide binding site is made of four phosphate binding loops (T-loops) and two sugar binding and guanine recognition sequences (Löwe, 1998).

FtsZ is a GTPase, which polymerizes into protofilaments with a head to tail arrangement by hydrolysing the GTP (*Figure1.4)*. Tubulin and FtsZ have similar GTP dependent longitudinal interactions. Activation of GTP hydrolysis occurs when the T7 region from one subunit enters the GTP binding site in the subunit below. The T7 loop region of FtsZ has conserved catalytic amino acid residues-N207, D209 and D212 that participate in the conserved GTPase function (Adams & Errington, 2009). No apparent conformational changes are seen in the FtsZ monomer during the nucleotide binding (M. A. Oliva, S. C. Cordell, & J. Löwe, 2004), however, recent cryo-EM studies have revealed subtle compaction in the GTP binding pocket when it is bound to GDP, which results in enfeebled longitudinal interactions (Ramírez-Aportela, López-Blanco, Andreu, & Chacón, 2014).

The C-terminal domain of FtsZ is not resolved in the crystal structure due to its high flexibility (Löwe & Amos, 1998). However, it plays a very important role in FtsZ assembly and interaction with other proteins (P. Buske & Levin, 2013; P. J. Buske & Levin, 2012; Gardner et al., 2013). The C-terminus can be divided into three domains: a variable length unstructured C –terminal linker, which is a short variable region at the extreme C-terminus (CTV), a highly conserved C terminal tail (CTT) (P. Buske & Levin, 2013). Each domain has its own function and is important for cell division and FtsZ assembly and interaction with other proteins. The C-terminal linker

ranges from 2-330 residues and it plays a role in the formation of FtsZ protofilaments and the architecture of the FtsZ ring *in vivo*. Whereas, the CTT and CTV serve as links between FtsZ and the other cell division components (Szwedziak et al., 2014).

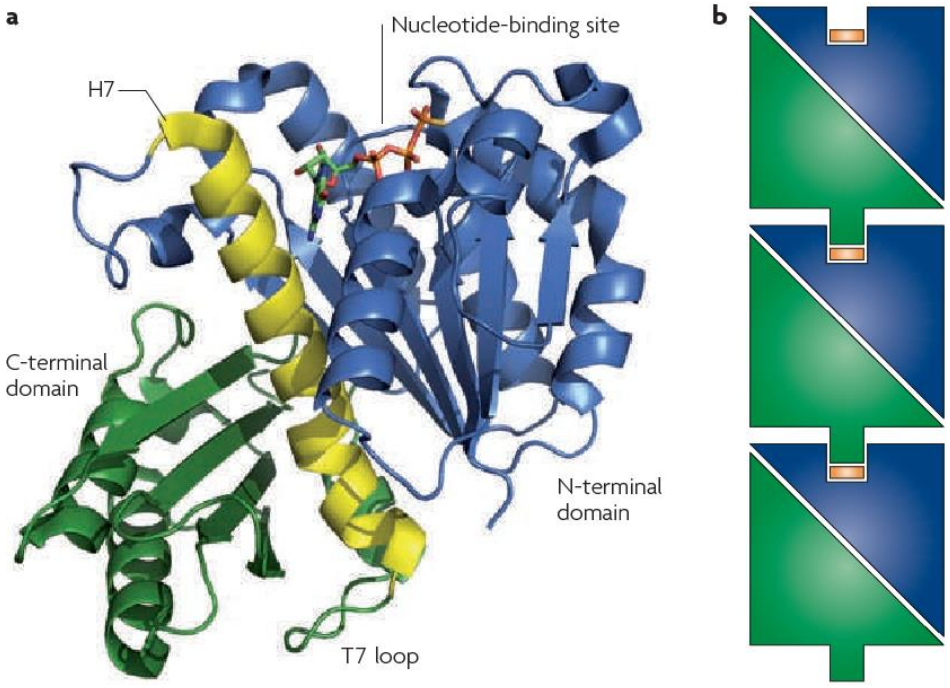

Figure 1.4: ***FtsZ polymerization model***

(A) The crystal structure of a Bacillus subtilis FtsZ monomer bound to GTP. FtsZ has two globular domains separated by a central core helix H7 represented in yellow. The N-terminal domain (blue) contains the signature motif and forms the nucleotide-binding site. C-terminal domain represented in green. (B) FtsZ polymerizes into a head-to-tail linear protofilament shown in blue and green and the GTP is shown in orange. Adapted from (Adams & Errington, 2009)

1.5.2 FtsZ polymers

Under standard conditions, GTP binding in FtsZ induces FtsZ self-assembly into the head to tail linear protofilaments of individual subunits, as opposed to head-to-tail stacking of heterodimers as in microtubules. The protofilament spacing in FtsZ is 42 Å which is close to the 40 Å spacing of microtubules (Erickson, 1995; M. A. Oliva et al., 2004; Romberg et al., 2001). The T7 synergy loop is thought to be inserted into the nucleotide binding site of the other FtsZ subunit, thus placing the catalytic residues close to the γ-phosphate and therefore allowing nucleotide hydrolysis to proceed (M. A. Oliva et al., 2004; Scheffers & Driessen, 2001). Depending on the experimental conditions, FtsZ can display cooperative assembly and a range of polymeric forms *in vitro* which range from single stranded protofilaments to mini rings, bundles, tubules and sheets (Adams & Errington, 2009; Mukherjee & Lutkenhaus, 1998). The data from electron microscopy and atomic force microscopy suggest that the distance between a pair of protofilaments fluctuates under different conditions, but most often their interaction is a loose association between the protofilament (Mingorance, Rivas, Vélez, Gómez-Puertas, & Vicente, 2010).

The FtsZ protofilament bundles are involved in weak association rather than a regular pattern of specific lateral bonds (Erickson, 2009). FtsZ bundling can be induced by several factors such as multivalent cations including DEAE dextran (Bramhill & Thompson, 1994) macromolecular crowding (González et al., 2003), calcium and magnesium (Mukherjee & Lutkenhaus, 1999; Yu & Margolin, 1997) as well as crossing liking of other cell division proteins like ZipA, FtsA (RayChaudhuri, 1999).

1.5.3 Dynamics of FtsZ polymers

To understand the process of various stages of Z ring dynamics during the cell cycle, it is necessary to study the behaviour and dynamics of pure FtsZ *in vitro*. Like microtubules, FtsZ polymers are dynamic in nature, owing to their ability to hydrolyse GTP. Specifically, turnover of the Z ring is powered by GTP hydrolysis (Stricker, Maddox, Salmon, & Erickson, 2002),is dependent on Mg^{2+} and stimulated by the presence of KCl. Similar to tubulins, the GTPase activity of FtsZ is found to be stimulated at the concentration of FtsZ that allows polymer

assembly. Structural data and mutagenesis studies of FtsZ also support the model of self–activation i.e., GTP hydrolysis in an active site that is shared by two monomers.

The dynamics of FtsZ polymerization has been studied by sedimentation and light scattering assays (Mukherjee & Lutkenhaus, 1999). FtsZ polymerizes above a critical concentration that corresponds to the concertation required for GTP hydrolysis. There is a close relation between GTP hydrolysis and polymerization that is evident from the observation that the presence of FtsZ polymers in solution is coupled to GTP hydrolysis, with polymer loss coinciding with GTP depletion. The coupling of GTP hydrolysis to polymerization then raises the question whether the FtsZ polymer contains GTP or GDP. Studies conducted by Erickson and co-workers (Erickson, Anderson, & Osawa, 2010) stated that GTP hydrolysis is coupled to conformational changes of straight to curved polymers that might drive ring constriction during cytokinesis. Isodesmic assembly of single FtsZ protofilaments with GTP and GMPCPP without self-activation have been shown (Romberg et al., 2001). This suggests that the polymerization is slow and lagging, and GTP hydrolysis occurs gradually throughout the FtsZ polymer. Although isodesmic polymerization accounts for the first step of association of FtsZ filament, it is likely that lateral contacts are required for the formation of stable polymers that lead to the model of cooperative assembly (discussed in section 1.4.2).

Although a number of accessory proteins are required for proper cell envelope constriction and cell separation, studies conducted by Erickson (Erickson, 2009) suggest that FtsZ itself may generate the force for membrane constriction. In addition, nucleotide hydrolysis has also been proposed to provide the force for constriction, whereby a nucleotide-dependent transition of conformational changes from a straight, GTP-bound polymer to a curved, GDP-bound polymer can transmit mechanical work to the membrane and subsequently generate force for constriction (Z. Li, Trimble, Brun, & Jensen, 2007; Lu, Reedy, & Erickson, 2000). However, the mechanism of force generation in bacterial cell division is complicated and remains controversial. Studies have shown *in vitro* Z rings can impact a force on tubular membrane (Osawa, Anderson, & Erickson, 2009) with the observation of both curved and straight filaments i*n vivo,* this reinforces the possibility of force generation through the straight to curved conformational changes of FtsZ polymers. However, computational modelling predicts that the Z ring transitions form a low-density state to a high-density state and generates sufficient contractile force to achieve division.

1.5.4 Z-ring assembly and regulatory system

The Z ring provides the framework for the division apparatus and determines the site of cytokinesis. Throughout the cell cycle, FtsZ exhibits different behaviours, such as mid-cell Z ring formation, maintenance of the ring and constriction and disassembly of the ring. The metamorphosis between the Z ring growth, maintenance and constriction is regulated by factors that influence FtsZ assembly (Anderson, Gueiros-Filho, & Erickson, 2004; Erickson, 2009; Romberg & Levin, 2003). Correlation between the cell cycle progression and Z ring behaviour exists. Z ring formation starts after the initiation of DNA replication and coincides with nucleoid segregation (Harry, Rodwell, & Wake, 1999; Regamey, Harry, & Wake, 2000). FtsZ assembly starts at the inner surface of the cell membrane forming an arc and then a ring like structure. This ring acts as a framework for assembly of other cell division proteins. According to the pioneering studies on FtsZ *in vivo*, using immunofluorescence and fluorescent proteins fused to FtsZ, FtsZ localized to mid-cell during most of the cell cycle (Anderson et al., 2004; Bi & Lutkenhaus, 1991). Around 20-30% of the total FtsZ available in the cell is integrated into the Z ring and the rest of the FtsZ is present in the cytoplasm as short polymers that continuously exchange with the Z ring (Anderson et al., 2004). The overall Z ring architecture constantly changes with time and is dynamic during constriction (Strauss et al., 2012). After constriction, the Z ring disappears and FtsZ reassembles in the daughter cells. The Z ring and its architecture *in vivo* is still not clear, however super-resolution techniques such as photoactivated localization microscopy, 3D-SIM, and cryotomography have increased the understanding of FtsZ ring formation *in vivo* and *in vitro*. An integral part of Z ring formation is the association between FtsZ and the cell membrane. It is important for FtsZ to have affinity, with help of other proteins, to the membrane in order to maintain structural integrity for septum formation and to transmit a constructive force to the membrane.

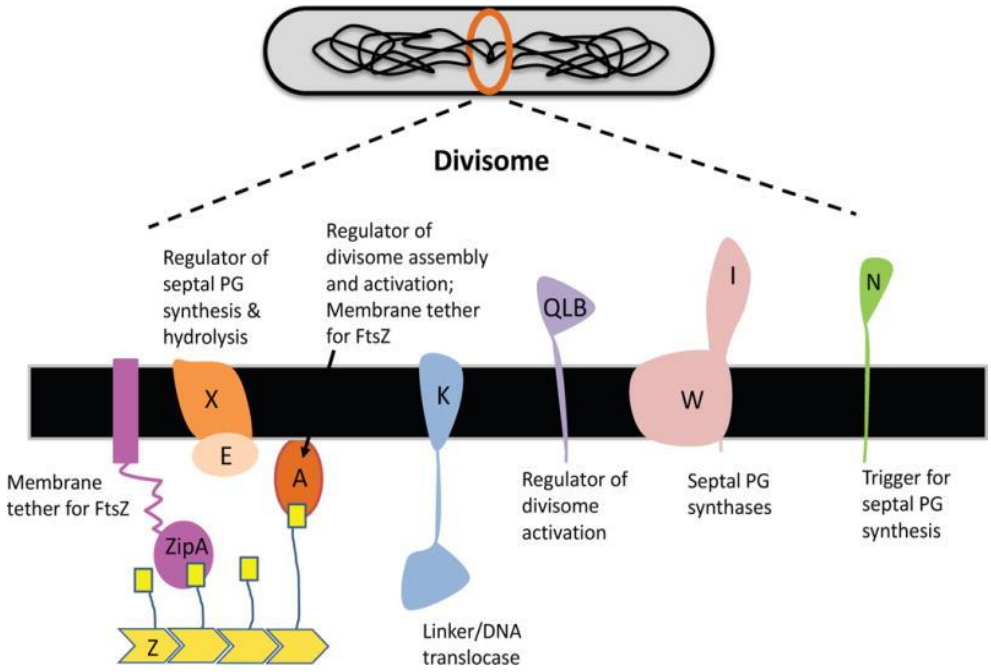

Figure 1.5: The Bacterial divisome

Schematic representation of a dividing E. coli cell. Proteins that assemble at the division site are shown along with their function. Taken from (Du & Lutkenhaus, 2017).

The completely assembled division machinery is called divisome and it is comprised of more than ten different proteins, whose precise functions are not fully understood (*Figure 1.5)*. FtsZ polymers are tethered to the cytoplasmic membrane by membrane binding proteins like FtsA, ZipA, ZapA, SepA and EzrA (Land, Luo, & Levin, 2014; Pichoff & Lutkenhaus, 2002, 2005). These proteins are essential for cell division, studies have shown that deletion of ZipA or FtsA causes no Z ring formation (Hale & De Boer, 1999). Changes in the FtsZ concentration also leads to aberrant cell division phenotypes: a slight overexpression of *ftsZ* enhances division frequency, resulting in the formation of minicells, whereas high levels of FtsZ inhibits cell division. (Ward Jr & Lutkenhaus, 1985).

The accessory protein FtsA, along with FtsZ, recruits enzymes for the septal peptidoglycan synthesis to the division site. FtsA and FtsZ form filaments that treadmill circumferentially around the division ring which drives the motion of peptidoglycan synthesizing enzymes (Bisson-Filho et al., 2017). FtsK is a bifunctional protein that links the process of cell division to DNA segregation. FtsW is a peptidoglycan polymerase which promotes septum formation. It is suggested that FtsQLB forms a complex connecting the Z ring to the septal peptidoglycan

synthesis machinery. Downstream proteins of the FtsQLB complex are presumably also involved in peptidoglycan metabolism (Pastoret et al., 2004; Ursinus et al., 2004). The rate of peptidoglycan synthesizing enzymes and cell division is dependent on the FtsZ treadmilling rate (Bisson-Filho et al., 2017).

The function, stability and assembly of the Z ring is regulated both temporally and spatially. Temporal regulation ensures that the septum formation occurs at a specific time during the cell cycle. Whereas, the spatial regulation makes sure the Z ring forms at the desired site for septum formation, and this is regulated by the Min system proteins (Rothfield, Taghbalout, & Shih, 2005). For example, in *E.coli*, positioning of the Z ring at the mid-cell is subjected to different forms of regulation like the *min* system and nucleoid occlusion. The *min* system has three proteins, namely MinC, MinD and MinE. They prevent cell division at the poles. MinC and D act together as the negative regulator of Z ring assembly and they oscillate together from cell pole to pole in a MinE dependent manner. MinE is present at the centre of the cell where it oscillates to repel MinC&D, and allows the Z ring to assemble (Lutkenhaus, 2007; Rowlett & Margolin, 2015). The nucleoid occlusion factors formation inhibits Z ring formation in its vicinity. According to the nucleoid occlusion model cell division takes place at any point along the length of the cell, but early in the cell cycle the unsegregated nucleoid prevents separation at mid-cell. Later in the cell cycle, the DNA segregation reveals a nucleoid free zone at the mid-cell that helps the assembly of the division apparatus (Romberg & Levin, 2003; Rowlett & Margolin, 2015; Wu & Errington, 2012).

FtsZ recruits the other divisome components. For example, in *B. subtilis*, the assembly of other proteins is a two-step process. First, the early cell division proteins - FtsZ, ZapA, FtsA and EzrA are recruited at the mid-cell and later on, a second set of proteins called the late cell division proteins - FtsL, DivIB, FtsW, Pbp2B and DivIVA arrive at the division site (Gamba, Veening, Saunders, Hamoen, & Daniel, 2009). In *E.coli* the assembly starts with FtsZ followed by FtsZ/ZipA, FtsK, FtsQ, FtsL/B, FtsW, FtsI and FtsN. However, it is found that protein FtsK, Q, L, B, W and I may assemble together with FtsA and are then recruited together as a complex (Goehring & Beckwith, 2005).

1.6 Tubulin superfamily proteins in Archaea

Archaea have a great diversity of tubulin superfamily proteins, including FtsZ in most of the major taxa, tubulins in some groups as well as archaea-specific families (Aylett & Duggin, 2017). They have different functions and frequently contain multiple homologues of these proteins (*Figure 1.6*). Yet some archaeal taxonomic groups do not contain any tubulin members or homologs and use alternative scaffolding components, such as homologs of eukaryotic *Endosomal Sorting Complex Required for transport* (ESCRT)-III complex (Makarova, Yutin, Bell, & Koonin, 2010). A third family of tubulin superfamily proteins, called CetZ, is wide-spread in Euryarchaeota phylum (Duggin et al., 2015).

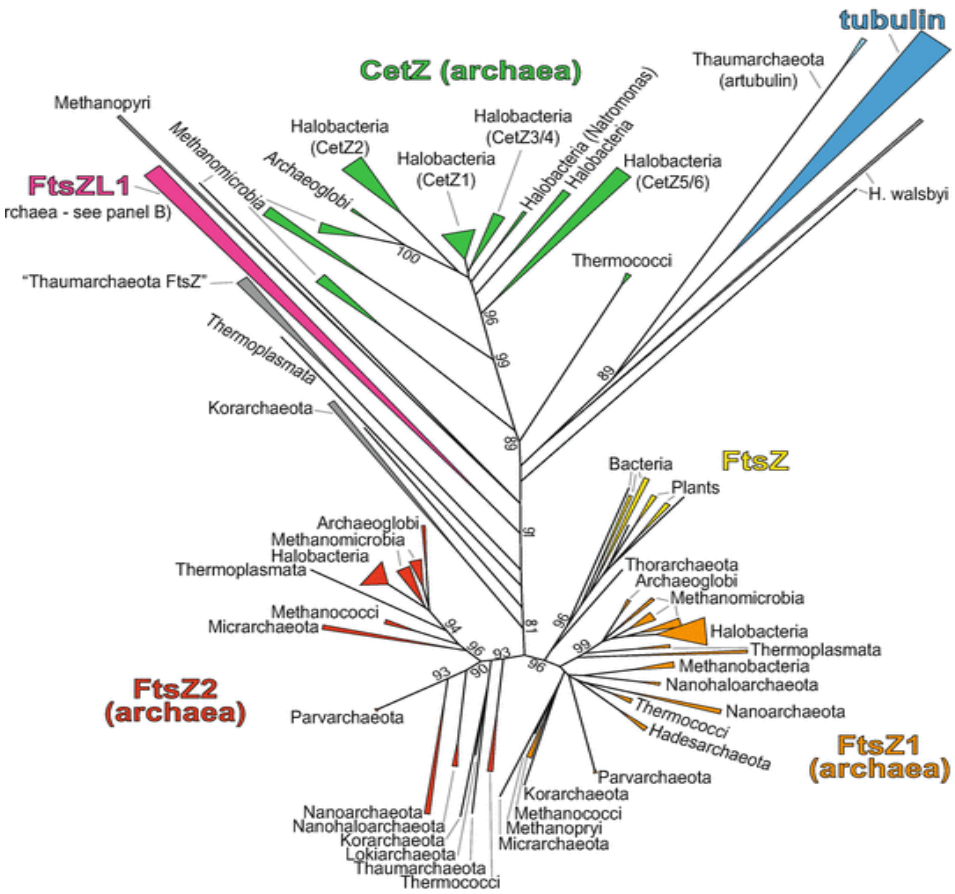

Figure 1.6**: **Molecular phylogeny of tubulin superfamily proteins in archaea.

Phylogram generated by Fasta Tree of tubulin superfamily proteins, generated by multiple sequence alignment of 271 tubulin super family members from across archaeal taxa including representative FtsZ and tubulins from bacteria and eukaryotes. Adapted from (Aylett & Duggin, 2017).

1.6.1 FtsZ family proteins in archaea

Like bacterial FtsZ, Archaeal FtsZs are GTPases which localize to the mid-cell plane of division. Most bacterial species have one FtsZ, but many archaea have two FtsZ homologs, each from separate families. FtsZ1 is evidently more closely related to bacterial and plant FtsZ while FtsZ2 is more phylogenetically distinct (Aylett & Duggin, 2017; Margolin, Wang, & Kumar, 1996; Wagstaff & Löwe, 2018). Recent studies have shown that *H. volcanii* FtsZ1 is capable of localising in preparation for Z ring formation at a very early stage of the cell cycle, a long time before the visible mid-cell constriction. Expression of a point mutant of FtsZ1 caused the hallmark cell division defects, in which cell division ceased but cell growth continued. That resulted in extremely large cells, suggesting that GTPase activity is essential for FtsZ1 function and for normal cell division (Duggin et al., 2015). Recently it was also shown that FtsZ1 and FtsZ2 co-localize at the mid cell and forms the division ring and FtsZ1 independently assembles and stabilizes the FtsZ2 in the ring. FtsZ1 has an impact on the cell shape and FtsZ2 has a function in constriction of the membrane (Liao, Ithurbide, Löwe, & Duggin, 2020). It will be informative to observe the assembly of archaeal FtsZ and compare them with the bacterial FtsZ function and division.

1.6.2 Tubulin family proteins in archaea

Few tubulin family homologs have been identified in archaea and bacteria. Genes encoding artubulins, distant relatives of the tubulin family, are found in genome of Thaumarchaeota (Yutin & Koonin, 2012). Artubulins stem at the base of the tubulin family and forms a sister group to the eukaryotic tubulins, which suggest that they likely are direct ancestors of tubulins. However, functions of artubulins are currently unknown, but since their genes are located adjacent to the ESCRT-III proteins, they may have possible roles in ESCRT-III mediated division.

Recently two archaeal tubulin family proteins were detected in metagenomics data for an organism that belongs to the Asgard superphylum (Imachi et al., 2020). The proteins are identified as another sister group to the eukaryotic tubulin but distinct from artubulins (Zaremba-Niedzwiedzka et al., 2017). The fact that this protein exists and was found in few

archaea supports the idea that the tubulin family arose in early archaea-like cells and then diversified during the course of evolution in eukaryotic cells.

1.6.3 CetZ family in archaea

Cell structure related Euryarchaeota Tubulin/FtsZ homologs (CetZ) are distinct group of cytoskeletal proteins within the tubulin superfamily proteins. Formerly known as FtsZ3, CetZ are widely distributed among Euryarchaeota including the Methanomicrobia. CetZ sequences diverge from eukaryotic tubulins as well as bacterial and archaeal FtsZs, but they share features with both. Along with FtsZ, many archaea have one or more additional tubulin superfamily protein from the CetZ family. *In vivo* studies recently carried out in the model Haloarchaeum, *Haloferax volcanii,* showed that it contains eight tubulin superfamily proteins in which two are FtsZs and six are CetZs. The CetZs are not individually required for cell division, but the most conserved homologue of the CetZs in *H. volcanii*, CetZ1, was required for differentiation of irregular plate-shaped cells into rod-shaped cells. Deletion of CetZ1 also resulted in a severe defect to motility, most likely due to their inability to form rods. CetZ1 forms dynamic cytoplasmic filaments that are required for cell shape change, but the mechanism by which CetZ1 modulates cell shape change is still unknown (Duggin et al., 2015). CetZ1 shares 80% sequence identity among homologs of Halobacteria. CetZ1 is the only protein from the CetZ family that has a known function in controlling cell shape (Liao, Ithurbide, de Silva, Erdmann, & Duggin, 2018).

1.6.3.1 CetZ structure

The recently solved CetZ protein structure shows some similarities and differences to the FtsZ and tubulin family proteins. The crystal structure of *Haloferax volcanii* CetZ1 and CetZ2 showed the typical fold for GTP binding and hydrolysis. The CetZ protein structure has two domains as seen in other tubulin superfamily proteins (*Figure1.7.d)*. In comparison to FtsZ and tubulin, variations are seen in H6, H9 and H11 regions of CetZ. Most CetZ, like tubulins, lack the N-terminal extensions to the GTP binding domain that is generally found in FtsZ. The H6 helix in the GTP binding domain is shorter and forms a single helical turn to form the

subunit-subunit interface. Whereas, the H9 helix is enlarged, thereby increasing the size of the C-terminal domain. Also, the H11 helix is long, forming the C-terminal extensions which align with the protofilament polymerization axis.

H.volcanii CetZ1 monomeric protein structure share remarkable similarity with FtsZ. Especially the conformation of T3 loop, the primary contact of the γ-phosphate of GTP in CetZs, is particularly identical to FtsZ. As compared to tubulins, the surface loops of CetZs are adjacent in conformation with those of FtsZ. However, the conserved regions of the amino acid sequence reveal that CetZs are more comparable with tubulins (*Figure1.7.b)*. For instance, the T7 loop that activates the γ-phosphate by nucleophilic attack contains a glutamate residue in CetZs and tubulins, whereas the equivalent residue in FtsZs is an aspartate. Also, a glutamate residue is found in CetZs at the top of the T1 loop that forms an essential protofilament contact with the T7 loop, but this is absent in FtsZ. Moreover, the guanine recognition site in the H7 loop has asparagine residue in the CetZ structure, which is similar to tubulin and TubZ proteins, but an aspartate residue is seen in FtsZ. The signature motif GGGTGS/TG is serine in both CetZs and tubulin proteins while it is threonine in FtsZ (Aylett & Duggin, 2017; Duggin et al., 2015).

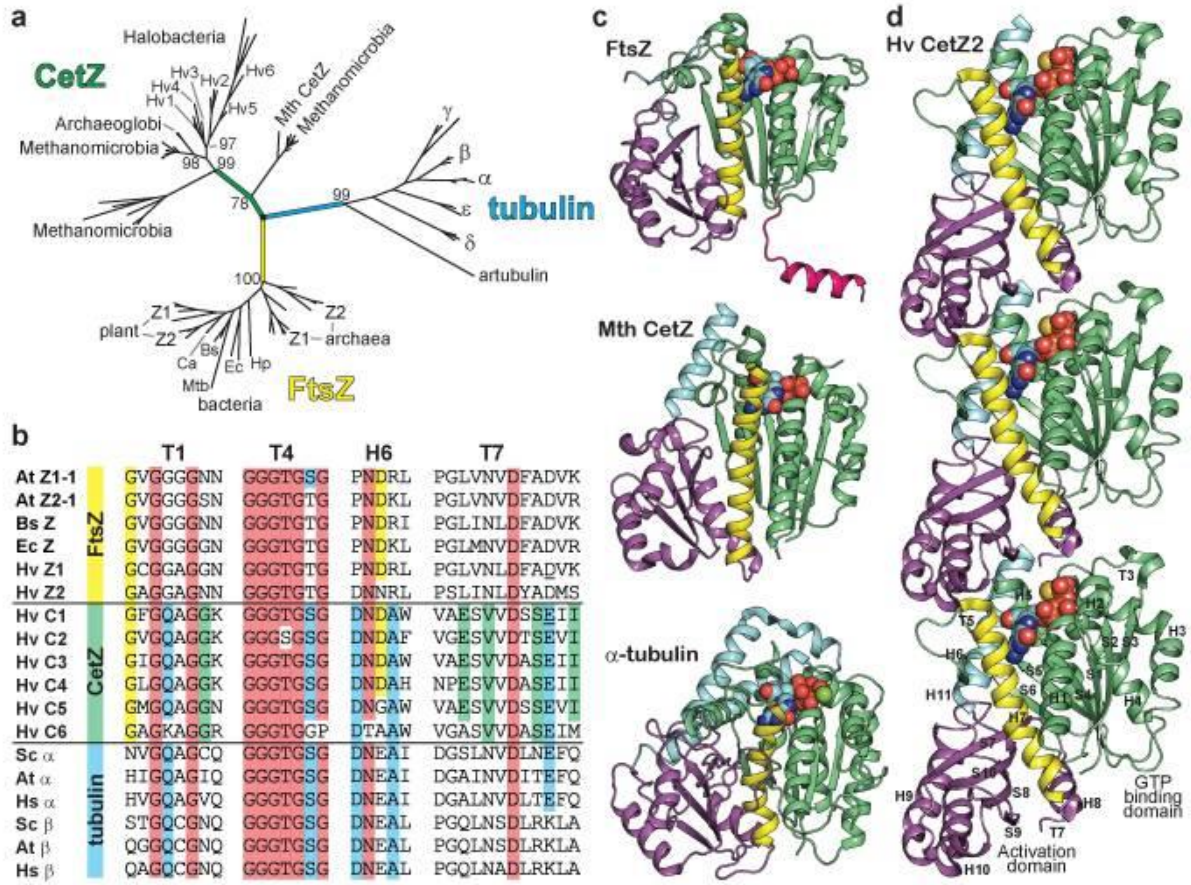

Figure 1.7**: **Conserved regions of CetZ, FtsZ and tubulin.

(a) Branch length indicates the degree of difference of proteins sequences, with major groups labelled. (b) Amino acid sequence alignments of conserved regions of FtsZ, CetZ and tubulin from a variety of species. Red indicates universal conservation, yellow shows the conserved region for FtsZ and CetZ, blue represents conservation between CetZ and tubulin, and green indicates conserved regions among CetZs only. (c) Structural comparison between different tubulin superfamily proteins - FtsZ, MthCetZ and α-tubulin. (d) Protofilament of CetZ2-GTP showing the straight and untwisted protofilament. Adapted from (Duggin et al., 2015)

1.6.3.2 Function of CetZ

Tubulin superfamily proteins have diverse functions, the primary function being cell division. Previous studies have used genetic approaches in attempt to establish functional roles of *H. volcanii* CetZ proteins. It was found that individual deletion of each of the six CetZs has no effect on the growth rate or cell size suggesting that CetZs are not required for cell division (*Figure 1.8.A*). Interestingly, knocking out the *cetZ1* gene inhibited the shapeshift from plate-

shaped cells to rod-shaped cells, thereby effecting swimming motility of *H. volcanii* (Duggin et al., 2015) (*Figure 1.8.B)*. Furthermore, upon overexpression of CetZ1 in liquid culture where cells are normally plate-shaped, rod development was stimulated (*Figure 1.8.C)*.

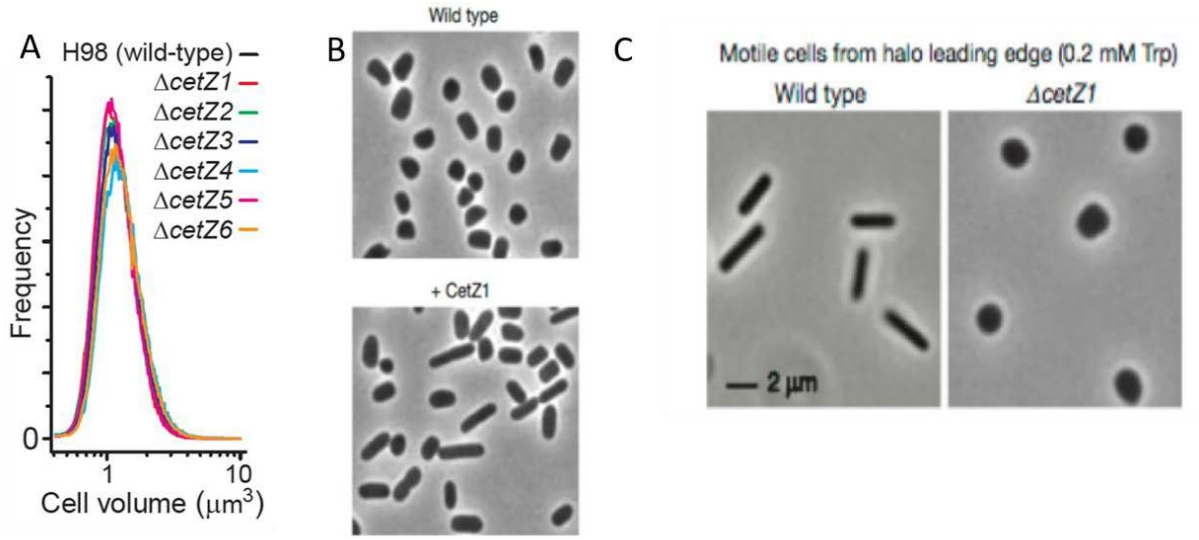

Figure 1.8: Phenotypes of CetZ1 deletion and overexpression

(A) A comparison of cell volume of all cetZ knockouts in mid-log phase to the cell volume of wild-type. (B) Phase contrast microscopy of wild-type H.volcanii mid-log cultures in HvCab medium shows plate shaped and overexpression of CetZ1 induces rod formation. (C) Phase contrast microscopy of cells from the leading edge of motility halos shows rods in wild-type and not in knockout CetZ1. Adapted from (Duggin et al., 2015).

Localisation studies using green fluorescent protein (GFP) tagged CetZ1 showed diffused fluorescence mostly throughout the cytoplasm, but foci or patches of varying intensity adjacent to the membrane. In rod-shaped cells, short filaments, and patches of CetZ1-GFP were observed in parallel with the long-axis of the rod cell elongation (Duggin et al., 2015) (*Figure 1.9.A)*. These localisation patterns were also seen with the use of second CetZ1 fusion protein- CetZ1-mTurquooise2, which was fully functional (De Silva, 2019) (*Figure 1.9.A)*. Expression of the CetZ1.GFP fusion protein has shown diffuse fluorescence, mostly around the cell periphery or at mid-cell. The pattern observed was highly dynamic in live cells and was dependent on the integrity of the GTPase active site. This dynamic localisation of CetZ1 implicates an important cytoskeletal role in modulating cell shape (Duggin et al., 2015).

However, the relationship between these localisation pattern and the function of CetZ1 still remains unclear.

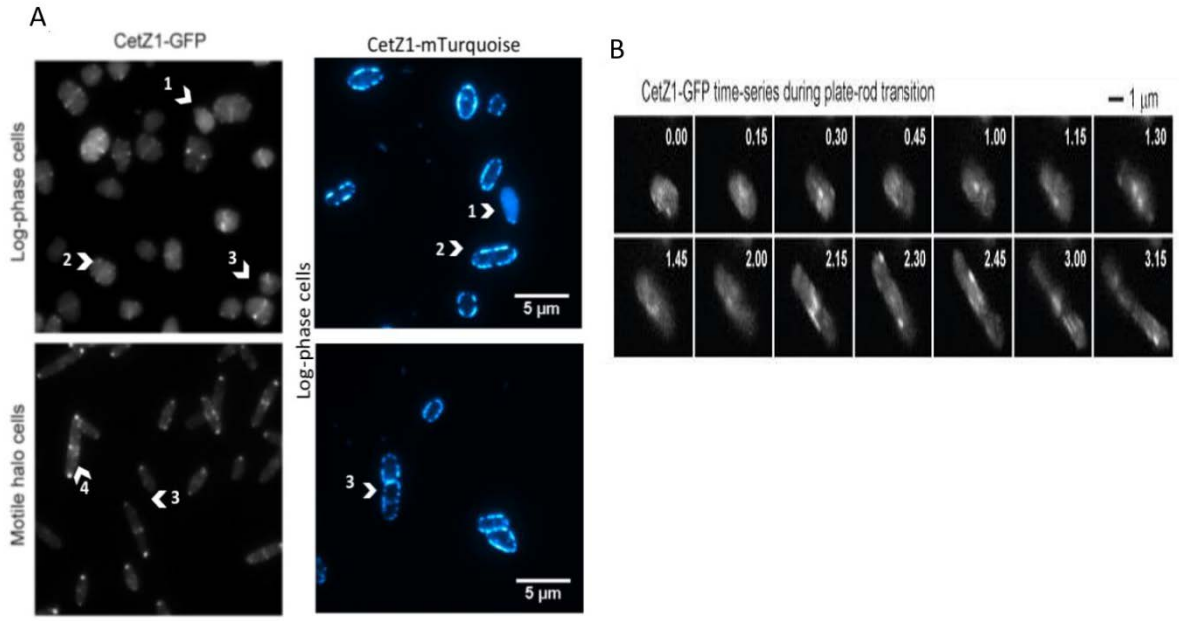

Figure 1.9 Localisation of CetZ1

(A) Fluorescence microscopy of CetZ1-GFP and CetZ1.mTurquoise showing detail of an end-capped cell and 3D-SIM showing single and multiple foci with short filaments. (B) The localisation dynamic of CetZ1-GFP during plate to rod shape transition. Adapted from(Duggin et al., 2015) and (De Silva, 2019).

1.6.3.3 Dominant inhibitory mutant of CetZ1

Mutation of a key catalytic residue (E218) from glutamate to alanine prevented GTPase activity of CetZ1, and inhibited the de-polymerization cycle, in a dominant inhibitory manner, creating hyper-stable localizations at the cell envelope and unusual cell shapes and structures. This mutation was made based on equivalent and well–characterised mutations of tubulin and FtsZ (Duggin et al., 2015). Additionally, it was also seen that strong overexpression of CetZ1.E218A caused a jagged cell shape phenotype in liquid cultures which often exhibited stalks and protrusions and partially inhibited rod development (Duggin et al., 2015) (*Figure1.10.A)*.

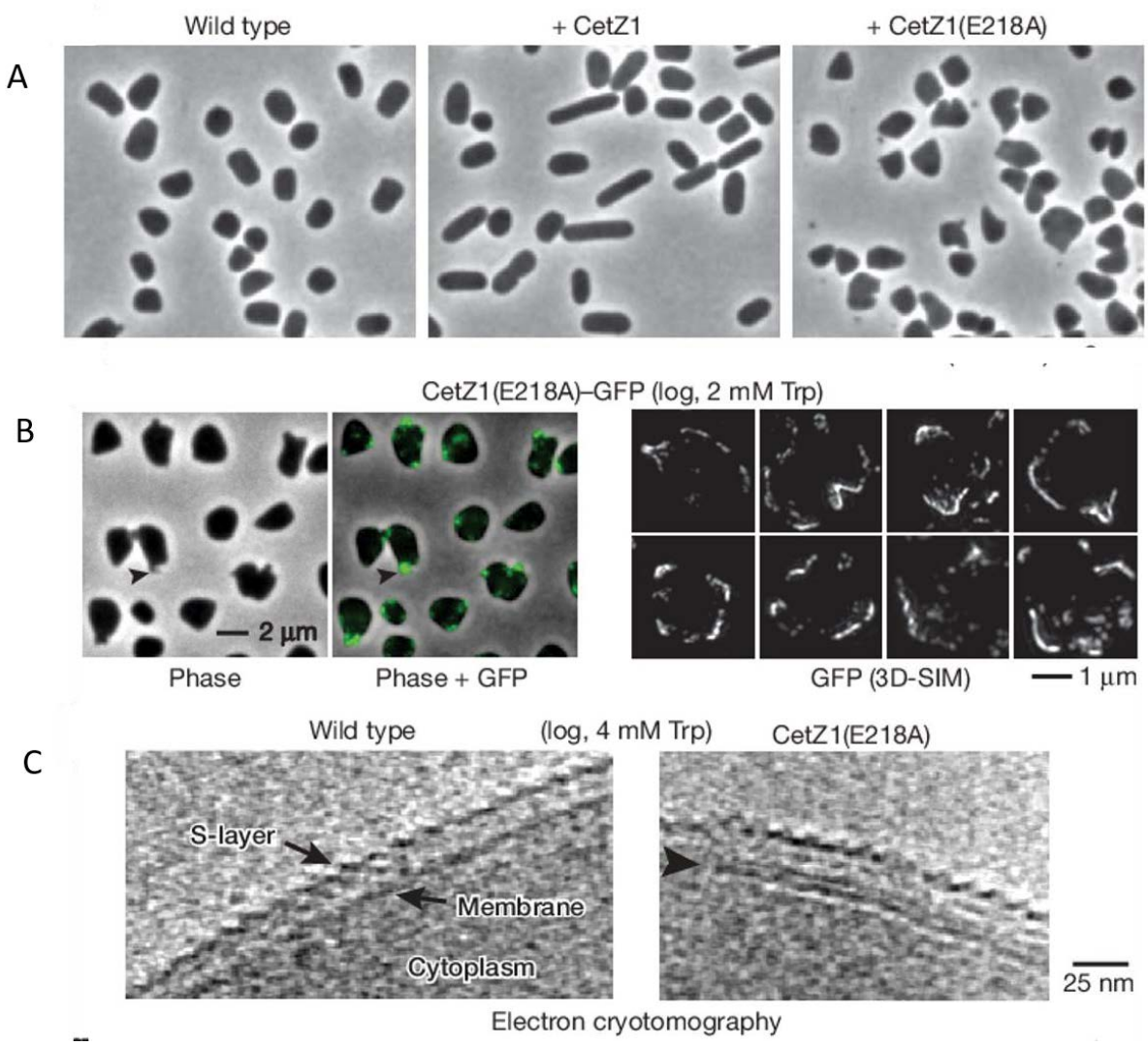

Figure 1.10 Localisation of CetZ1.E218A

(A) Phase contrast microscopy images of cells showing wild-type, CetZ1 overexpression and CetZ1.E218A overexpression. (B) Fluorescence microscopy and 3D SIM of CetZ1.E218A during mid-log growth. CetZ1.E218A localizes generally at high curvature regions of the membrane. (C) Extra layer at the inner surface of the envelope due to overexpression of CetZ1.E218A. Adapted from (Duggin et al., 2015).

The localisation of CetZ1.E218A tagged with GFP was different from that of CetZ1. It did not localise dynamically throughout the cytoplasm and instead was seen to show stronger foci adjacent to the membrane (*Figure1.10.B)*. The foci were mostly observed at the regions of high membrane curvatures. This may be due to the loss of the CetZ1 depolymerization and the dynamics of polymer turnover. Similar outcomes have been seen for GTPase defective mutations in FtsZ and tubulins. Together CetZ1 knockout studies and the CetZ1.E218A

phenotypes indicate that CetZ1 is certainly important for the rod cell development and controls the cell shape.

CetZ2 overexpression does not induce a shape phenotype. However, CetZ2 overexpression causes cells to become hyper motile on soft-agar motility assays. This hyper motility cannot rescue the motility defect caused by CetZ1 deletion (Brown et al; unpublished data). However, the GTPase defective mutant of CetZ2 (E212A) showed cell shape effects similar to that of CetZ1.E218A. Suggesting that CetZ2 is likely to have an indirect or non-dominant role in controlling cell shape and motility in conjunction with CetZ1, and may be have other additional cellular functions (Duggin et al., 2015). Possible higher order cytoskeletal structure was evident in CetZ1 from a cryoEM analysis which strongly indicated an additional layer near to plasma membrane during the overexpression of the GTPase mutant of CetZ1 (*Figure1.10 C)*. Moreover, the CetZ2 resolved as a sheet-like structure which resembles the subunit arrangement in the microtubule wall. However, further investigation is needed to confirm this observation.

The relationship between the localisation and function of CetZ1, and the mechanism through which it influences cell shape is still uncharacterised. However, since previously conducted localisation studies show foci form adjacent to the membrane, and the CetZ1 GTPase mutant causes an additional layer close to the inside of the membrane as well, it is hypothesised that CetZ1 may modulate cell shape via interaction with the archaeal membrane, either directly or indirectly.

Despite the fact that there is preliminary understanding of CetZ1 function, the insights of structural-functional relationship of CetZ1 remains a prediction, based on what is known about FtsZ and tubulins. Investigating the structural-functional roles of CetZ1 in *H.volcanii* will enable a greater understanding of fundamental process that contribute to cell shape control in archaea. Additionally, characterisation of CetZ1 proteins and their interactions with other proteins and lipids will help in understanding how these proteins influence cell shape and will facilitate our understanding of a major cytoskeletal component in archaea. CetZ1 may also represent an evolutionary intermediate between FtsZ and tubulin-based cytoskeletons across the domains of life. Moreover, investigation of the CetZ family proteins can contribute greatly to our understanding the evolutionary and elementary biology of cytoskeletal proteins in general. Recently it has also been shown that archaeal species reside in the human gut and

skin, and can now be explored as an alternative option for drug delivery and drug development options such as archaeosomes (Kaur, Garg, Rath, & Goyal, 2016).

1. 7 Project Aim

The overall aim of this project is to gain insight in the biochemistry of the CetZ1 protein, and the mechanisms of its self-association. This aim was addressed through the following key objectives:

1. Study the self-association (polymerization) of CetZ1 in vitro by comparing the pure wild-type CetZ1 protein, and its several site-directed mutants that are predicted to be defective in polymerization, to characterize the quaternary arrangements of CetZ1 molecules and the important regions of the protein involved in polymerisation. (Chapter III)
2. Investigate the potential actions of CetZ1 on lipid membranes at the molecular level and its possible roles in envelope remodelling. (Chapter IV)

Finally, an overview of the main conclusion is presented in Chapter V with some perspectives for future research.

Tubulin superfamily proteins have several defining biochemical characteristics such as self-interaction, membrane localisation and lipid binding capabilities that are seen in FtsZ and tubulin. With no prior work done on CetZ1 *in vitro*, these characteristics were studied using a range of biochemical assays. The standard assays used to study CetZ1 were light scattering, sedimentation, electron microscopy and GTPase assay.

Lipid binding capabilities were established using i*n vitro* binding assays analysed by light microscopy and electron microscopy, as well as co-sedimentation assays.

As described above, eukaryotic and prokaryotic tubulin homologs have different structures, functions, mechanisms of action, and regulation. Structural and biochemical analysis presented in this study will provide the foundation to understand the role of CetZ cytoskeletal proteins in archaea and will thereby help understand the intermediate stages that occur during the evolution of tubulin superfamily proteins.

Chapter II
General Materials and Method

2.1 Growth Media

Bacterial and archaeal growth media used in this study are listed in Tables 2.1 and 2.2, respectively. All media were made in ROW and sterilised by autoclaving or 0.2 μm filtration or from sterilised components.

Table 2.1 Bacterial Growth Media

Media	**Composition**
LB	25 g of LB broth base in 1 L of MQW (0.5 % (w/v) Yeast extract, 1 % (w/v) Tryptone, 0.05 % NaCl)
LB agar	25 g of LB broth in 1 L of MQW, 1.5 % (w/v) bacteriological agar
2TY	1.6 % (w/v) Tryptone, 1 % (w/v) Yeast extract, 0.5 % (w/v) NaCl
SOC	2% (w/v) Tryptone, 0.5% (w/v) Yeast extract, 10 mM NaCl, 2.5 mM KCl, 10 mM $MgCl_2$. 20 mM Glucose in MQW was added after autoclaving.

Table 2.2 Archaea Growth Media

30% BSW	24 % (w/v) NaCl, 3 % (w/v) $MgCl_2.6H_2O$, 3.5 % (w/v) $MgSO_4.7H_2O$, 0.7 % (w/v) KCl, 0.02 M Tris-Cl (pH 7.4), 0.005 M $CaCl_2$
HvYPC	60 % (v/v) 30 % BSW, 0.1% (w/v) Casamino acid, 0.5% (w/v) Yeast extract, 0.1% (w/v) Peptone, 15% (w/v) Sucrose, PH 7.4

2.2 Bacterial Strain and Plasmids

Tables 2.3, 2.4 and 2.5 list the general bacterial, archaeal strains and plasmids used in this work, respectively. All the strains were stored as stationary phase cultures with 20 % (v/v) glycerol at -80^{o}C.

Table 2.3 General Bacterial Strains used

Species	Strain	Relevant genotype	Reference/Source
E. coli	C41(DE3)	*E. coli B F- ompT gal dcm hsdSB (rB-mB) (DE3)*	Jan Lowe MRC Cambridge UK (Hartman et al., 2010) (Dumon-Seignovert, Cariot, & Vuillard, 2004)

Table 2.4 General Archaeal Strains used

Species	Strain	Relevant genotype	Reference/Source
Haloferax volcanii	H26	Δ*pyrE2*	T. Allers (Hartman et al., 2010) (Duggin et al., 2015)

Table 2.5 General Plasmids used

Plasmid	Relevant features	Reference/Source
pHis17	Protein overexpression vector, T7 promoter, *Amp* resistance gene	Cordell and Lowe, 2001

pHis17 with CetZ1/mutant	Protein overexpression vector, T7 promoter, *Amp* resistance gene with CetZ1 or mutant	(De Silva, 2019)

2.3 Chemicals, Reagents and Solutions

Most chemicals and reagents used in this work are outlined in *Table 2.6.* These chemicals were analytical reagent (AR) grade. Commonly used aqueous buffer and solutions in this work are listed in *Table 2.7.*

Table 2.6 commonly used Chemicals

Chemical	Source
40% Acrylamide (ratio of acrylamide to bisacrylamide is 37.5:1)	GE Healthcare, Sweden
Agarose	Bioline , Australia
Ampicillin	Genlantis, USA
AM1-43	Thermo-Fischer Scientific , USA
Bio-lab Pre-Stained Broad Range Protein Standard	New England Bio-Labs, USA
Coomassie Brilliant BlueR-250	Sigma-Aldrich, USA
Difco™ LB Broth Base(Luria-Bertani)	Thermo-Fischer Scientific , USA
Glycerol	Sigma-Aldrich, USA
GTP	Sigma-Aldrich, USA
Oxoid™ Agar (Bacteriological Agar No 1)	Thermo-Fischer Scientific , USA

Table 2.7 Buffers and General Solutions

Buffer/Solution	Composition
1 X PBS	150 mM potassium phosphate, 50 mM Tris-Cl, pH 7.4
4 X SDS-PAGE loading buffer (SDS-LB)	250 mM Tris-Cl, 8 % (w/v) SDS, 40% (v/v) Glycerol, 20 % (v/v) 2- β mercaptoethanol, 0.4 % (w/v) Bromophenol Blue, pH 6.8
Coomassie Destain	20% (v/v) Ethanol, 10 % (v/v) Acetic Acid
Coomassie Stain	50% (v/v) Ethanol, 10% (v/v) Acetic acid, 0.5% (w/v) Coomassie brilliant Blue R
Liposome Buffer	50 mM Tris-Cl, 100 mM NaCl, 1 mM EDTA pH 7.5
SDS-PAGE Running Buffer	25 mM Tris, 190 mM Glycine, 0.1% (w/v) SDS, pH 8.3
TAE	40 mM Tris-Cl, 20 mM acetate, 1 mM EDTA, pH 8.6

2.4 Growth conditions and preparation of *Bacterial* cells

2.4.1 Normal growth conditions for *E.coli*

E. coli strains were cultured by streaking a loop full of bacteria from a frozen glycerol stock on to a LB agar and incubated overnight at 37^{o}C. A single colony from the above agar plate was used to inoculate in 50 mL LB broth with ampicillin antibiotic. This liquid culture was then incubated at 37^{o}C with shaking at 150 rpm.

2.4.2 Preparing electro competent cells of *E.coli*

C41 *E. coli* cells were grown up to mid-log phase (A600 nm: 0.5-1). Cells were pelleted at 4000 x g max for 15 min at 4 ^{o}C. Then the cells were washed by resuspension in an equal volume of sterile water and centrifuged as above. This washing step was repeated twice with half the

initial volume of sterile water and 1/50th of the initial volume of 10% v/v glycerol in sterile water, respectively. Cells resuspended in 10% v/v glycerol were stored in aliquots at -80^{o}C.

2.4.3 Transformation of *E. coli* by electroporation

Pre-chilled 40 µL of electro competent cells were mixed with 1-2 µL of plasmid DNA in a prechilled 1.5 mL eppendrof tubes. The mixture was kept on ice for 40 sec, then transferred to a 0.2 cm electroporation cuvette. A pulse of 25µF capacitor with a 2.5 kV for 200 resistance in parallel was set. One millilitre of SOC medium was added immediately and the electroporation cells were transferred to a different tube to incubate at 37^{o}C for 1 h with shaking at 250 rpm. Cell suspension was then spread onto a LB agar plate with ampicillin antibiotic.

2.5 General growth conditions for *Haloferax volcanii*

H.volcanii stains were cultured by streaking a loop full of archaea from a frozen glycerol stock on to a HvYPC agar (*Table 2.2)* and incubated 3-5 days at 45^{o}C. A single colony from the agar plate was used to inoculate 50 mL HvYPC broth and incubated at 45^{o}C with shaking at 150 rpm (Robinson et al., 2005).

2.6 General Method used in this work

2.6.1 SDS-PAGE Analysis

Throughout the work, all the protein samples and *in vitro* studies were analysed using SDS-PAGE using the following protocol. Resolving gel (12%) was prepared using the components shown in *Table 2.8*. Ammonium persulphate (APS) and TEMED were added immediately before loading the gel into the casting apparatus (Bio-Rad Mini-Protean 3). The stacking gel (4%) was poured on top of the resolving gel and the appropriate comb was immediately inserted into the gel to create wells. After the gels solidified they were placed in a Bio-Rad Mini-Protean 3 system. The inner tank was filled completely and the outer tank up to 2 cm height with 1x running buffer (*Table 2.7)*. To prepare the samples, 4x SDS-LB (*Table 2.7)* was added to a final concentration of 1x and 10 µl of each sample was loaded into the

polyacrylamide gel along with a pre-stained blue protein board range standard. The gel was run at a constant current of 20 mA with 100 V per gel for 60 min. After the run was completed, the gel was stained with Coomassie Blue stain (*Table 2.7)* for 10 mins and destained using Coomassie destain (*Table 2.7)*. The gels were imaged using the Amersham 600 gel imager.

Table 2.8 SDS-PAGE Gel Components

Resolving Gel (12 %) for 10 mL	**Stacking gel (4 %) for 5mL**
40 % Acrylamide solution – 3 mL	40 % Acrylamide solution– 500 µL
MQW – 4.4 mL	MQW – 3.2 mL
1.5 M Tris-Cl pH 8.8 – 2.5 mL	0.5 M Tris-Cl pH 6.8 – 1.25 mL
Ammonium persulphate (10% w/v frozen stock) – 100 µL	Ammonium persulphate (10% w/v frozen stock) – 50 µL
TEMED – 10 µL	TEMED – 5 µL

2.6.2 DNA Electrophoresis

Generally, 1 % agarose gels with TBE (*Table 2.7)* were used in this study. Gels were pre-stained by adding 0.5 µL of 10mg/ml Ethidium Bromide per 50 mL of agarose solution and cast on a horizontal wide mini gel apparatus. Samples containing DNA were mixed with 1x loading buffer(Thermo Fisher) and were loaded into the wells and run at 100 V for 60 min in an electrophoresis chamber containing TBE. The gels were visualised via UV light using a transilluminator (Ingenius3; Syngene) and imaged using a charge–coupled device camera (Synoptics CAM-FLXCM; Syngene).

2.6.3 Imaging Liposomes using microscopy

For most microscopic imaging, 2 µL of sample was placed directly on a slide and covered with 1.5 number coverslip. Phase contrast images were acquired with the Zeiss Axio Plan @ system with a 1.4 NA phase- contrast objective (Carl Zeiss, Germany).

Chapter III
In vitro assembly studies of CetZ1 from *Haloferax volcanii*

3.1 Introduction

Tubulin superfamily proteins are one of the main components in the cytoskeleton across all the domains of life. The key feature of tubulin superfamily proteins is the GTP dependent polymerization and depolymerisation of protein subunits (Scheffers & Driessen, 2001). These tubulin superfamily proteins from Bacteria, Eukaryotes, and Archaea have a high level of primary amino acid sequence conserved at the GTP site and belong to the broader P-loop family of GTPases (Mukherjee & Lutkenhaus, 1998). Although these proteins share a common basic monomeric structure, their quaternary structures and mechanism of action have diverged. The tubulin superfamily proteins can be grouped into three main branches: (a) FtsZ found in bacteria, archaea and some eukaryotic organelles; (b) tubulins primarily found in eukaryotes; (c) CetZ found in archaea (Aylett & Duggin, 2017; Vaughan, Wickstead, Gull, & Addinall, 2004). These proteins can all polymerize in a GTP dependent manner, assembling into filaments and disassembling by hydrolysis of GTP to GDP. Specific structural and functional changes in the cell are regulated by the location, timing and polymerizing cycle of the tubulin superfamily proteins (Löwe & Amos, 2009).

Tubulin and FtsZ polymerization have been intensively studied *in vitro* and many different structures of filaments have been described depending on the nucleotides, accessory proteins, and assembly buffer included in the polymerization reaction. Previously observed tubulin and FtsZ filament structure includes straight, curved, sheets, tubes and bundles. (Erickson et al., 2010). Although, the architecture of these proteins *in vivo* is not yet fully understood, studies done by electron cryo-tomography have shed some light on how these proteins might assemble into complex structures. Archaea have been contributory in understanding the evolution of many complex biological processes such as the protein modifier system in eukaryotes and replication of eukaryotic DNA (Nunoura et al., 2011). The recently discovered third group of tubulin superfamily protein, CetZ, is distributed mainly among halophilic and methanogenic archaea, and is expected to be crucial in providing insights into the evolution of tubulin superfamily proteins. The primary function of CetZ1 is to modulate cell shape change from plates to rods, most likely to assist in motility and this has been observed in a number of conditions such as a motility assay (Duggin et al., 2015) and

trace element depletion (De Silva, 2019). In the same study it was found that CetZ proteins are not individually required in cell division. But instead, knocking out the *cetZ1* gene inhibited the shapeshift from plate-shaped cells to rod-shaped cells, thereby inhibiting *H. volcanii* swimming motility. It was seen that *H. volcanii* can exhibit different types of motility behaviour, but rods were the fast swimmers. Mutation of a residue E218A (glutamate substituted to alanine at position 218) in the CetZ1 GTPase active site directly affected changes in the cell shape, and blocked rod formation, even when the wild-type endogenous genomic copy of *cetZ1* gene was present. This may be due to the hyper stability of CetZ1 polymers upon incorporation of the CetZ2.E218A GTPase dead monomer, since GTP hydrolysis is required for polymer disassembly and turnover in tubulins (Duggin et al., 2015; Liao et al., 2018). The study therefore suggests that CetZ1 polymerisation and depolymerisation dynamics are essential for CetZ1's function in cellular morphology.

Structural dynamics such as cell motility and division are maintained by the force generated by a cytoskeleton. To understand the force generation mechanism of CetZ protein and how this is regulated, first we must understand how CetZ protein polymerizes and depolymerizes. In this study, to understand the CetZ1 protein structure and its function we studied amino-acid mutations on specific regions of the CetZ1 protein to check how well-defined modifications to the amino acid sequence affect protein function. These mutations have been analysed at two different levels: first, by looking at their effect *in vivo* on their dynamic localisation and cell shape change in *H. volcanii* (done by former PhD student)*(De Silva, 2019)*, and secondly, by analysing their effect in polymerization assay *in vitro* (the current study). Since it has been hypothesised that residues involved in the lateral interactions between protofilaments and in the C-terminal tail region would be important for the formation of CetZ1 polymers, mutations were designed within this region to determine their importance in CetZ1 polymerisation. Also, mutation was designed to study the functional importance for GTP binding domain and GTPase domain (De Silva, 2019).

Mutation to disrupt the lateral interactions:

Mutations in the C-terminal domain of CetZ1 were made, in order to test whether these disrupt the lateral interactions between protofilaments, as predicted based on the CetZ2 filament crystal structure and the arrangement of subunits in the microtubule wall. The mutation E188G (Glutamic acid substituted to glycine at position 188) and a double mutant,

R276E K277E, were made in the C-terminal domain as the double mutant appeared to have close contact with the adjacent subunit as shown in *Figure 3.1.a*. In tubulins, the surface-exposed M-loop region has been shown to be crucial for the maintenance of lateral interactions of microtubules (Amos & Löwe, 1999; Mitra & Sept, 2008). Interestingly, CetZ1 has a relatively long M-loop rich in leucine between S7 and H9 of its M-loop region and a conspicuous hydrophobic patch near its centre. The M-loop region is not resolved in the CetZ1 crystal structure suggesting an intrinsically disordered structure. The CetZ1 M-loop region might be involved in stabilizing the lateral interactions, like tubulins, and since it also has the exposed hydrophobic patch it might also be involved in membrane association of CetZ1. To investigate its functional importance a mutation in the M-loop sequence ^{248}LLSRL^{252} was substituted with SASRA, to decrease its hydrophobicity (De Silva, 2019).

Mutation in the T4 loop region (GTP binding) to disrupt the longitudinal interactions:

In FtsZ and tubulin, the T4 region is involved in GTP binding and hence polymerization of protein. Exploring the functional importance of the T4 region in CetZ1 will be crucial to test the longitudinal interaction of CetZ1. Therefore, a mutation G108S (glycine is changed to serine) was made to the top surface (T4 nucleotide binding surface) of CetZ1 protein as shown in *Figure 3.1.b*.

Mutation in the GTPase domain to disrupt the longitudinal interactions:

In tubulin superfamily proteins such as tubulin and FtsZ, the GTPase domain in the C- terminal domain is involved in the polymerization of protein (*Figure 3.1.a)*. Mutation E218A was done in the CetZ1 protein to explore the importance of the GTPase domain. E218 is located in the part of the 'synergy' loop and probably is in contact with the GTP of the subunit below, to bring about GTP hydrolysis and promote filament disassembly.

Mutation in the C-terminal tail region:

Membrane association of FtsZ has been studied and it is seen that flexible C-terminal tail region of FtsZ is important for its membrane interactions via cell division associated proteins such as ZipA (P. J. Buske & Levin, 2012) (Shen & Lutkenhaus, 2009). Therefore, to study the importance of C-terminal tail of CetZ1, mutations were made in the CetZ1 C-terminal tail by

changing the sequence ^{390}LSESLF^{394} to AESGG (unresolved in the crystal structure) (De Silva, 2019).

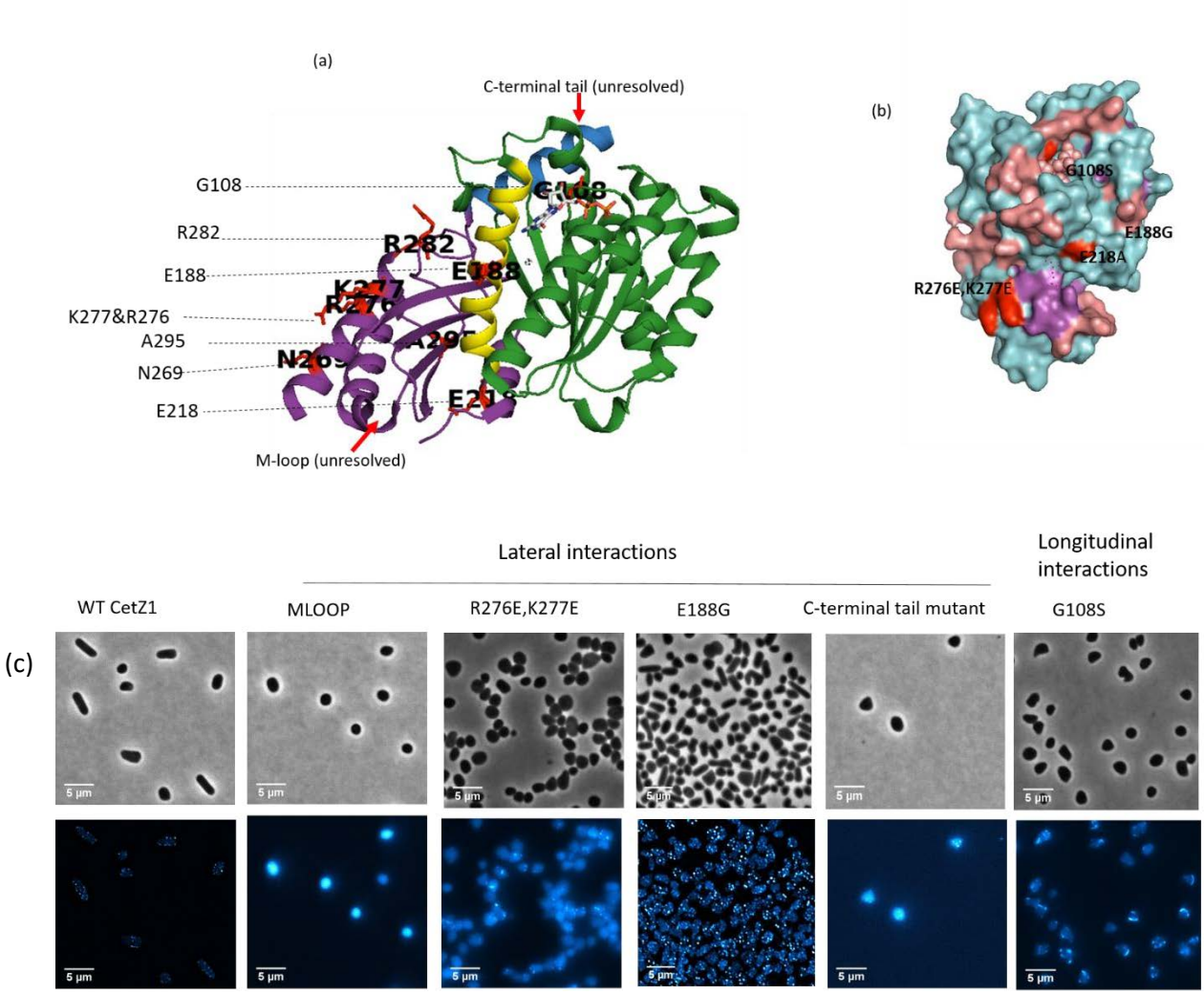

(d)

	Mutation and Amino acid change	Location of mutation
Lateral interaction mutants	**M-loop LLSRL-SASRA**	S7-H9 C-terminal domain
	E188 Glutamic acid (E) change to Glycine(G)	H7 helix C-terminal domain
	R276,K277 Arginine &Lysine (R,K) change to Glutamic acid(E)	H9 helix C-terminal domain
	C-terminal tail LESLF-AESGG	C-terminal tail
Longitudinal interaction mutants	**G108 Glycine(G) change to Serine(S)**	T4 loop N-terminal domain (GTP-binding site)
	E218 Glutamic acid (E) change to Alanine(A)	T7 loop C-terminal domain (GTPase activation site)
	Wild type CetZ1	–

Figure 3.1: Locations of the CetZ1 point mutations designed to disrupt the lateral and longitudinal interactions.

(a) Marked are the positions of all the point mutations in the CetZ1 monomer. The mutation that affects the longitudinal interaction (G108) is marked in the N-terminal domain shown by green colour and the mutation that affect the lateral (A295,E188,R282,N269,R276,K277) and GTPase interaction (E218) are marked in the purple-coloured C-terminal domain. The C-terminal tail domain and M-loop are not resolved in the protein structure. (b) The surface view of the monomer showing the marked longitudinal and lateral mutations are shown in red colour. This highlights the GTP binding site mutation inside the GTP binding pocket and the position of lateral contact mutants on the bottom side of the CetZ1 monomer. (c) Phase contrast and fluorescence images of the in vivo localization for wild-type CetZ1 and CetZ1 mutant tagged with mTurquoise2. (d) tabular representation of the mutation with amino acid change and the location of mutation.

***In vivo* localisation of mutants**: The study done for *in vivo* localization by (De Silva, 2019) showed that the mutants displayed different localization patterns (*Figure 3.1.c)*. Wild-type CetZ1 showed localization close to the cell envelope, whereas the M-loop mutant displayed a highly diffuse localization. The CetZ1 double mutant displayed intense filament-like localisation. CetZ1.C-terminal tail mutant showed diffused localization. CetZ1.G108S mutant displayed an intense peripheral localisation. CetZ1.E188G showed filament like intense localisation (De Silva, 2019) (*Figure 3.1.c)*.

In this work, we have studied the CetZ1 polymerization in vitro by right-angle light scattering, electron microscopy, sedimentation. Light scattering is a standard method that has been used to study tubulin and FtsZ polymerization in real time (Mukherjee & Lutkenhaus, 1998; Walker, Gliksman, & Salmon, 1990). These methods allow a relatively rapid characterization of CetZ1 polymerization and its activity. This chapter reports the results from the right-angle light scattering to investigate the increase in polymer size and dynamic behaviour of CetZ1 protofilaments in real time, electron microscopy of negatively stained samples to characterise the CetZ1 polymer structure, and an attempt was made to measure the kinetics of inorganic phosphate (Pi) released from GTP hydrolysis which is catalysed by CetZ1 protein.

3.2 Methods

3.2.1 Protein Overexpression

The pHis17 plasmids, with cloned CetZ1 or the CetZ1 mutants (De Silva, 2019), were transformed into *E.coli* C41 via electroporation for the overexpression of the protein and plated on an ampicillin agar plate on day one. On day two, the transformed colonies were scraped off the agar plate and inoculated into 50 ml of 2TY media containing 0.1 mg/mL ampicillin. Initially the culture was incubated at 37^{o}C for one hour with shaking at 200 rpm, after that the culture was transferred to a 5 L flask containing 1.6 L of 2TY media with ampicillin at 37^{o}C with 200 rpm shaking. Periodically, the OD (A_{600}) was checked until the culture reached OD (A_{600}) of 0.4, after which the cultures were then placed in an incubator at 18^{o}C with shaking at 150 rpm for 10-12 min. At this point 1 mL of culture was taken as a "pre-induction" sample and the cell pellet was stored at -20 ^{o}C for the later SDS-PAGE comparison. After 10-12 min 1 mM IPTG was added to induce the protein expression and was left overnight at 18^{o}C with shaking at 150 rpm. On day three the OD (A_{600}) was checked by diluting the sample by 1/10th and 1 mL sample was again removed as "post-induction" sample. The remaining cells were then centrifuged using Hitachi R9A rotor at 9000 rpm for 30 min at 4^{o}C. The pellet was stored at -80 ^{o}C until future use. From this step onwards, all procedures were carried out at 4^{o}C.

3.2.2 Cell lysis

The frozen pellet was thawed in 40-50 mL of 25 mM Tris buffer pH 8.5, 1mM EDTA, 20 % glycerol and lysed by using sonication on ice for 10-15 min with 30 second intervals, or by passage through a homogenizer. The lysate was then centrifuged at 18,000 rpm using Hitachi R18A rotor for 30 min at 4^{o}C to remove debris and unbroken cells. The supernatant was collected in new tube and 0.2 % of PEI was added and left on ice for 10 min. The cells were then centrifuged using a Hitachi R18A rotor at 10,000 rpm for 15 min at 4^{o}C to remove any nucleic acid impurities, and the supernatant was subjected to subsequent chromatographic purification.

3.2.3 Protein purification by Ion exchange and Gel filtration chromatography

The supernatant of the sonicated culture was subjected to further purification by using an AKTA pure chromatography system (GE Healthcare Life Science). All the solutions used in the chromatography were filtered sterilised by 0.2 µm membrane filter and pre-chilled at 4^{o}C. Ion exchange and gel filtration columns were used for the protein purification. Before each purification, all the chromatography columns and the system were first washed with ROW water and secondly with 25 mM Tris buffer pH 8.5, 1 mM EDTA, and 20 % glycerol (buffer A). All the buffers used for the purification contained 1 mM EDTA and 20 % glycerol in them.

3.2.3.1 Ion Exchange Purification

CetZ1 has a predicted isoelectric point of pI = 4.8 and was initially purified using an ion exchange chromatography. The final supernatant was passed through the HiTrap Q DEAE column, bed volume of 5 mL which was equilibrated with 25 mM Tris buffer pH 8.5, 1 mM EDTA, and 20 % glycerol as buffer A. The column was washed with 5 volumes of buffer A and the CetZ1 sample was passed through the column at a flow rate of 5 mL/min using a sample-loading pump. A gradient of 0 -500 M KCl at a flow rate of 0.4 mL/min, over the course of 10 column volumes was then performed to remove unbound or weakly bound protein. Fractions of 2 ml were collected and screened via SDS-PAGE and protein containing fractions were pooled and concentrated in 20 mL capacity, 30 kDa cut-off centrifugal concentrators (Vivaspin) to obtain a final volume of 0.5 mL.

3.2.3.2 Gel Filtration Purification

The concentrated protein from the ion exchange chromatography was further purified by size exclusion Superdex 200 Increase 10/300 GL column (GE Healthcare) chromatography. The column was equilibrated with 25 mM Tris buffer pH 7.5, 1 mM EDTA, and 20% glycerol containing 200 mM KCl at 0.1 mL/ min speed. The protein sample of 0.5 ml was loaded with a flow rate of 0.1 mL/min and 2.5 mL fractions were collected. As per the UV_{280nm} readings, fractions containing protein were analysed by SDS-PAGE, then pooled and concentrated.

3.2.4 Ultracentrifuge sedimentation assay

The sedimentation assay was carried out using the purified CetZ1 and CetZ1 mutant proteins. The reaction mixture was prepared by addition of 12 µM CetZ1 mutant in 800 mM PIPES buffer pH 7.5, 3 M KCl, 10 mM $MgCl_2$ to a final volume of 50 µL in an ultracentrifuge tube. The tubes were incubated for 2 min with shaking at 300 rpm at 37^{o}C. Polymerization was initiated by adding 1 µL of 2 mM GTP, and incubating for 2 min. The tubes were transferred to a Beckman TLA100 rotor and spun down for 10 min at 90, 000 rpm at 20^{o}C. After spinning, the tubes were removed carefully, and supernatant was immediately transferred into a clean tube. The pellet was washed with PIPES buffer and solubilised with SDS-LB (*Table 2.7)* and samples were analysed by SDS-PAGE (Section 2.6.1) (Król & Scheffers, 2013).

3.2.5 Right angle (90^{o}) light scattering assay

90^{o} Light scattering assay measurements were carried out using a Shimadzu RF-6000 Spectrofluorophotometer to monitor the dynamics of CetZ1 polymerization and depolymerization. The spectrophotometer was switched on 15 min prior to the assay to avoid thermal fluctuations and readings were taken at room temperature. The operating parameters with 300 volts of the detector were as follows. Emission and excitation wavelengths were both set to 350 nm with a slit width of 1.5 nm and the time base acquisition to 2000 seconds duration. The quartz cuvette with 10 mm path length were used and cleaned thoroughly with water and then with ethanol between each measurement. 200 µL of reaction mixture was prepared by adding CetZ1/mutant protein to a final concertation of 12 µM in 800 mM PIPES buffer, pH 7.5, 3 M KCl, 1 mM $MgCl_2$ (De Silva, 2019). The mixture was mixed thoroughly and incubated at 37^{o}C for 2 min. 196 µL of mixture was transferred to the quartz cuvette and placed in the spectrometer, this solution was used as the blank for the measurements. Data acquisition was started and sustained until the signal was stable. Polymerization was initiated by adding 4 µL of 100 mM GTP/GDP (2 mM final concentration) to the mixture and mixed briefly by pipetting up and down. Acquisition was resumed, and data was collected, with readings taken every 10 seconds (De Silva, 2019; Król & Scheffers, 2013).

3.2.6 Transmission Electron microscopy

Samples were prepared like those in the sedimentation assay; however, the final volume was reduced to 10 µL. Polymerisation of 12 µM of CetZ1/mutant in 800 mM PIPES buffer pH 7.5, 3 M KCl, was initiated with the addition of 1 µL of 2 mM GTP added and incubated for 2 min at 30 ^{o}C at 300 rpm shaking. The reaction mixture was then spun for 2 mins in a bench top centrifuge. 2 µL of sample was applied onto a glow-discharged 400 mesh carbon coated copper grid and incubated for 2 min. The grid was blotted dry by gently touching the grid parallel to a piece of filter paper. The grid was stained with 4 µL of 2 % uranyl acetate solution, and excess stain was removed by filter paper. The grid was left to dry completely and viewed using a Tecnai T20 transmission electron microscope operating at 120 kV.

The average filament length for the mutant and the wild-type was measured by manually counting more than 50 filament length for the polymers seen in the TEM images. The polymer length was measure using the ImageJ software, where single filaments were measured from different TEM images and then using Prism software the average length and *Mann-Whitney test* was performed to see significant difference.

3.2.7 GTPase assay

The experiment is set up in such a way that GTP hydrolysis of CetZ1 is stopped after various times by mixing the malachite green reagent. Malachite green working reagent and phosphate standards (40-0 µM) were prepared as describe in the Sigma malachite green phosphate assay kit user guide. 96 well PCR plate was used to carry out the experiment. 12 µM CetZ1 and mutant protein final concertation was prepared in 800 mM PIPES buffer pH 7.3, 3 M KCl. Only Buffer without protein was used as a control. GTP was added at 1 mM final concentration to each CetZ1 protein at different time points starting from 0 to 30 min in the 96 well plates. The malachite green reagent was added and mixed to each well in the 96 well plate at different time points as the GTP. The final concertation of GTP was 0.25 mM in all the reaction mixtures. The absorbance for the reaction in the 96 well plate was measured at 620 nm using a Tecan plate reader. The free phosphate in every sample reaction were calculated using the phosphate standard calibration curve. The data was plotted as phosphate release per minute/CetZ1 protein from the liner rage of the curve.

3.3 Results

To investigate the biochemical properties of CetZ1 protein, purified CetZ1 and CetZ1-mutant proteins were required. CetZ1/mutants were expressed and purified with the final goal being the use of the proteins for *in vitro* analysis of nucleotide-dependent self-association.

3.3.1 Expression and purification of CetZ1

In the preparation for the subsequent experiments, CetZ1 was overexpressed from a pHis17 plasmid and induced using IPTG. After harvesting of cells in mid-log phase, overexpression of CetZ1 was confirmed using SDS-PAGE. The results revealed successful over-expression of CetZ1 as evident from the high abundance protein band at 42 kDa in the cell lysate of transformed post-induction samples *(Figure 3.2)*. The position at which the band appeared in the gel correlated with the size for the CetZ1 which was not seen in the pre induction samples.

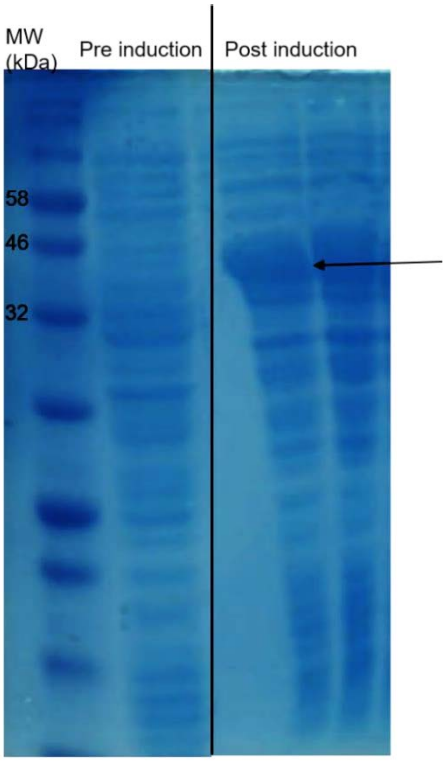

Figure 3.2: CetZ1 over expression

SDS-PAGE analysis of whole cell lysates from representative C41 cultures. The gel demonstrated successful over-expression of CetZ1, as evident by a protein band of high abundance at ~ 42 kDa post-induction (arrow). This band was absent in the pre-induction sample.

After the confirmation of CetZ1 overexpression, CetZ1 was then purified by ion exchange chromatography, with 10% glycerol in the buffers. CetZ1 eluted at around 450 mM KCl in the salt gradient. As seen in the SDS-PAGE analysis *(Figure 3.3)*, the ion exchange purification was successful but only provided a moderate level of purification. Numerous impurities were evident both above and below the band of interest corresponding to the molecular weight of CetZ1. The impurities could be either bound to the column directly or bound to the recombinant protein under the specific native conditions (*Figure 3.3.b)*.

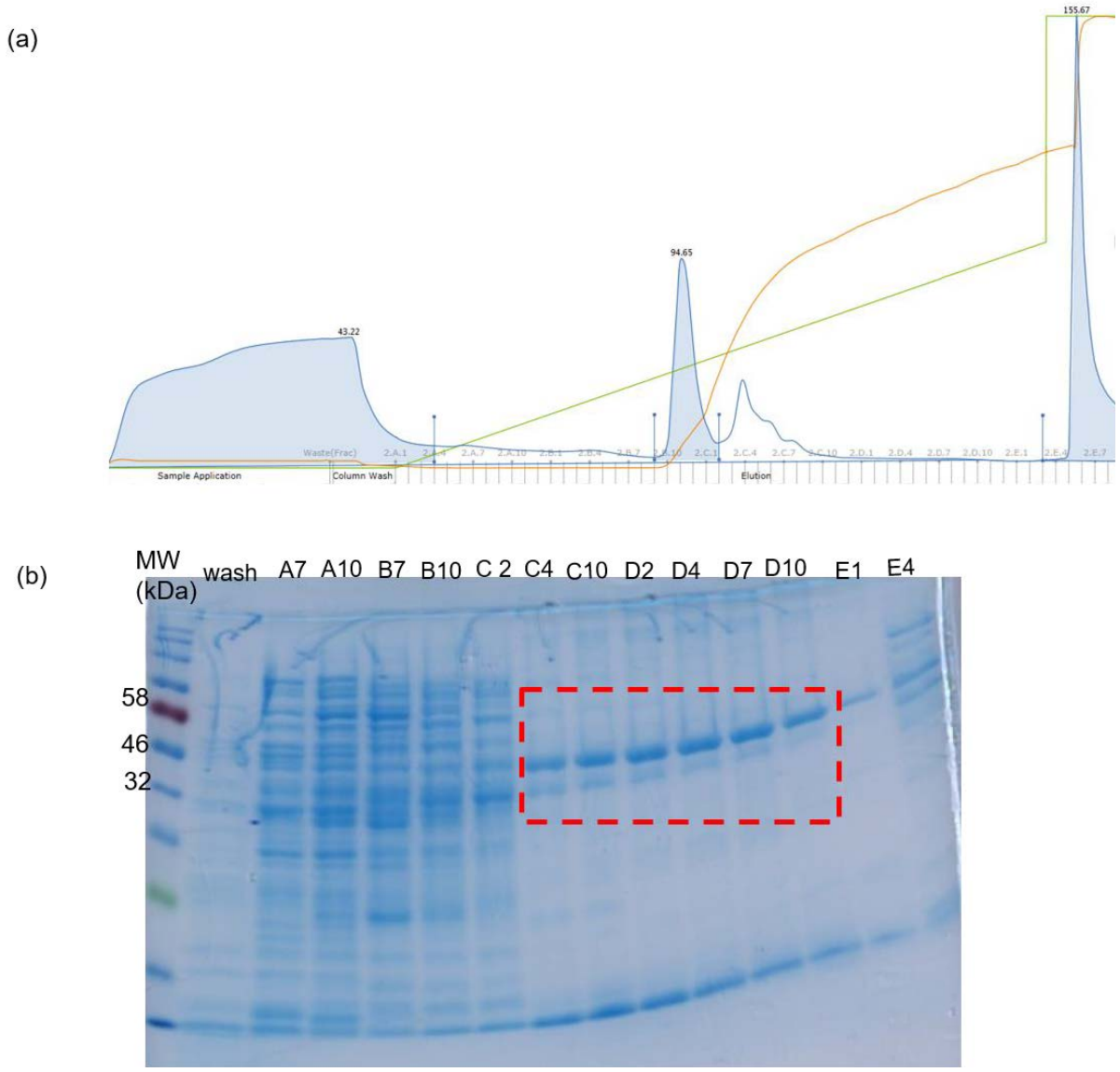

Figure 3.3 Ion exchange Purification of CetZ1

Ion exchange chromatogram and SDS-PAGE analysis of the collected fractions from ion exchange purification. (a) Representation of the chromatogram for CetZ1 ion exchange purification with 10 % glycerol in buffers. The green line represents KCl gradient and the orange line represent the conductivity. (b) SDS-PAGE gel analysis of the collected fractions from the above chromatogram purification; (MW) is the molecular weight standard, (wash) is the column wash and elution fractions (A7-E4) which show successful binding and elution of CetZ1 from the ion exchange column with the presence of an overloaded protein band of ~ 42 kDa, corresponding to the predicted MW of CetZ1. Fractions C4-D10 were pooled together for further purification shown by the red dotted box.

The purified CetZ1 fractions were pooled together and concentrated using a 30 kDa cut off Vivaspin concentrating column (GE Healthcare, Sweden). Gel filtration chromatography was then performed to further improve the purity of protein. As seen in the SDS-PAGE gel in *Figure 3.4*, the gel filtration chromatography was successful in removing some of the impurities from the CetZ1 protein. Interestingly, in the gel filtration of the CetZ1, evidence of potential moderate aggregation was seen (*Figure 3.4.a)*. The peaks representing higher molecular weight species were incompletely separated. The purest fractions were collected and concentrated using Vivaspin concentrating column and stored at -80^{o} until further use. The purified protein concentration was calculated using spectrophotometry with an assumed extinction coefficient and the BCA assay.

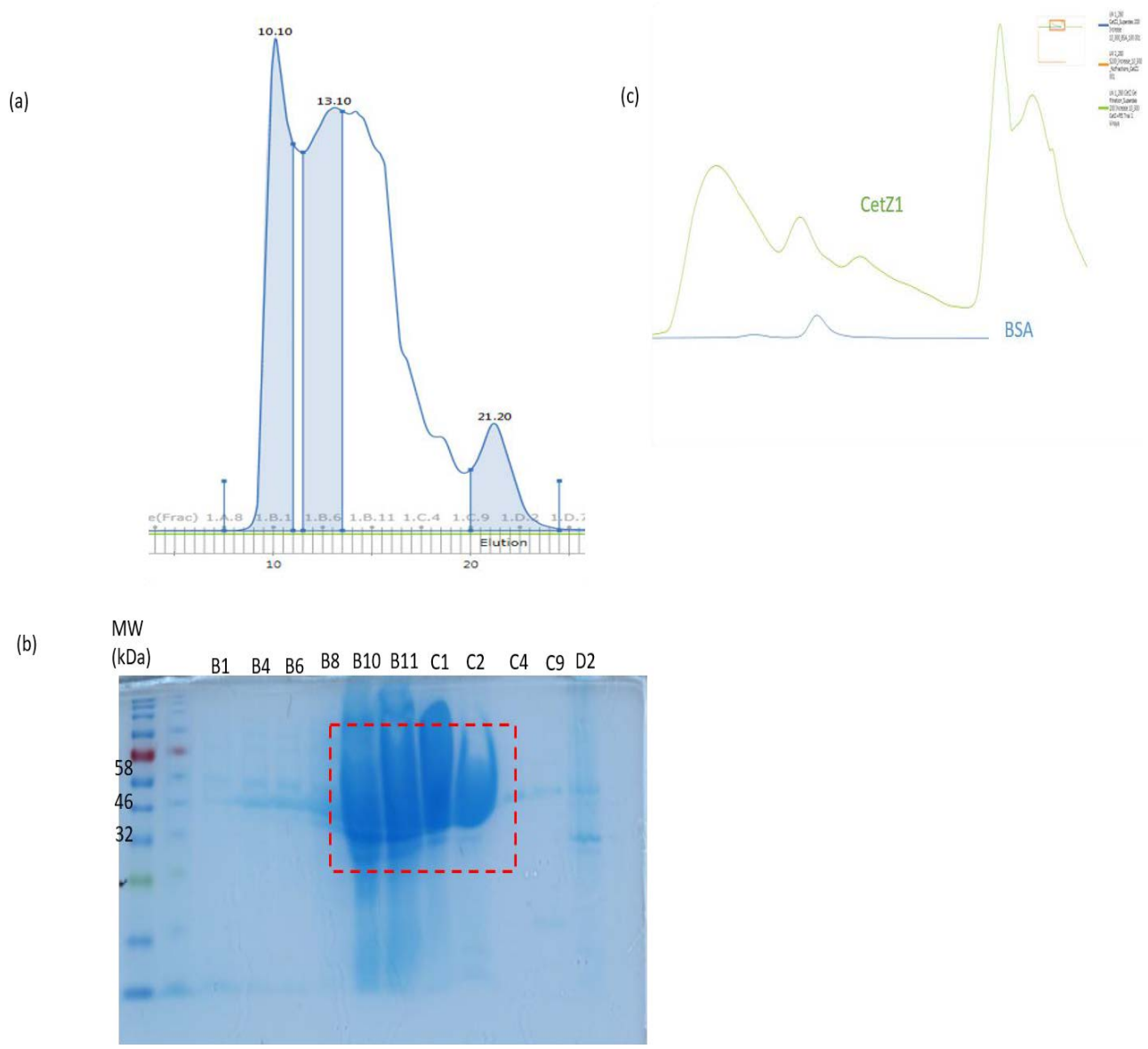

Figure 3.4: Gel filtration purification of CetZ1

Gel filtration chromatogram and SDS-PAGE analysis of the collected fractions from Gel filtration purification with 10 % glycerol in buffers. (a) Representation of the chromatogram for CetZ1 gel filtration purification. (b) SDS-PAGE gel analysis of the collected fractions forms the above chromatogram purification; (MW) is the molecular weight standard, and elution fractions (B1-D2) showed elution of CetZ1 from the gel filtration column with the presence of an overloaded protein band of ~ 42 kDa, corresponding to the predicted MW of CetZ1. Fractions B10-C2 were pooled and concentrated as shown by the red dotted box. (c) Comparison of purified CetZ1 with BSA protein. CetZ1 (42 kDa) peak eluted before BSA (66 kDa) peak in a gel filtration purification, due to aggregation in the CetZ1 protein.

When compared with the BSA protein on a gel filtration column, as a standard to compare the size of protein it was seen that CetZ1 (42 kDa) peaks eluted before the BSA (66 kDa) peak. This may be due to the aggregation of the CetZ1 protein during purification (*Figure 3.4.c)*. Cytoskeletal proteins possess an intrinsic tendency to aggregate together (Rivas & Minton, 2016), and CetZ1 also showed this tendency of aggregation when in high concentration during the protein purification by displaying broader or multiple unresolved peaks. It was considered important to purify CetZ1 in the monomeric form, so that its polymerization dynamics and molecular interactions could be studied from a homogenous starting solution. To do this, the buffers for the protein purification were changed by replacing 10 % glycerol to 20 % glycerol, which helped in preventing the non-specific protein aggregation which were evident from the SDS-PAGE gels. The amphiphilic nature of glycerol helps to interact with the hydrophilic surfaces of the protein, thereby preventing the stabilisation of unwanted intermediate and unfolding of the proteins (Leibly et al., 2012).

Upon measuring the protein concentration, the UV- absorbance spectra were consistent with some nucleic acid contamination. To eliminate this contamination, 0.2 % polyethyleneimine (PEI) was used after the lysis step in an additional purification procedure. An anion exchange column has positively charged resin, negatively charged particles bind to the column. Nucleic acids (DNA & RNA) possess negative charge, and therefore have a high tendency to bind to the column strongly and possibly with a higher affinity than CetZ1. PEI was therefore used to precipitate the DNA & RNA from the cell lysate. This further added in the efficiency of CetZ1 binding to the column.

Addition of 20 % glycerol proved fruitful to ensure stability of the CetZ1 purified protein which was evident from the *Figure 3.5.a* where the purified protein was re-applied on the gel filtration column to see if any aggregates are present showed non-symmetrical peak suggests some impurity/association, but the pooled final protein for the fractions chosen gives a single peak consistent with monomer size and also when compared with BSA, as a standard to compare the size of the protein it was seen that CetZ1 (42 kDa) eluted after the BSA (66 kDa) peak. The final concentration of CetZ1, calculated using the extinction coefficient at 280 nm 21430 /M cm for CetZ1, was found to be 23.75 mg/mL, with approximately 90% purity seen.

Together, these changes to the purification buffers improved the stability of the protein and prevented the non-specific aggregation.

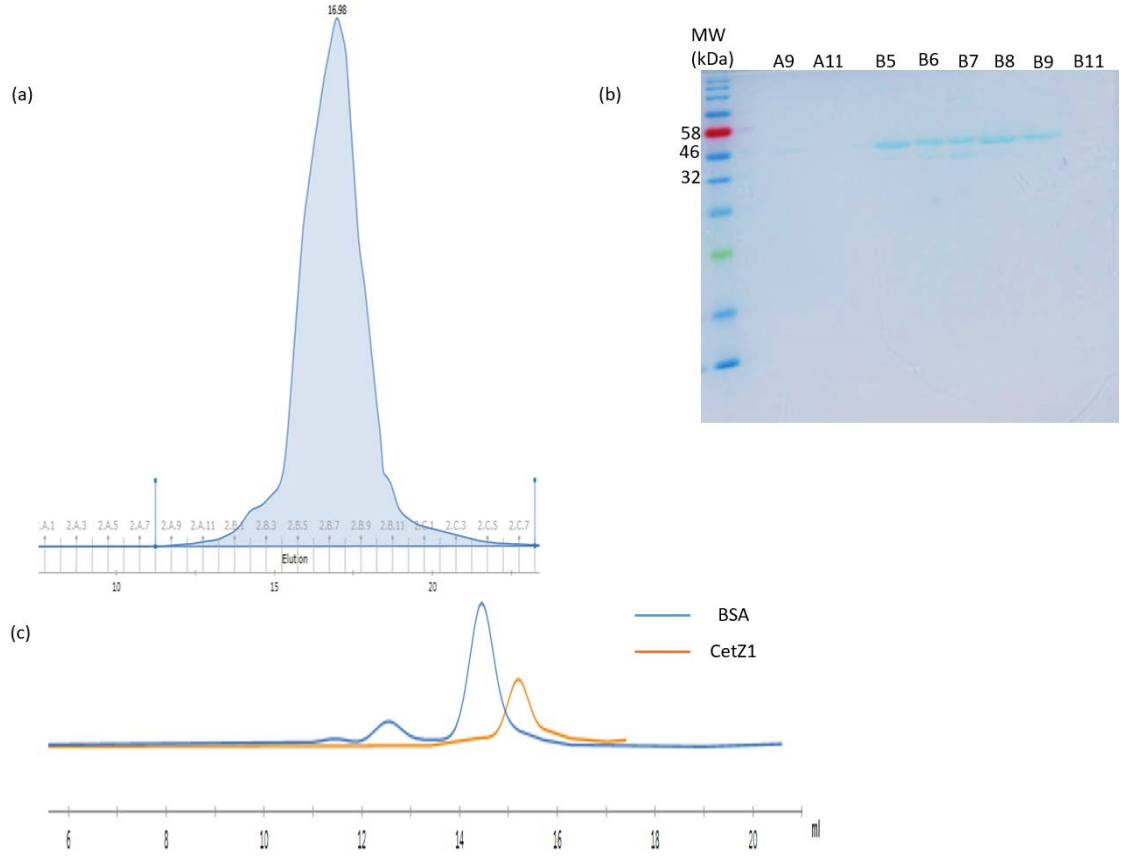

Figure 3.5: Comparison of purified CetZ1 with BSA

(a) A diagnostic gel filtration chromatogram for purified CetZ1 with 20 % glycerol in buffer shows improvement of CetZ1 elution in the monomeric form. (b) SDS-PAGE gel analysis of the collected fractions from the gel filtration chromatogram purification; (MW) is the molecular weight standard, and elution fractions (B5-B9) showed elution of CetZ1 from the gel filtration column with the presence of a protein band of ~ 42 kDa, corresponding to the predicted MW of CetZ1. Fractions B5-B9 were pooled and stored at – 80 ^{o}C for further use (c) Comparison of purified CetZ1 with BSA protein. CetZ1 (42 kDa) peak appears after BSA (66 kDa) peak in a gel filtration purification, consistent with the monomeric form of CetZ1.

3.3.2 Polymerization of CetZ1 analysed by right-angle light scattering assay

Using a right-angle light scattering assay, we investigated CetZ1 polymerization efficiency in real time. The assay works in such a way that highly bundled polymers will produce a larger signal than the unbundled polymers, because the difference in the physical size of the molecules assembled will be different and therefore the difference in the light scattering will be observed (P. J. Buske & Levin, 2012). The delta light scattering, which is the change in light scattering after the addition of GTP to the reaction is shown in the result, plotted as a function of time (*Figure 3.6*).

For polymerization assays, buffer conditions that have previously shown to facilitate tubulin polymerization *in vitro* were used, as preliminary studies had shown that these can be used to detect CetZ1 polymerization (De Silva, 2019). A 1,4-Piperazineethanesulfonate (PIPES) buffer (80 mM PIPES, pH 6.9, 2mM $MgCl_2$ and 0.5 mM EGTA) has been commonly used for tubulin polymerization *in vitro*. The concentration of PIPES buffer changes the degree if polymerization in tubulin; in a study by Waxman *et al*, the highest tubulin polymerization was achieved by using 800 mM PIPES at pH 6.9. (Waxman, Del Champo, Lowe, & Hamel, 1981) (De Silva, 2019).

Similarly, it was observed that CetZ1 can polymerize in 800mM PIPES buffer at pH 7.3 with 3 M KCl (De Silva, 2019). Therefore, in this study the same conditions were applied to study the CetZ1 and mutant polymerization (as stated in section 3.2.5). The light scattering assay showed that with the addition of 2 mM GTP, CetZ1 polymers assembled rapidly, reaching a peak and then transitioning to an approximate steady state (*Figure 3.6)*. To explore the GTP dependence of CetZ1 polymerization, controls such as 2 mM GDP instead of GTP and BSA instead of CetZ1 were compared to the CetZ1 polymerization. No scattering was observed in the controls, showing that the CetZ1 has a GTP dependent polymerization.

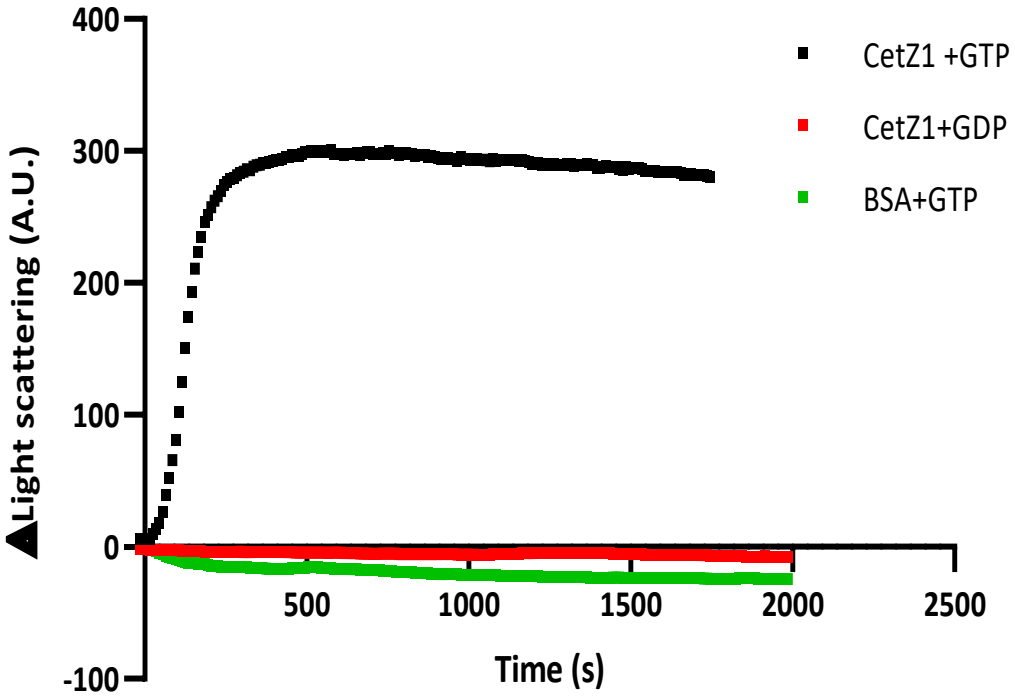

Figure 3.6: Analysis of CetZ1 polymerization by right angle light scattering

Dynamic behaviour of CetZ1 was observed by the increase in the light scattering after the addition of the GTP. Polymerization was initiated by the addition of GTP (final concentration 2 mM) to 12 µM CetZ1 in 800 mM PIPES buffer pH 7.3, 3 M KCl and 10 mM $MgCl_2$. Measurements were collected every ten seconds at room temperature. As a control GDP was added instead of GTP and BSA instead of CetZ1. The X axis indicates the time in seconds and the Y axis shows the delta light scattered during the polymerization.

3.3.3 Morphologies of CetZ1 structures under transmission electron microscopy

The morphology of CetZ1 polymers formed in presence and absence of GTP were examined by negative stain electron microscopy using transmission electron microscopy. The samples were prepared with 12 µM CetZ1 in 800 mM PIPES buffer, pH 7.3, 3M KCl. GTP was added to form the polymers and GDP was used as a control.

CetZ1 assembled into obvious GTP-dependent filaments in the PIPES buffer and the filaments where then placed on the EM grid to be visualized under electron microscopy (Figure 3.7 a).

The structure in the negative stain image suggests a straight polymer structure (Figure 3.7 b), and some were bundled together (Figure 3.7 e). The results were in accord with the CetZ1 right angle light scattering assay. In the presence of GDP, no filaments were observed on the grid (Figure 3.7 f). These results suggest that CetZ1 polymers are regulated by GTP.

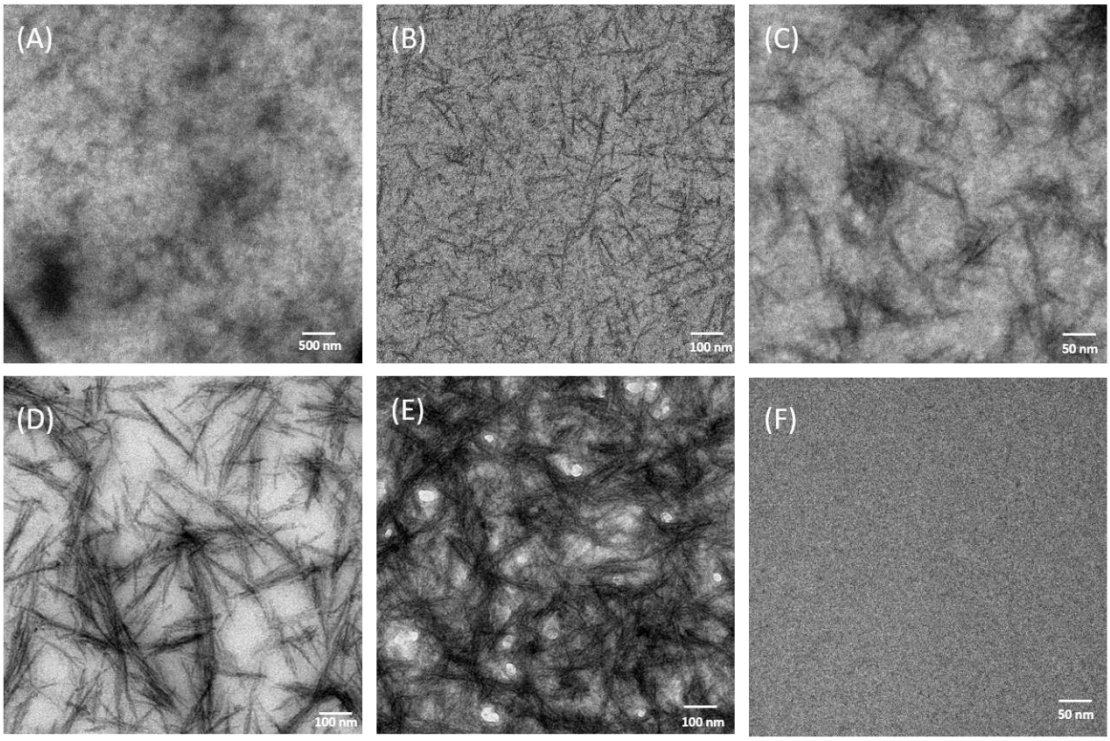

Figure 3.7: Structure of CetZ1 polymers visualized by transmission electron microscopy

(A-F) Images of filaments observed after polymerization of 12 µM CetZ1 protein in 800 mM PIPES buffer pH 7.3, 3M KCl polymerized with 2 mM GTP/GDP and stained with 2 % uranyl acetate. (A) View of negative stain grid showing dense polymers. (B-C) CetZ1 in buffer with GTP displaying linear filaments. (D-E) CetZ1 in buffer with GTP displaying dense bundles of polymers. (f) CetZ1 in buffer with GDP as a control with no filaments formed.

The morphology of CetZ1 filaments was also studied at different time points of incubation after the addition of GTP during polymer formation to see the different filament length and bundling properties of CetZ1. Firstly, after polymerization with GTP the samples were quickly loaded on to the grid without any specific incubation period (*Figure 3.8 a)*. The polymers were not as clustered as seen for other incubation periods. Samples loaded after 10 and 20 min of

incubation appeared to show greater polymer length and density and were often bundled together and stacked upon each other (*Figure 3.8 b-c)*.

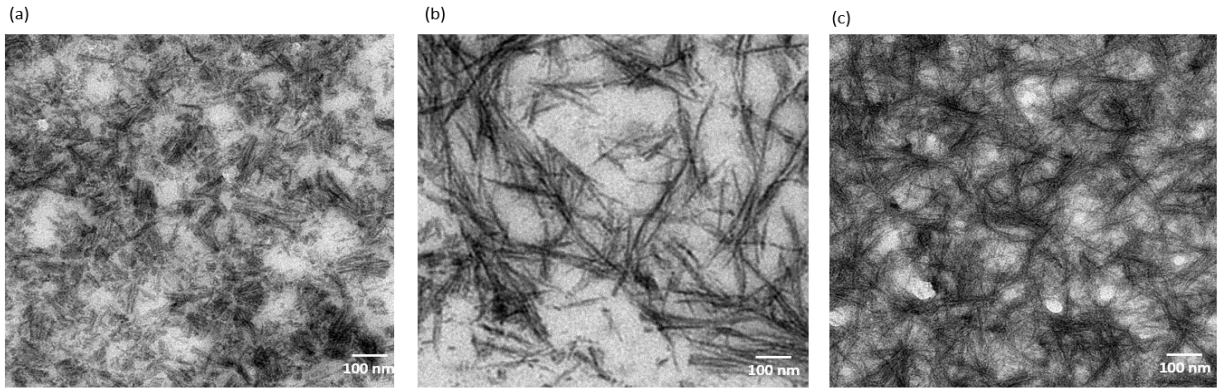

Figure 3.8: Structure of CetZ1 polymers visualized by transmission electron microscopy at different time point

(a) Image of short CetZ1 polymers seen immediately after adding GTP to the CetZ1 in PIPES buffer with no incubation time. (b) Image of CetZ1 polymers in PIPES buffer with 10 min of incubation after adding GTP. (c) Image of long, dense and bundled CetZ1 polymers after 20 min of incubation.

3.3.4 Purification of CetZ1 point mutants

CetZ1 point mutants that affected CetZ1 function and localization *in vivo* were identified and were selected for the *in vitro* studies. The selected CetZ1 mutants were E218A, G108S, M-loop, R276E & K277E (double mutant), E188G and C-terminal tail mutant (*Figure 3.1.a)*. Investigating *in vitro* polymer dynamics of these point mutants would further highlight the important regions of CetZ1 structure that may be responsible for the function and molecular interactions of CetZ1. CetZ1 itself displayed a highly dynamic, filament- like localisation *in vivo* during morphogenesis suggesting that CetZ1 cytoskeletal structure formation is needed for its function (De Silva, 2019).

The protein purification procedure for all the CetZ1 point mutants was like that of wild-type CetZ1. SDS-PAGE results revealed successful over-production of CetZ1 point mutants, as

evident by a protein of high abundance at ~ 42 kDa in the post induction cell lysate *(Figure 3.9)*.

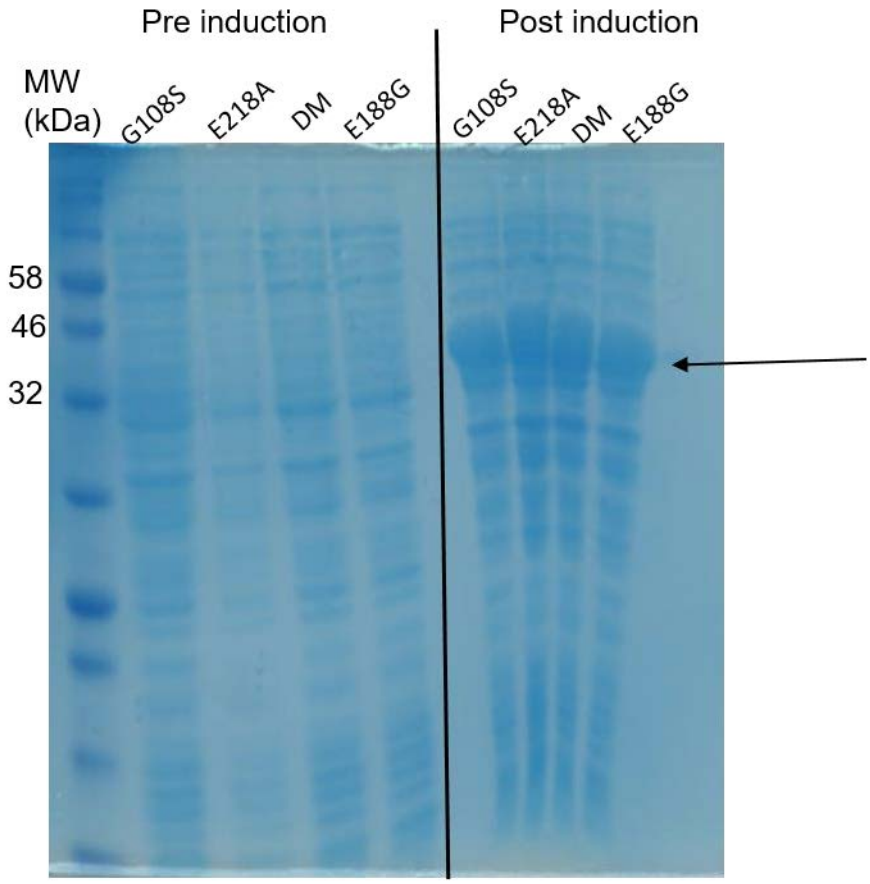

Figure 3.9: CetZ1 mutant over expression

SDS-PAGE analysis from whole cell lysates fractions generated from transformed cultures. The gel demonstrated successful over-expression for CetZ1 point mutant (G108S, E218A, double mutant and E188G), as evident by a protein band of high abundance at ~ 42 kDa post indication indicated by arrow. This band was absent from the cell lysates pre-induction. MW is the protein molecular weight standard.

Next, CetZ1 point mutants were purified using anion exchange chromatography and gel filtration chromatography with 10% glycerol in buffers as done for wild-type CetZ1. However,

similar to wild-type CetZ1 the mutant protein showed aggregation therefore, to resolve this problem we added 20 % glycerol to all the chromatography buffers instead of 10 % and re-purified all the mutant CetZ1 proteins again. Since glycerol helps in preventing non–specific binding of protein to each other thereby avoiding the oligomerization seen in the point mutants. The CetZ1 mutant proteins were purified as described in the methods section 3.2.3.1. The CetZ1 point mutants were successfully bound to and purified to ~80% pure from the ion exchange column as determined from the SDS-PAGE gel. Like the wild-type CetZ1 protein, numerous impurities evident from the SDS-PAGE (*Figure 3.10.b)* both above and below the band of interest at the corresponding molecular weight of CetZ1. Gel filtration was conducted subsequently for further purification of the point mutants. The gel filtration purification was successful in removing some unwanted impurities in the protein samples (*Figure 3.10.d).*

(a)

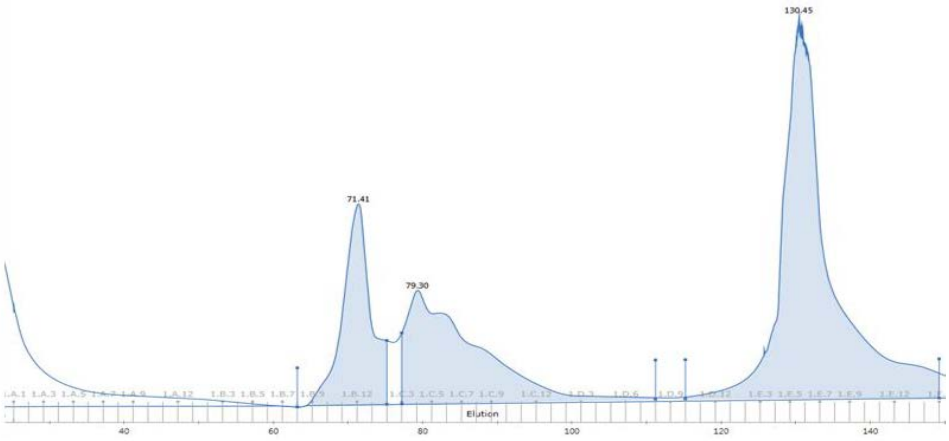

(b)

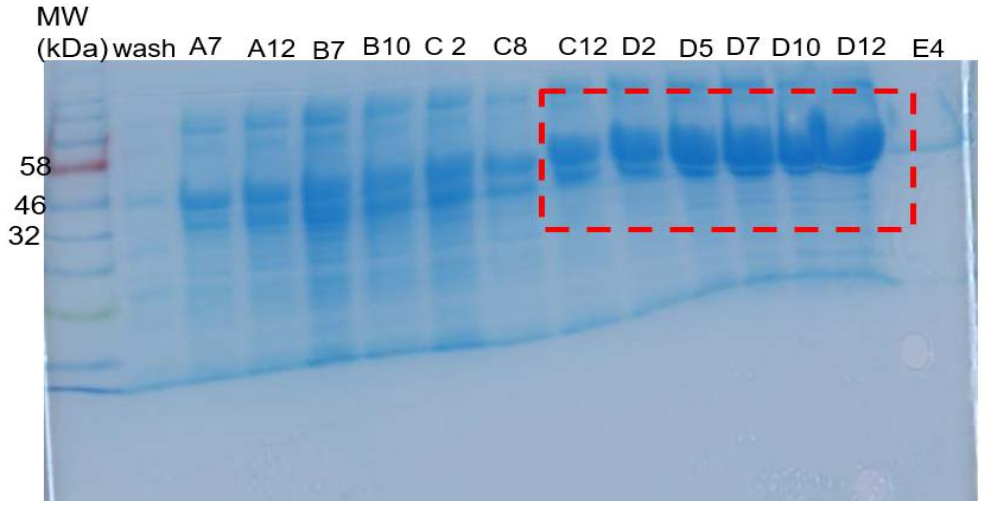

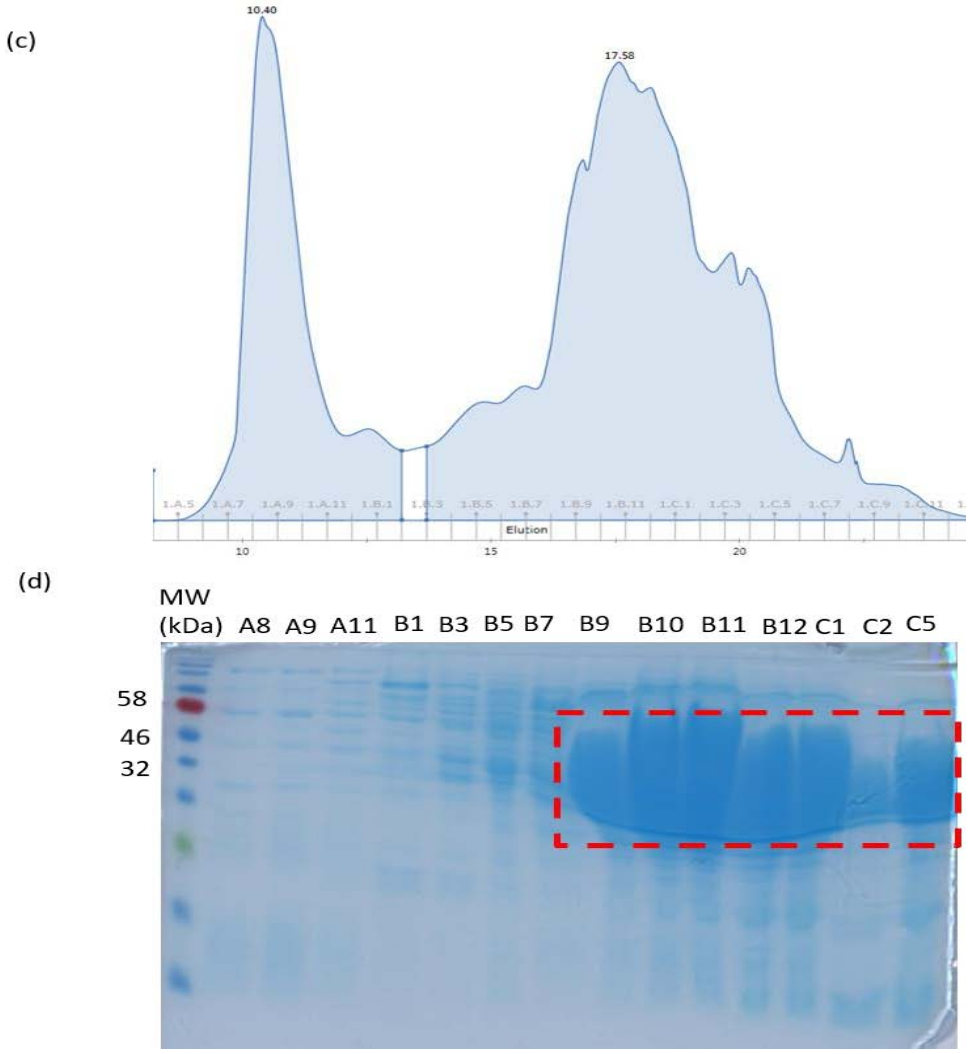

Figure 3.10 Purification of the CetZ1.E218A mutant

Ion exchange chromatogram and SDS-PAGE analysis of the collected fractions from ion exchange purification. (a) Represent the chromatogram for CetZ1.E218A mutant ion exchange purification. (b) SDS-PAGE gel analysis of the collected fractions from the above chromatogram purification; (MW) is the molecular weight standard, (wash) is the column wash. Elution fractions (A7-E4) showed successful binding and elution of CetZ1.E218A from the ion exchange column with the presence of an overloaded protein band of ~ 42 kDa, corresponding approximately to the predicted MW of CetZ1. Fractions C12-D12 were pooled together for further purification shown by the red dotted box. (c) Representation of the chromatogram for CetZ.E218A gel filtration purification. (d) SDS-PAGE gel analysis of the collected fractions from the above chromatogram purification; (MW) is the molecular weight standard. Elution fractions (B9-C5) showed elution of CetZ1 from the gel filtration column with

the presence of an overloaded protein band of ~ 42 kDa, corresponding to the predicted MW of CetZ1. Fractions B9-C5 were pooled and concentrated as shown by the red dotted box.

During gel filtration chromatography all the mutants displayed additional apparent higher oligomeric peaks compared to the monomeric wild-type CetZ1 (supplementary data 1). This may be due to the mutations in the CetZ1 protein structure that might have inflicted change in the normal monomeric conformation in the mutant CetZ1 leading to increase unspecific oligomerization compared to the wild-type CetZ1.

3.3.5 Polymerization of CetZ1 point mutants by right-angle light scattering assay

Using right-angled light scattering I investigated the effect of point mutations on the polymerization ability of CetZ1, since light scattering signal corresponds to the average polymer size. Polymer and polymer bundles scatter more light than smaller monomer structures, although a limitation of right-angle light scattering is that it cannot distinguish between a large number of relatively small structures and fewer large structures. Similar conditions as that of wild-type CetZ1 (as stated in section 3.2.5) were used to carry out light scattering for all the point mutants. For all the mutation, light scattering intensities were compared to the wild-type CetZ1 light scattering results (*Figure 3.11*). To explore the GTP-dependence of CetZ1 mutant polymerization controls such as 4 µL of 2 mM GDP was used instead of GTP, no scattering was observed in the controls.

(A)

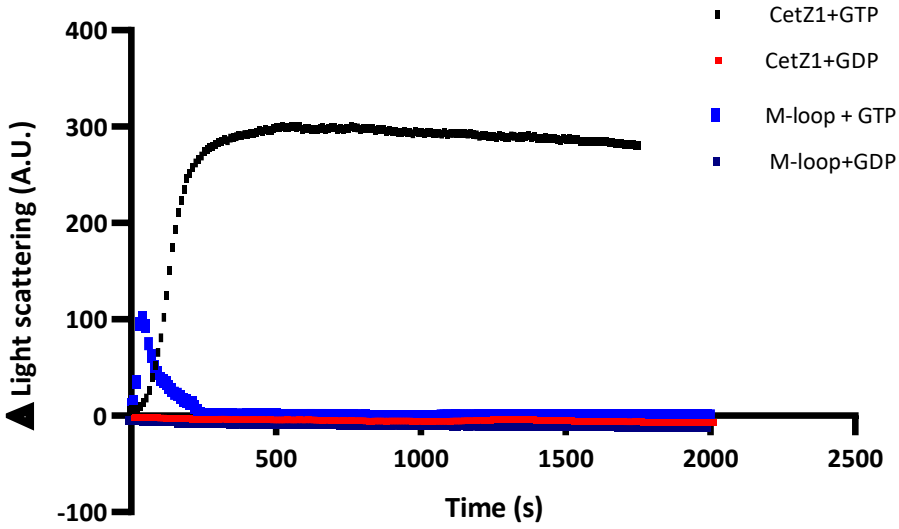
CetZ1+GTP
CetZ1+GDP
M-loop + GTP
M-loop+GDP
Light scattering (A.U.)
400
300
200
100
0
-100
500
1000
1500
2000
2500
Time (s)

(B)

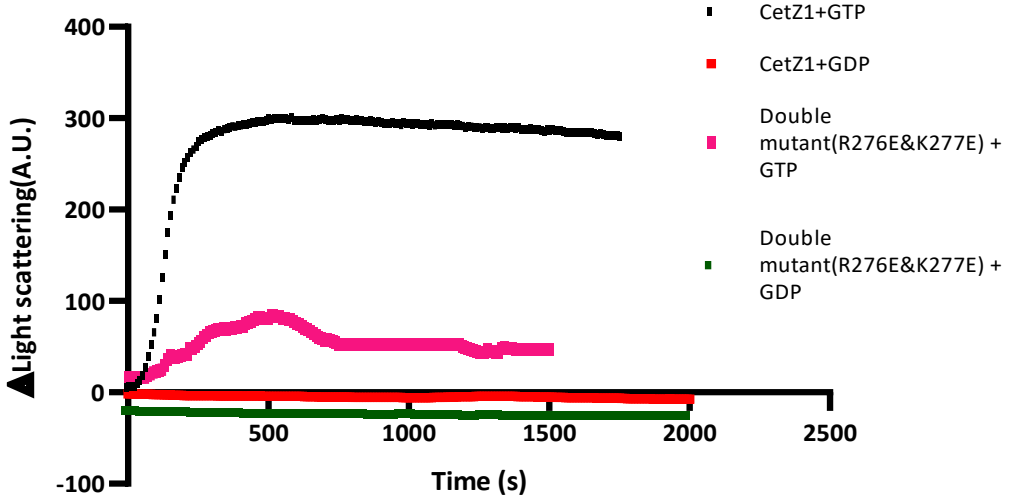
CetZ1+GTP
CetZ1+GDP
Double mutant(R276E&K277E) + GTP
Double mutant(R276E&K277E) + GDP
Light scattering(A.U.)
400
300
200
100
0
-100
500
1000
1500
2000
2500
Time (s)

(C)

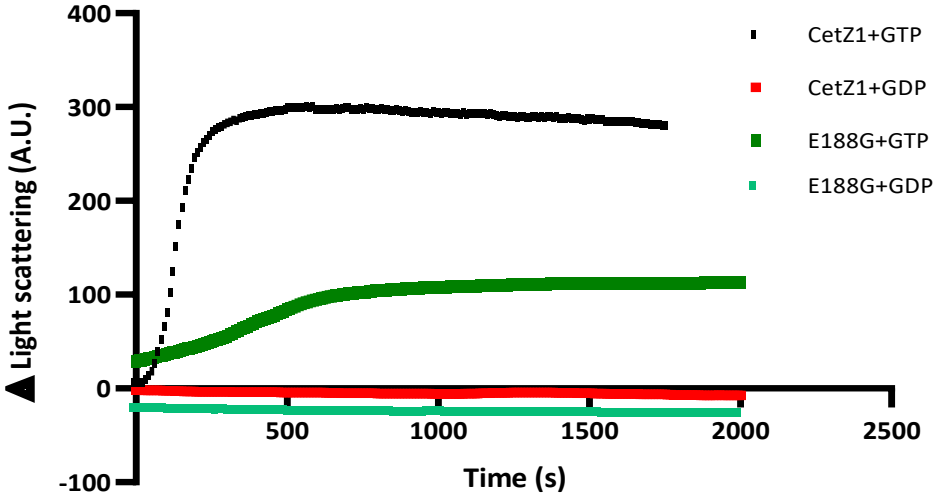
CetZ1+GTP
CetZ1+GDP
E188G+GTP
E188G+GDP
Light scattering (A.U.)
400
300
200
100
0
-100
500
1000
1500
2000
2500
Time (s)

(D)

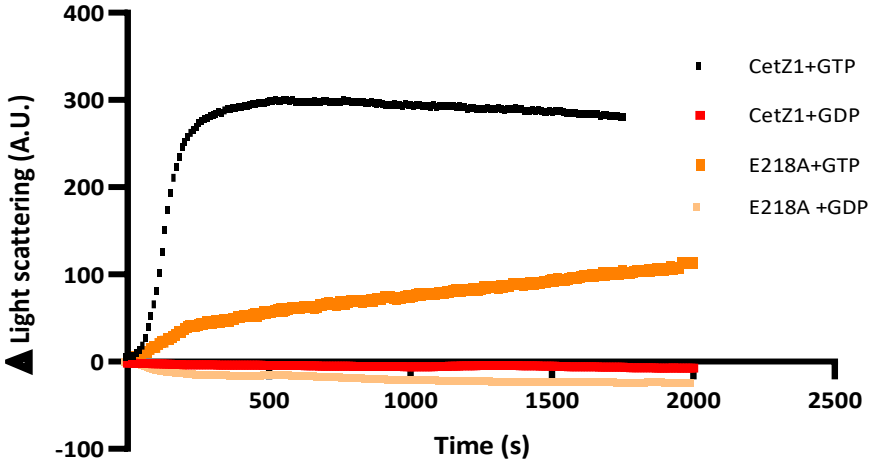
400
300
200
100
0
-100
Light scattering (A.U.)
500
1000
1500
2000
2500
Time (s)
CetZ1+GTP
CetZ1+GDP
E218A+GTP
E218A +GDP

(E)

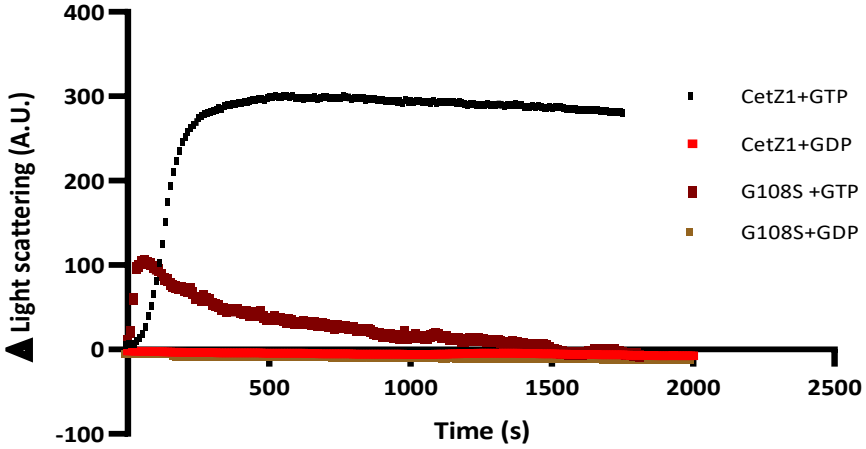
400
300
200
100
0
-100
Light scattering (A.U.)
500
1000
1500
2000
2500
Time (s)
CetZ1+GTP
CetZ1+GDP
G108S +GTP
G108S+GDP

(F)

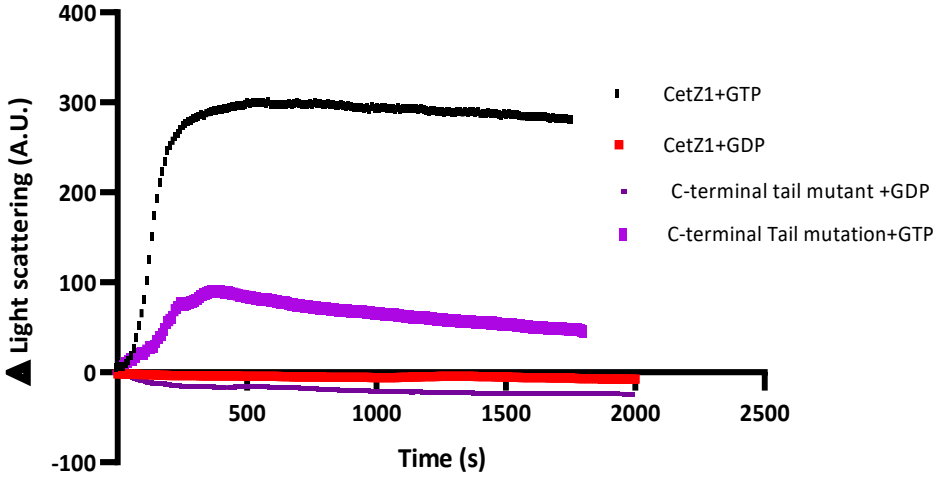
400
300
200
100
0
-100
Light scattering (A.U.)
500
1000
1500
2000
2500
Time (s)
CetZ1+GTP
CetZ1+GDP
C-terminal tail mutant +GDP
C-terminal Tail mutation+GTP

Figure 3.11: Analysis of CetZ1 point mutant polymerization by right angle light scattering

Polymerization assembly of CetZ1 point mutants was observed by the increase in the light scattering after the addition of the GTP. Polymerization was initiated by the addition of GTP (final concentration 2 mM) to 12 µM point mutants in 800 mM PIPES buffer pH 7.3, 3 M KCl and 10 mM $MgCl_2$. Data was collected every ten seconds at room temperature. As a control GDP was used instead of GTP. Polymerization assembly of (a) M-loop; (b) double mutant; (c) E188G; (d) E218A; (e) G108S; (f) C-terminal tail mutant. All the mutant polymerization assembly was compared to wild-type CetZ1 polymerization.

For the CetZ1.M-loop mutation, it was observed that the increased in light scattering was seen when GTP was added which indicate the polymerization of M-loop protein molecules, but polymerization was quickly reduced and then disassembly of polymers was seen, suggesting that M-loop appears to be important for polymer stability. (*Figure 3.11.A)*.

The double mutant, R276E&K277E, showed initiation in polymerization after the addition of GTP but with time the signal decreased in intensity then remained constant, (*Figure 3.11.B)*.

For the CetZ1.E188G mutation, the initiation of polymerization was observed after the addition of GTP and the intensity increased to some level with time which later remained constant (*Figure 3.11.C)*. All the mutations that effected the lateral interaction, including M-loop, double mutant and E188G, showed less average peak light scattering value than wild-type CetZ1 suggesting that there was consistent reduction in the average number of filaments lesser light scattering intensity was seen.

The CetZ1.E218A mutant that is hypothesised to affect the GTPase activity displayed a continuous increase in polymerization at a slower rate than the wild-type CetZ1 (*Figure 3.11.D).* This behaviour suggests that the mutation might affect the rate of polymerization but does not completely disrupt the polymerization efficiency of E218A.

Another mutation, CetZ1.G108S, that is also hypothesised to affect longitudinal interaction by disrupting the GTP binding activity, displayed initiation of polymerization upon addition of GTP, but the polymeric structure became destabilised as indicated by the decrease in signal. The reduced polymerization is presumably due to the defect near to the GTP binding pocket

which therefore reduces the GTPase activity, making the polymers to disassemble quickly (*Figure 3.11.E).*

The mutation that affects the C-terminal tail showed initiation of polymerization after the addition of GTP, but then disassembly of polymers occurred slowly, which was evident through the decreased in the intensity. The C-terminal tail mutation displayed a similar polymerization trend to wild-type CetZ1 but was 3-fold less than that of the wild-type CetZ1 (*Figure 3.11 F)*.

All the mutations showed decreased intensity of light scattering compared to wild-type CetZ1, indicating that each mutation impeded the polymerization ability of CetZ1, presumably due to reduced turnover of subunits within the protofilaments of CetZ1 mutants.

3.3.6 Morphologies of CetZ1 point mutants under transmission electron microscopy

We examined the morphology of CetZ1 mutant polymers formed in the absence and presence of GTP by negative stain electron microscopy using TECAN T20 transmission electron microscope which allowed direct visualization of CetZ1/mutant structures. Like the wild-type CetZ1, the samples were prepared with 12 µM of CetZ1 mutant protein in 800 mM PIPES buffer, pH 7.3, 3M KCl. GTP was added to the above mixture to form the polymers and GDP was used as a control.

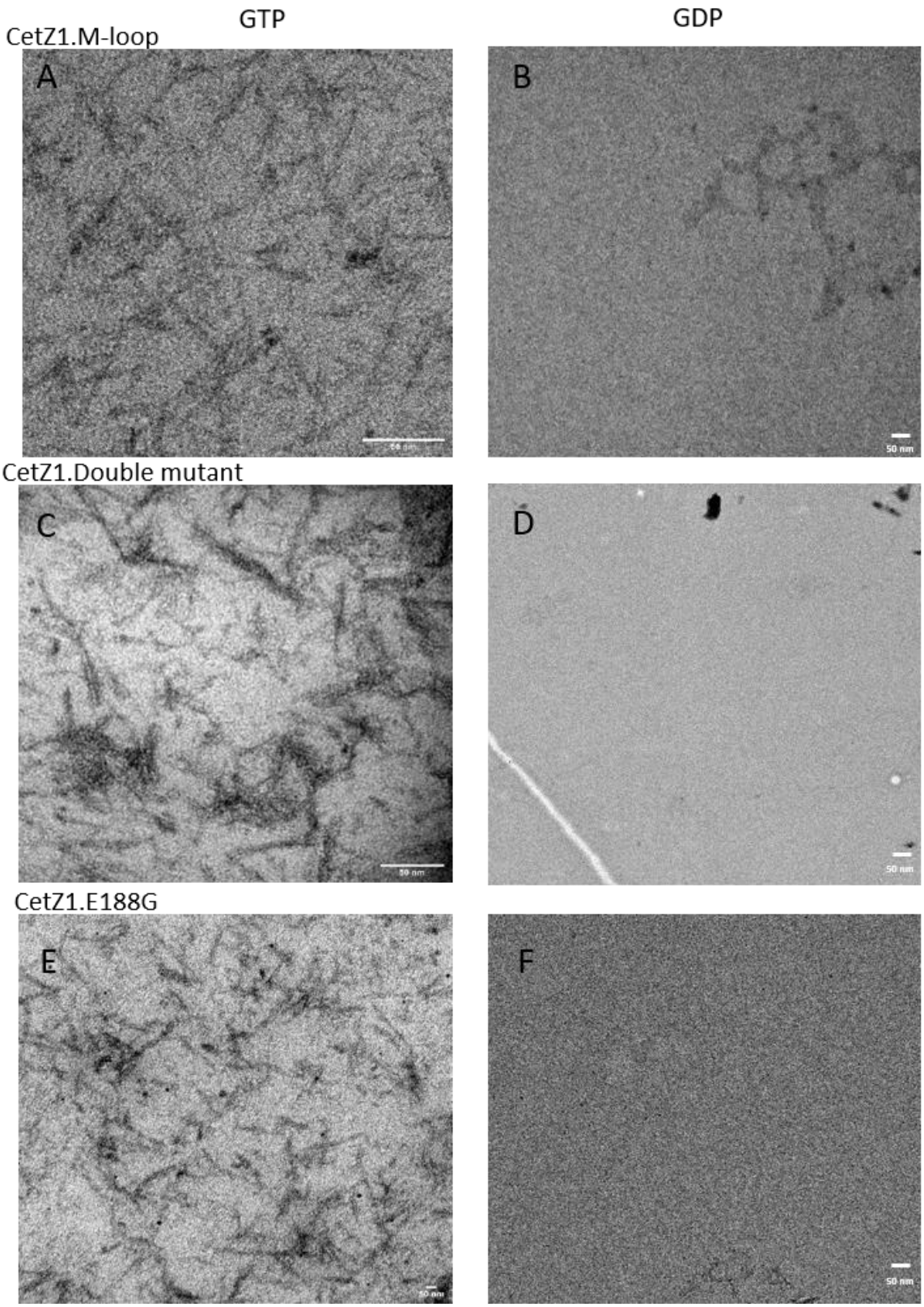
GTP
GDP
CetZ1.M-loop
A
B
CetZ1.Double mutant
C
D
CetZ1.E188G
E
F

GTP

GDP

CetZ1.E218A

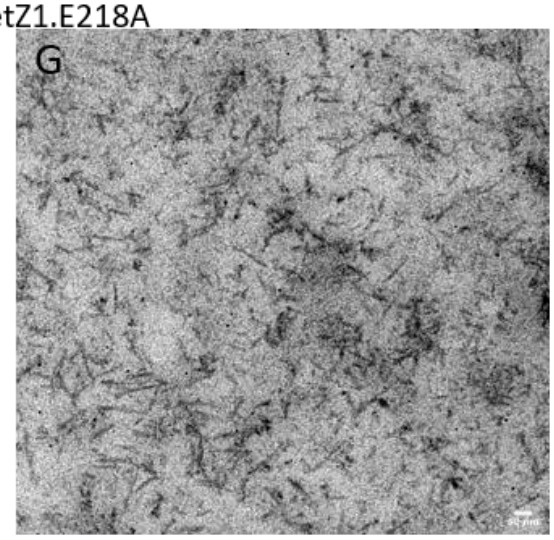

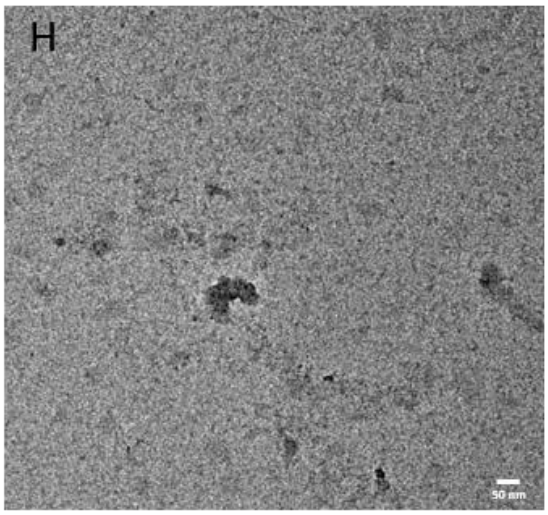

CetZ1.G108S

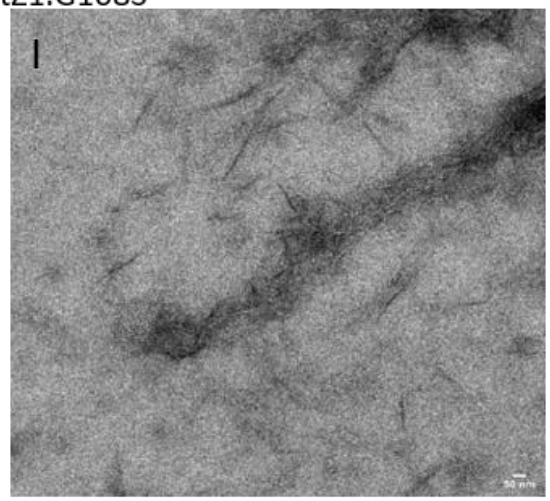

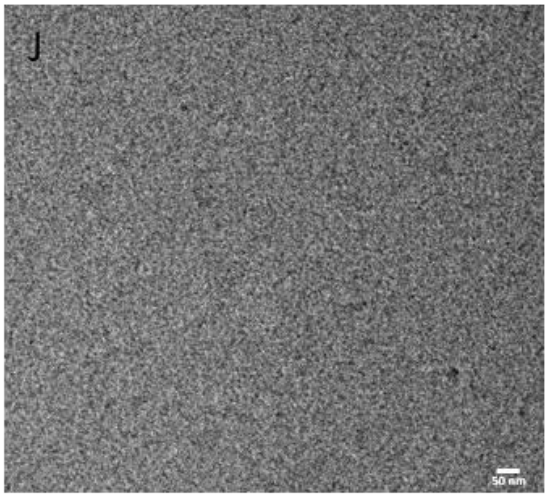

CetZ1.CTTM

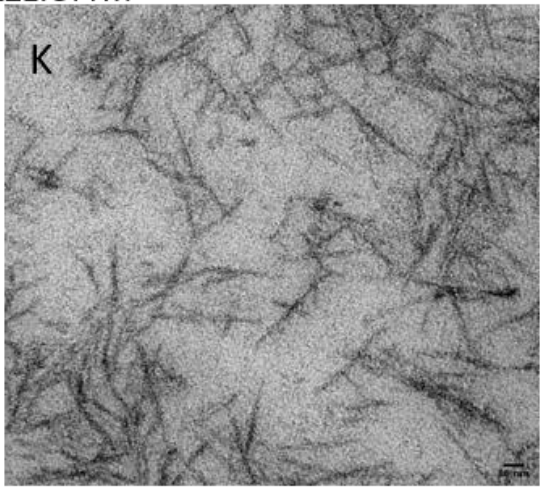

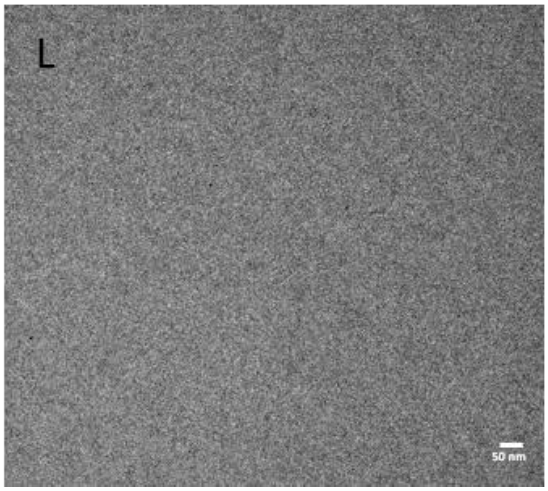

Figure 3.12 Structure of CetZ1 mutant polymers visualized by transmission electron microscopy

Images of 12 µM CetZ1 point mutants in 800 mM PIPES buffer pH 7.3, 3M KCl polymerized with 2 mM GTP/GDP and stained with 2% uranyl acetate. (A-C) Mutant in the C-terminal domain predicted to affect the lateral interaction, (A) CetZ1.M-loop polymerized with 2 mM GTP and in next panel (B) as a control GDP was used instead of GTP. (C) CetZ1.Double mutant polymerized with 2 mM GTP. (E) CetZ1. E188G. (G-J) Mutation affecting the longitudinal interaction were polymerized in 2mM GTP, CetZ1.E218A and CetZ1.G108S respectively. (K) CetZ1. C-terminal tail mutant polymerized in 2 mM GTP. (B, D, F, H, J&L) As a control GDP was used. Scale bar 50 nm.

The CetZ1.M-loop mutant formed single–stranded unbundled filaments (*Figure 3.12 a)*. In comparison to the wild-type CetZ1 filaments, the M-loop mutant does not show high propensity to from stable lateral interactions. CetZ1.M-loop filaments were shorter in length than the wild-type CetZ1, averaging 75.51 ± 75.28 nm in length versus 144.8 ± 28.48 nm for wild-type CetZ1 (*Figure 3.13)*. To confirm the right-angle light scattering results for CetZ1.M-loop mutant, 300 sec of incubation after the addition of GTP were observed under the TEM and still, no filaments were seen.

The CetZ1.Double mutant produced single-stranded unbundled filaments (*Figure 3.12 b)*. CetZ1.Double mutant filaments averaged 44.55 ± 21.98 nm in length, significantly shorter than wild-type CetZ1 filaments. CetZ1.E188G produced short filaments that were singular, and no bundling was observed (*Figure 3.12 c)*. CetZ1.E188G filaments were shorter (33.41 ± 14.10 nm versus 144.8 ± 75.28 nm) than the wild-type CetZ1. Altering the residues involved in the lateral interaction of the CetZ1 protein structure, therefore significantly affect the filament length and they were less clustered as compared to wild-type CetZ1. All three mutants did not display any bundling of filaments.

The E218A mutation that disrupts the GTPase activity by affecting the longitudinal interaction of CetZ1 displayed very short, single-stranded filaments, whereas the CetZ1.G108S mutant produced single stranded structure of filaments and were very few in number as compared to that of wild-type CetZ1 filaments. Residues in the T7 loop provide the active site for the GTPase activity, which is largely dependent on polymerization as one subunit provides

catalytic residues to the active site of the next subunit. While the E218A and G108S mutations showed polymerization, the GTPase activity was comprised despite retaining some residual activities, and therefore short and few filaments were observed in the TEM analysis of these mutants (*Figure 3.12 d & e).* CetZ1.E218A produced the shortest filaments that measure 30.68 ± 13.24 nm, whereas CetZ1.G108S average filament measured 56.70 ± 29.72 nm as compared to that of wild-type CetZ1.

The mutation made in the C-terminal tail of CetZ1 displayed single-stranded filaments, however, no bundling was observed (*Figure 3.12 f)*. CetZ1.CTTM filaments were typically somewhat shorter 71.78 ± 30.28 nm than the wild-type CetZ1 filaments. As a control, GDP was used for all mutants, and in this condition no filaments were observed on the grid. The results for the CetZ1 mutation by TEM were in accord with the right-angle light scattering assay.

Table 6.1 represent the summary of the results presented in section 3.3 for the *in vitro* assay done in this study for wild-type CetZ1 and mutants.

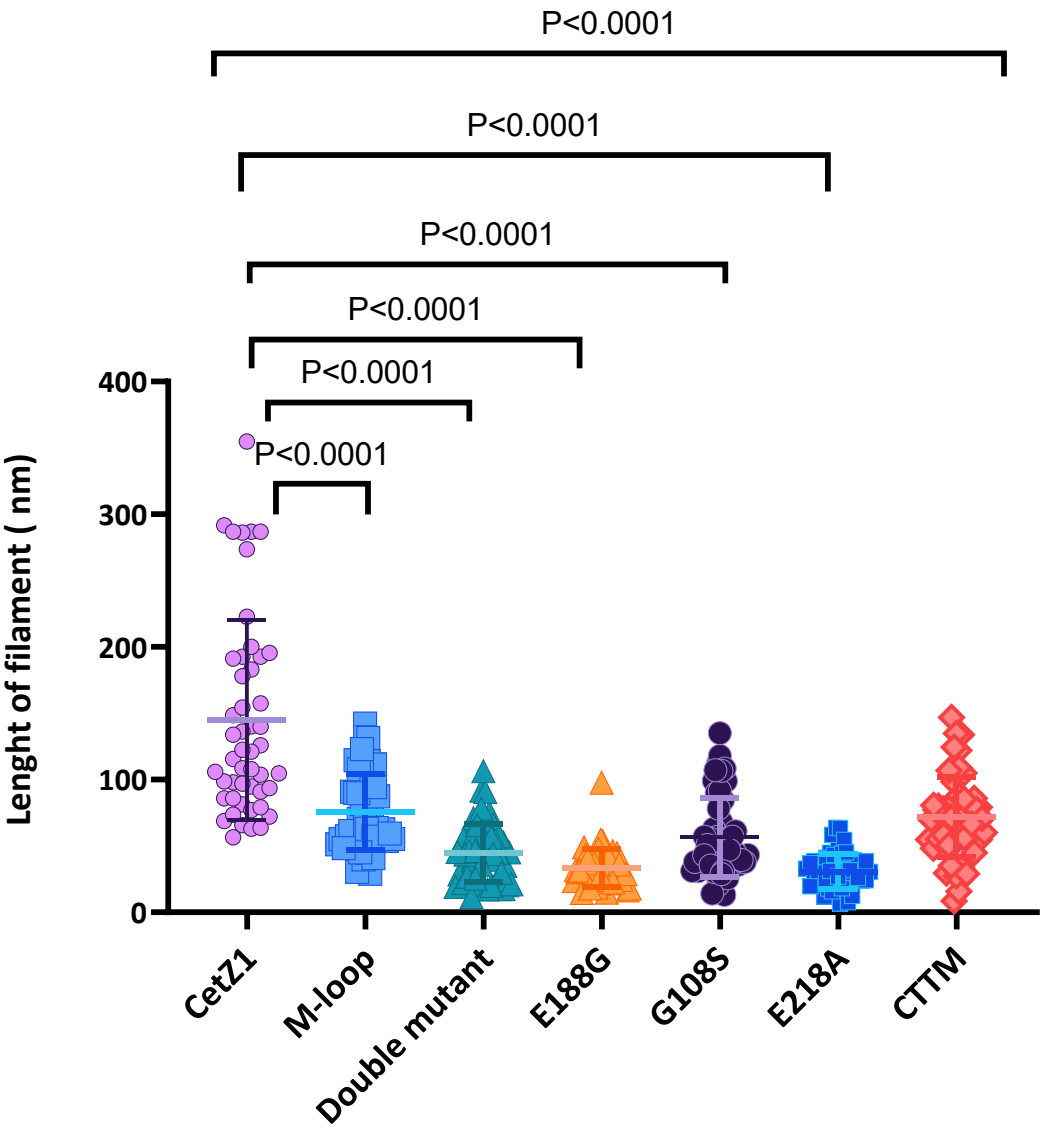

Figure 3.13: Filament length of CetZ1 and mutant polymers

Scatter plots shown for filament length in nm for CetZ1 and mutants polymers. Error bars represent the mean filament length ± SD. More than 50 filaments each were measured manually for CetZ1 and CetZ1 mutants. Each mutant is represented by different shape and colour and compared to the wild-type CetZ1 shown in purple colour circles. Mann-Whitney rank test was used to statistically analyse the data for significant changes in the filament length.

3.3.7 Sedimentation assay of CetZ1 and mutants

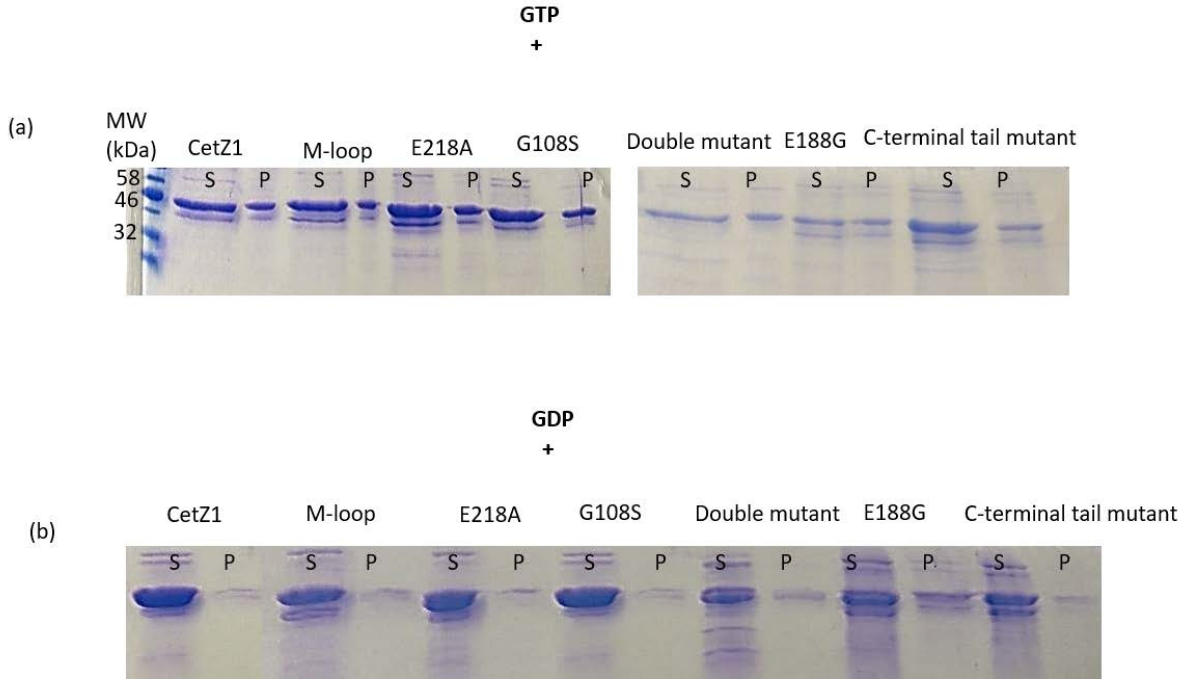

Fig 3.14 Quantification of CetZ1 and mutant polymerization by sedimentation.

12 µM CetZ1 and mutant were polymerized in the presence of 2 mM GTP/GDP in PIPES buffer at pH 7.3 and 3 M KCl. (a) Representative results from Coomassie stained gels revealed that CetZ1/mutant sedimented in the presence of GTP. (S) Supernatant, (P) pellet fractions from the experiments. (b) Coomassie stained gels for CetZ1 / mutants in the presence of GDP, where no sedimentation was seen in the pellets

The polymerization was also explored by performing co-pelleting/sedimentation assay. The sedimentation assay was used to investigate whether the wild-type CetZ1 or mutant induced polymerization in the presence of GTP. Through ultracentrifugation, the larger polymers pellet down and can be identify by SDS-PAGE. At the high velocity only large structures of

CetZ1 were pelleted, for example the large bundles/tubules of CetZ1 filaments. (*Figure3.14.a)* SDS-PAGE analysis revealed increasing amount of CetZ1/mutant in the pellet of the reaction containing GTP. For control GDP was used for a specific sedimentation as seen in the SDS-PAGE analysis, suggesting that CetZ1/mutant polymerize only in the presence of GTP and not GDP (*Figure3.14.b)*.

3.3.7 Quantification of inorganic phosphate by Malachite green assay

The GTPases activity of CetZ1 was measured using a colorimetric assay for free phosphate that used the dye malachite green which forms the green complex formed between malachite green, molybdite and free orthophosphate. The rapid colour formation absorbance from the reaction was measured at 620 nm. The change in absorption at 620 nm allows quantification of the Pi consumed in the reaction. Since the buffer itself gives high absorbance with malachite green, the buffer values were subtracted from the protein absorbance values. CetZ1 protein (12 µM) was polymerized in 800 mM PIPES buffer, pH 7.3, 3 M KCl and 1 mM GTP.

Upon addition of GTP, Pi was released from the GTP hydrolysis catalysed by CetZ1 with a GTPase activity of $4.6x10^{-3}$ moles of GTP hydrolysed per mole of CetZ1 per minute.

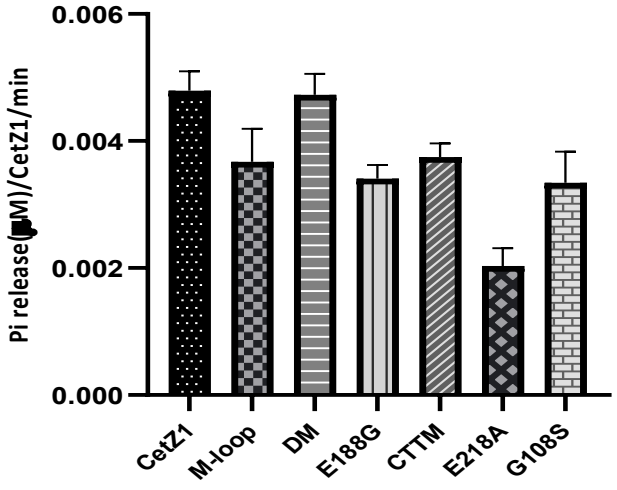

Fig 3.15: GTPase activity of CetZ1 and mutant protein.

The kinetics of Pi released from the enzymatic conversion of GTP to GDP catalysed by CetZ1 using 800 mM PIPES buffer was measured using a colorimetric assay that measures absorbance at 620 nm.

The kinetics of Pi release for CetZ1 mutants in PIPES buffer were measured. As seen from *Figure 3.15* CetZ1.E218A, the GTPase mutant, had the lowest values for the phosphate release as compare to the wild-type CetZ1 and other mutants. The GTPase activity, CetZ1.double mutant, which is predicted to disrupt the lateral interaction is almost equal to that of wild-type CetZ1. This assay has been previously used to measure GTPases activity of FtsZ and tubulins (Król & Scheffers, 2013). But the major problem with this assay was the high absorbance for PIPES buffer, which was used as the negative control. The 3 M KCl concertation in the PIPES buffer (buffer only control) interferes with the malachite green assay. May be high KCl concertation destabilises constituents that contribute to the green colour of the complex.

Table 6.1 in the appendix section was made as a summary of the results presented in section 3.3 and can be referred to for discussion.

3.4 Discussion

We have described a set of methods that allow quick analysis of the CetZ1 biochemical activity. Various methods such as right-angled light scattering assay, sedimentation assay as well as electron microscopy have been widely used to study FtsZ and microtubule polymerization (Król & Scheffers, 2013; Mukherjee & Lutkenhaus, 1999; Waxman et al., 1981). We have used similar methods to study the CetZ1 protein and describe conditions that best suits its polymerization. Studying the *in vitro* polymerization dynamics of CetZ1 could unravel how the protein might assemble into a higher order quaternary structure. This study mainly provided evidence suggesting that CetZ1 polymerization is dynamic and regulated by GTP hydrolysis and has begun to describe the structurally important regions that are required for CetZ1 polymerization.

CetZ1 was successfully purified using ion exchange and gel filtration chromatography. However, CetZ1 initially posed problems with the appearance of non-nucleotide dependent aggregates. But attempts were made to purify the protein in its monomeric form using the *E. coli* expression system. Buffer conditions allowing the purification of protein in its monomeric form, which is necessary to understand the pure polymer dynamics, were identified and utilized. The use of glycerol (20% v/v) was found to be important for optimal purification of monomeric CetZ1 protein. Most cytoskeletal proteins are prone to aggregation, since they possess an intrinsic ability to make polymers (Rivas & Minton, 2016). Like other cytoskeletal proteins, CetZ1 showed high propensity to aggregate when is highly concentrated, therefore improvising the buffer was necessary. Additional reagents have been demonstrated to reduce non-specific aggregation. For example, kosmotropes such as ammonium sulphate and glycerol, reducing agents like DTT and ligands or co-factors at low concentrations have been helpful in preventing non-native aggregates (Leibly et al., 2012).

FtsZ and tubulin both have displayed variations in polymerization depending on the buffers used for the assay and the additives such as Mg^{2+}, CaCl or KCl (Mukherjee & Lutkenhaus, 1998) (Waxman et al., 1981). Addition of the crowding agent into the reaction was shown to increase the polymerization for FtsZ, probably because of its resemblance to the naturally crowded environment of the cytoplasm (P. Buske & Levin, 2013) (Monterroso, Reija, Jiménez, Zorrilla, & Rivas, 2016). In case of CetZ1 polymerization buffer, the strength and the

concentration of KCl used in the study showed maximal polymerization, but how this buffer mediates the polymerization is unclear (De Silva, 2019). *H. volcanii* has a high cytoplasmic KCl concentration as an adaptation to their high salt environment they live in. Therefore, the 3 M KCl concentration required for the CetZ1 polymerization could resemble the natural cytoplasmic conditions of CetZ1 (De Silva, 2019) (De Silva, 2019). CetZ1 showed cooperative polymerization (De Silva, 2019). Subunits interact with one another in cooperative polymerisation to form the initial polymer nucleus, which then provides several interaction sites for the polymer to expand. As a consequence, lagging of the nucleation causes polymer assembly to be delayed at low subunit concentrations. In addition, polymerisation initiation necessitates a "sensitive" subunit concentration, which refers to the bare minimum subunit concentration required for polymerisation. Single subunit nucleation is typically the rate-limiting stage because it is energetically unfavourable, and at low protein concentrations, nucleation does not occur frequently enough to facilitate extension polymerisation (Miraldi, Thomas, & Romberg, 2008). For CetZ1, 12 µM was the concentration where no lag was seen during the light scattering assay with the PIPES buffer (De Silva, 2019).

The different regions of the CetZ1 protein structure were studied via structure-guided site directed mutagenesis. Mutations that disrupted the predicted longitudinal and lateral interaction surfaces of CetZ1, forming the protofilament interface with reference to the filament structures of FtsZ and tubulin, were selected for the *in vitro* studies (Arjes, Lai, Emelue, Steinbach, & Levin, 2015; Dhaked et al., 2016; Guan et al., 2018; Lu, Stricker, & Erickson, 2001). Mutations such as the E218A, that disrupt the T7 synergy loop that is conserved in tubulin superfamily proteins, disrupts the GTPase activity of the CetZ1 protein. The ‘top’ surface mutant G108S was used to study the importance of the T4 region involved in GTP binding and polymerization of CetZ1. The remaining mutants, including the M-loop mutant, C-terminal tail mutant, E188G mutant, and double mutant, were hypothesised to inhibit lateral interactions with a neighbouring subunit of an adjacent protofilament. For the purification of CetZ1 mutations it was noted that depending upon the mutation, the propensity for aggregation of the proteins differed; this may be due to the altered surface properties caused by each specific mutation.

Light scattering assays for the point mutants E218A and G108S, that we presume to affect the longitudinal interaction by disrupting the GTPase activity and GTP binding site respectively

(T7 and T4 loop region) of the CetZ1 protein, resulted in partial impairment in polymerization, causing slow and continuous polymer growth for the E218A mutant. The mutant also showed shorter filaments and apparently a reduced GTPase activity. The *in vivo* localization patterns for E218A mutant displayed an intense, less dynamic and peripheral localisation pattern (De Silva, 2019), and continuous and slow polymer formation in light scattering assay suggest that this mutation therefore probably affects the polymerization and depolymerization rate of CetZ1. Whereas short polymerization and a fast depolymerization for G108S mutant suggest that the mutation in the N-terminal domain of CetZ1 containing the GTP-binding site affected the monomer-monomer interactions within the single protofilament and therefore reduced polymerization was seen. Although the mutation displayed an intense peripheral localisation *in vivo, (De Silva, 2019)* the mutation formed shorter filaments *in vitro*.

In tubulins, growth both *in vivo* & *in vitro* (Dougherty, Sage, Davis, & Farrell, 2001). The mutation in addition to slow growth showed slow depolymerization, suggesting that rate of polymerization is probably associated with the rate of depolymerization (Dougherty et al., 2001). The analogous mutation in The T4 region of FtsZ in *E. coli*, G104S (*ftsZ84),* increases the temperature sensitivity of the cells. The *ftsZ84* mutant exerted a normal cell division at 30 ^{o}C and displayed defective growth at 42^{o}C. Although the top surface is mainly associated with the polymerization, mutations showed reduced depolymerization (Lu et al., 2001). Similarly, the mutation made in the T7 and T4 regions of CetZ1 protein showed impairment near to the GTP active site, thus affecting the polymerization. Slow polymerization due to weak interaction, which is sufficient to stimulate GTPase activity was shown *in vitro* by these mutants; suggesting that CetZ1 can add and remove subunits in the polymers from both ends. Therefore, it would be interesting to explore the kinetic polarity of the CetZ1 polymer in future studies.

The goal in making the lateral mutants was to target amino acids making lateral contacts between protofilaments. The polymerization of the potential lateral surface-interaction mutation was explored by measuring the light scattering of CetZ1.M-loop, CetZ1.Double mutant and CetZ1.E188G made in the C-terminal domain of CetZ1. CetZ1.M-loop mutant destabilises the CetZ1 polymeric structure as little to no light scattering was seen. This may be due inhibition of subunit addition, leading to disassembly of the filaments. The mutation made in the M-loop region decreased the hydrophobicity of the region and therefore other

forces such as salt bridges between specific residues or van der Waals interaction play role in CetZ1 polymerization and lateral interaction. The poor polymerization seen with the M-loop mutant is consistent with the diffused i*n vivo* localisation shown by this mutant (De Silva, 2019). The major surprise with the M-loop mutant in the C-terminal domain which failed to polymerize suggests that M-loop region is crucial for CetZ1 polymerization.

CetZ1.double mutant and CetZ1.E188G were able to polymerize and they appeared to have normal GTPase activity. It may happen because the GTPase is thought to be activated by assembly into protofilament and does not involve the lateral interactions also the mutation showed patchy peripheral *in vivo* localization. The double mutant (R276E & K277E) and E188G showed less scattered light intensity than wild-type, possibly due to conformational change that effects the interconnection within the monomers. One reason might be the differences in the protein purification of the mutants, as oligomerization was seen. It may have resulted in moderate differences in the protein concentration and therefore effective signal differences were seen for all the mutant proteins.

In the double mutation, the positively charged residues were replaced by negatively charged glutamic acid, which might have impact on the lateral interactions and therefore the reduced light scattering signal. Mutations located on the top surfaces of the C-terminal domain of tubulin have been shown to uncouple the conformational changes in the microtubule structure, maintaining the straight conformation which reduces the microtubule shrinkage (Geyer et al., 2015). In the FtsZ of *B. subtilis,* the mutation R191A of FtsZ showed reduced level of polymerization by a conformational change that disrupts the interactions between the monomers (Dhaked et al., 2016). The C-terminal tail mutation of the CetZ1, which we presume to affect the lateral and membrane interaction of the CetZ1 polymers, displayed less dynamic polymerization than the wild-type CetZ1 *in vitro* as well as *in vivo*. It will be attractive to identify the conserved residues on the CetZ1 C-terminal tail that are involved in stabilizing the putative lateral or membrane interactions.

Negative-stain electron microscopy (TEM) was used to characterize the assembly of CetZ1 and mutant proteins. CetZ1 showed dynamic filaments which were regulated by GTP. The mutants displayed a variety of filament assembly structures and all showed significantly reduced average length of filaments, which were straight and singular, with no bundling as compared to that of wild-type CetZ1. This suggests that the various mutation affects the

polymerization ability of CetZ1, and that they have a specific role in modulating interactions between subunits of individual protofilaments. For example, the GTPase mutant CetZ1.E218A may increase nucleation rates without altering elongation rates, which may lead to the formation of a higher number of shorter filaments due to overall reduction in the total number of CetZ1 subunits that are available for assembly. The findings highlight the need for closer examination of the kinetics assembly dynamics of wild-type CetZ1, as well as the point mutations to illustrate the factors that contribute to CetZ1 filament length.

Attempt was made to calculate the GTPase activity with Malachite green phosphate assay, but due to presence of high KCl in the PIPES buffer we hypothesised that the 3M KCl might have interfered with the assay that contributes to the green colour development and therefore the assay could not measure the CetZ1 GTPase activity under these conditions. Different assay which utilises the radioactive phosphate can be used to detect the GTPase activity of CetZ1 to study the kinetics of CetZ1 polymerization in future studies. A future detailed analysis of the activity of these mutant CetZ1 proteins could include studies of the GTPase activity, GTP binding and GTP concentration dependence of polymerization, to determine whether these are related to changes in nucleotide biochemistry of the mutants.

The investigation of protein biochemical characteristics poses many difficulties and challenges surrounding both the experimentation and the results that are generated. Despite these difficulties, *in vitro* work allows a glimpse at the linkage between molecular structure and cellular function. In this set of experiments, we attempted to answer some of the fundamental questions surrounding CetZ1 and its dynamic biochemical properties an essential step in supporting characterising CetZ proteins as members of the tubulin-superfamily. This is thus, the first such investigation into the polymer activities and structure of CetZ1.

In summary, an initial investigation into the biochemical features of CetZ1 dynamics has been conducted and showed promising results. This is the first study to show the *in vitro* polymer formation of CetZ1, and CetZ1 point mutants by electron microscopy. The polymers formed by the CetZ1 are GTP dependent and dynamic in nature. Furthermore, mutation to the residues in certain parts of the protein structure helped our understanding of the important structural parts of CetZ1 that are involved in polymerization. In future research, cryo-EM and/or GFP fusions would allow a more detailed look into the polymerization of CetZ1 both

in vivo and *in vitro*. This biochemical study of the CetZ1 protein dynamics will continue to enhance a deeper understanding of the archaeal cytoskeleton. The multi-functionality and biochemical properties shared by CetZ1 with tubulin superfamily proteins are yet remained to established just prokaryotic and eukaryotic members of tubulin superfamily proteins.

Chapter 4
In vitro interaction of CetZ1 and point mutant polymers with liposomes

4.1 Introduction

Phospholipid bilayer membranes are the boundary of living cells. They are two-dimensional self-organized structures with many cellular functions. The shape of a cell is determined by the interaction of cytoskeletal structures with large numbers of proteins at the cell membrane. These interactions can be highly complex and can involve many components. Hence, understanding the coordination between the cytoskeleton and the membrane can also be difficult and sometimes requires simplification. One way to understand this complex set of functions and interactions is to reconstruct cellular functions *in vitro*. Microtubules, actin and FtsZ have been polymerized inside synthetic liposomes, an effective cell free approach (Miyata & Hotani, 1992; Pontani et al., 2009) (Osawa, Anderson, & Erickson, 2008; Pinot et al., 2009). Such approaches can be used to study archaeal cytoskeleton proteins *in vitro* to explore their potential interactions with the membrane, and to further understand their function.

Protein-membrane interactions have been observed in FtsZ and other cytoskeletal proteins in bacteria, by studying the FtsZ polymers formed in the presence of anchor proteins on lipid membrane surfaces by electron microscopy (Milam, Osawa, & Erickson, 2012). Cell division in most bacteria depends on FtsZ and many other proteins like ZipA and FtsA, which from an annular structure at mid-cell. ZipA binds to the membrane through its N-terminal domain and FtsA binds through its C-terminal helix. Together these proteins stabilize the Z ring and anchor polymers to the membrane (Hale & de Boer, 1997; Ohashi, Hale, de Boer, & Erickson, 2002; Pichoff & Lutkenhaus, 2002). MreB, a bacterial homolog of actin, is essential for cell shape formation in bacteria (Lee, Cha, Zerbv, & Stewart, 2003). MreB has shown to interact with the membranes directly and induce negative curvature in purified liposomes (Salje, van den Ent, de Boer, & Löwe, 2011).

The CetZ protein is homologous to the eukaryotic tubulin and prokaryotic FtsZ. The primary function of CetZ1 in the model archaeon *H.volcanii* is to control cell differentiation from plates to rods. *In vivo*, CetZ1 forms highly a dynamic localization pattern, producing filament like structures adjacent to the membrane, suggesting it may interact with the inside of the cell membrane (Duggin et al., 2015). Cells expressing CetZ1.E218A-GFP have shown intense patches of localization of CetZ1.E218A at the cell envelope, mostly at regions of high

curvature. Moreover, the electron cryotomography sections of cells showed regions with an additional layer at the envelope, most likely produced by CetZ1.E218A filaments. This implies that CetZ1 has an effect on the cell envelope, and it was hypothesized that it may even directly remodel the cell envelope. (Duggin et al., 2015). CetZ1 polymerized filaments, however, have unique properties distinct from microtubules and FtsZ (chapter 3), and CetZ1 interaction with the membrane may differ from that of FtsZ and tubulins. The *in vivo* localization studies carried out for CetZ1 and it mutants such as M-loop, C-terminal tail mutant showed a diffused localization pattern (De Silva, 2019), likely due to impairment in CetZ1 polymerization or structure (Chapter 3). Moreover, mutants such as the C-terminal tail mutant and C-terminal domain mutants showed decreased cell envelope localization, suggesting that the disordered C-terminal region of CetZ1 may be involved in membrane interaction, similar to the membrane interactions seen for FtsZ. However, the mechanism by which CetZ1 interacts with the membranes is unknown.

Functionally important features of biological molecules are conserved during evolution. The identification of functionally important regions in a protein structure is vital in understanding how complex structures emerged during evolution to exert specific functions. Therefore, in the present study the ability of CetZ1 to bind and modulate the shape change in lipid membranes in a GTP dependent manner was explored. We attempted to obtain phase contrast and transmission electron microscopy images of the CetZ1 filaments with *Haloferax volcanii* lipid membranes. The current preliminary data in this literature suggests that the shape changes in liposomes may be induced by CetZ1 polymerization, as CetZ1 localizes to the membrane. Although it is still undetermined whether CetZ1 interacts with the membrane directly or indirectly on the liposome membrane.

4.2 Methods

4.2.1 Purification of archaeal membranes

Archaeal membrane lipids were extracted as described by De Silva et al (De Silva, 2019). The cells of *H. volcanii* strain DS2 were harvested in the late exponential phase of growth by centrifugation using Hitachi R18A rotor at 7000 rpm for 10 mins. The cells were washed by re-suspending in 50 mL of 18% BSW and centrifuged using Hitachi R18A rotor at 6500 rpm for 10 min. The supernatant was discarded, and the pellet was washed with 50 mL 18 % BSW. The supernatant was removed, and the cell pellet was freeze-dried for 24 h. A mixture of methanol, dichloromethane (DCM), and phosphate buffer (8.7 g/L KH2PO4, pH 7.4) at a ratio of 2:1:0.8 (v/v) was prepared. The solvent mixture was mixed well, ensuring phases were not separated. The solvent mixture was added to the freeze-dried cells to extract the lipids, using about 5 mL per 1 g of dry cell mass. The cells were then re-suspended by vortexing, followed by sonication in a water bath sonicator (40 kHz, 700W) for 5 min. The cell suspension was centrifuged using Hitachi R18A rotor at 6500 rpm for 5 min and the supernatant was transferred in a new tube. The extraction procedure was again repeated on the pellet, and the supernatant was collected with the first extract. Two further extractions were carried out with 0.8 volumes of 5 % trichloroacetic acid, pH 2 instead of the phosphate buffer, as trichloroacetic acid improves the extraction. 0.5 volumes of dichloromethane and MQW water were added to the pooled supernatant extracts. They were vortexed and centrifuged using Hitachi R18A rotor at 6500 rpm for 5 min. The phases were separated by keeping the mixture still for some time, and the organic phase was collected in a different tube. The aqueous phase was washed with 5 mL dichloromethane per 1 g of original dry mass, followed by vortexing and centrifugation using Hitachi R18A rotor at 6500 rpm for 5 min. The second dichloromethane phase was pooled with the main organic phase. The organic phase was washed with an equal volume of pure water, followed by centrifugation and collected with the organic phase. Several aliquots of the final organic phase in glass vials were evaporated under a stream of dry N2 in a fume hood. The vials were sealed while under N2 flow to minimize the oxygen in the vial and stored as the total lipid extracts at – 20^{o}C until further use.

4.2.2 Archaeal liposome preparation

The liposomes were prepared by re-suspending the extracted lipids in filter sterilized liposome buffer (50 mM Tris-Cl, 200 mM KCl, 1 mM EDTA pH 8.5), adding 5 mL of liposome buffer per 10 mg of lipids. The mixture was vortexed for several seconds, then sonicated in a water bath sonicator (Power Sonic420, 40 kHz, 700W) for 30 – 45 min. Liposomes were stored at 4 ^{o}C and used within 7 days.

4.2.3 Co-sedimentation assay for liposomes

The co-sedimentation assay was performed using sonicated liposomes (Section 4.2.2). Purified CetZ1 was centrifuge using Beckman TLA 100 rotor at 50,000 rpm for removed any aggregated protein. Liposomes were mixed with pre-spun 12 µM CetZ1/mutant protein in 800 mM PIPES buffer, and the polymerization reaction was initiated by adding 2 mM GTP to the mixture. The mixture was centrifuged at 55 000 rpm at 20 ^{o}C for 15 min in a Beckman TLA 100 rotor. The supernatant and pellet were removed and stored separately in new tubes for analysis by SDS-PAGE.

4.2.4 Phase contrast microscopy

To 10 µL of liposomes, 10 µL of 12 µM CetZ1/mutant protein and 1 mM GTP was added, and incubated for 15 min. In some samples, liposomes were then stained with the membrane stain 5 µL of AM1-43 (5 µg/mL). For most microscopic imaging, 2 µL of sample was placed directly on a slide and covered with #1.5 coverslip (WPI). Phase contrast images were acquired with Zeiss AxioPlan microscope with a 1.4 NA phase-contrast objective (Carl Zeiss, Germany).

4.2.5 Transmission electron microscopy

Samples were prepared similarly to that of the co-sedimentation assay; however, the final volume was reduced to 10 µL. 12 µM of CetZ1/mutant protein was mixed with liposomes and polymerized in 800 mM PIPES buffer pH 7.5, 3 M KCl. 1 µL of 2 mM GTP was added and incubated for 2 min at 30 ^{o}C at 300 rpm. The reaction mixture was then spun for 10 mins at 10,000 rpm. 2 µL of sample was applied onto a glow discharged 400-mesh carbon-coated

copper grid and incubated for 2 min. The grid was blotted dry by gently touching the grid parallel to a piece of filter paper, then stained with 4 µL of 2 % uranyl acetate solution. Excess stain was removed by blotting with filter paper. The grid was left to dry completely and viewed in Tecnai T20 transmission electron microscope operating at 120 kV.

4.3 Results

4.3.1 Liposome preparation from *Haloferax volcanii* membrane

In vivo CetZ1 displayed a high cell envelope localization during the morphogenesis studies. Therefore, the ability of CetZ1 to interact directly with the cell membrane was explored by purifying the archaeal cell membrane. *H. volcanii* lipids were extracted and dried under nitrogen gas (*Figure 4.1.a)* as described in section 4.2.1. The liposomes were prepared by re-suspending the lipids in Tris buffer (filter sterilised 50 mM Tris-HCl, 200 mM KCl, 1mM EDTA, pH 8.5) and sonicating for 30 min. The liposomes showed small particles of varying sizes with a diameter of 1-3 µm when using a phase-contrast microscope (*Figure 4.1.b)*. Initially, the liposomes were observed to be heterogeneous in size, so to control the size of the liposomes, the sonication time was increased from 30 min to 45 min, but no improvement to the uniformity of size was seen.

(a)

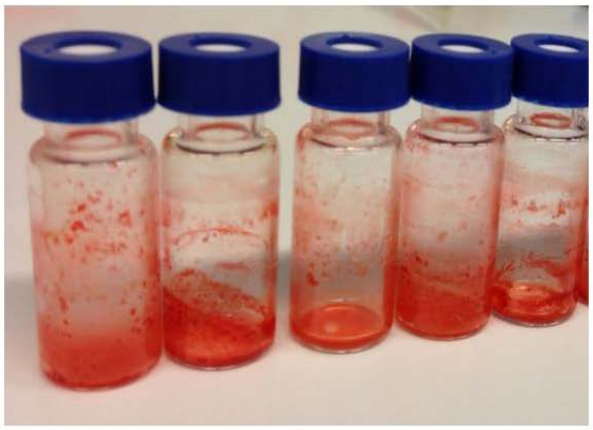

(b)

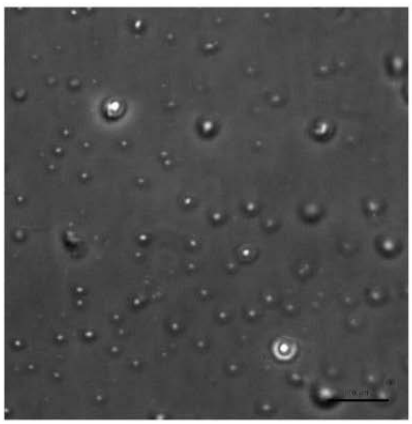

Figure 4.1: Liposomes of H.volcanii

(a) The lipids (pink color) from H. volcanii after the extraction with solvents and evaporated under the nitrogen gas. (b) Phase-contrast image of prepared liposomes by sonication having a diameter of 1-3 µm.

4.3.2 Electron microscopy images for CetZ1 interaction with lipid membranes

The ability of CetZ1 to interact directly with the cell membranes was explored by transmission electron microscopy. Samples were prepared similar to the co-sedimentation assay, as described in section 4.3.1. The CetZ1 liposomes mixture was polymerized with GTP and examined by negative stain electron microscopy. As a control, only liposomes without proteins were used (*Figure 4.2.A),* producing only spherical liposomes.

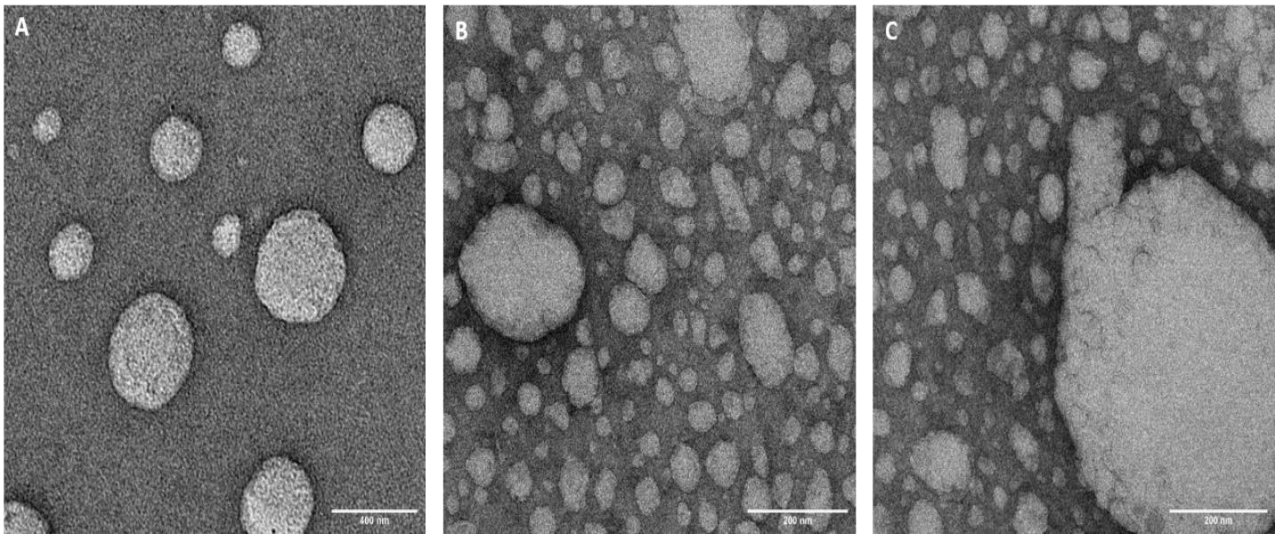

Figure 4.2: EM images of negative stain liposomes with CetZ1

(A) Liposomes only as a control, produced from H. volcanii. (B-C) wild type CetZ1 with liposomes polymerized in 800 mM PIPES buffer and GTP.

Negative stain EM showed changes in the liposome shape when incubated with CetZ1 polymerized protein. The liposomes where typically on average 200 nm wide when no CetZ1 protein was present (*Figure 4.2.A)*, while in presence of CetZ1 the liposomes became distorted and formed shapes similar to those observed by phase contrast (*Figure 4.*3). Liposome protrusions were also observed, beginning to project outwards from the liposome in areas which were adjacent to concavities.

Some CetZ1 polymer structures were seen in *Figure 4.2.B&C,* making distortions that bend the membrane in several places, suggesting protein–lipid assemblies. The bending projects outward from the liposome.

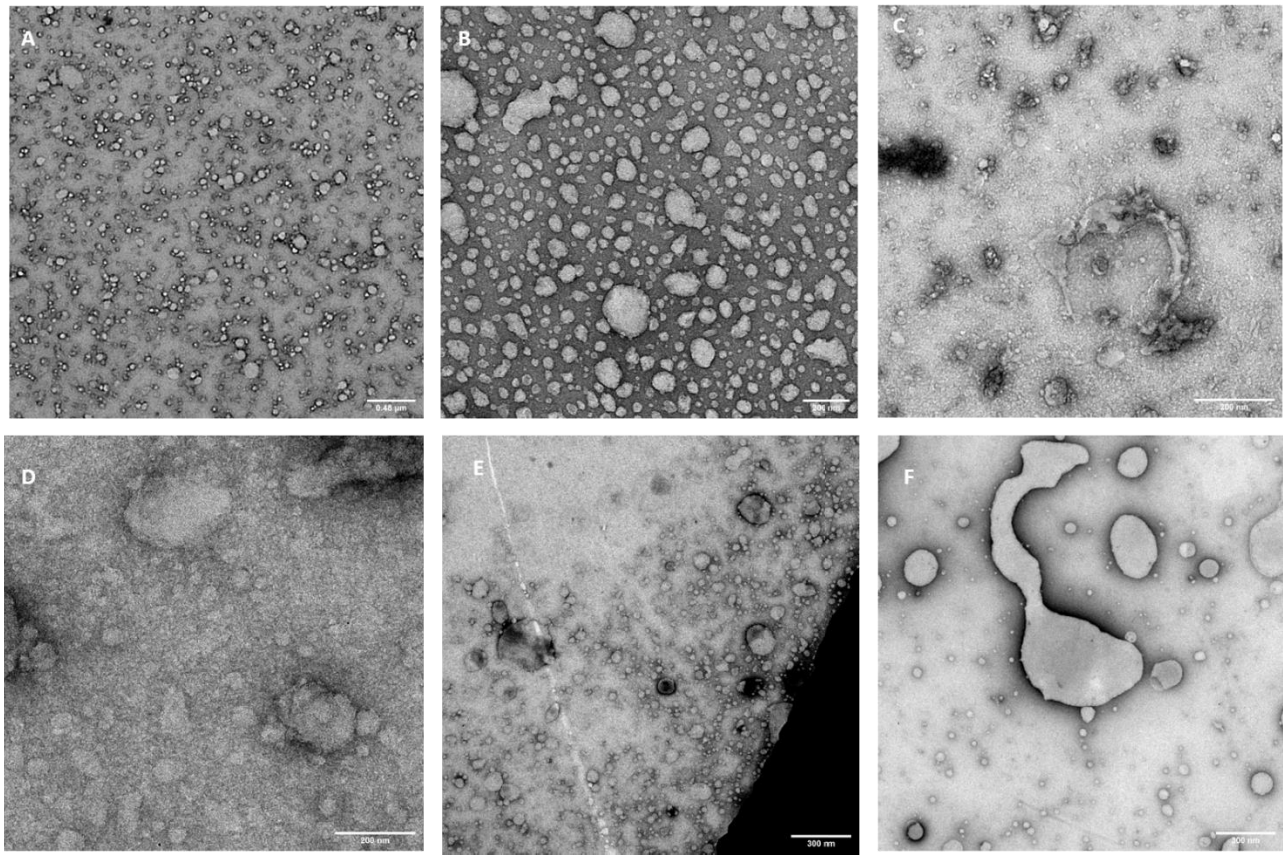

Figure 4.3: EM images of negative stain liposomes with CetZ1 point mutants

Liposomes mixed with (A) CetZ1.M-loop; (B) CetZ1. Double mutant; (C) CetZ1.E188G; (D) CetZ1. E218A; (E) CetZ1. G108S; and (F) CetZ1. CTTM. All proteins were polymerized in 800 mM PIPES buffer with 3M KCL and 2 mM GTP and incubated for 10 -15 min. Changes in the liposome shapes are visible over the concavities.

The effect of point mutations on the interaction of CetZ1 with liposomes was explored by transmission electron microscopy. The, CetZ1. M-loop and CetZ1.E188G mutant (*Figure 4.3.A & B)* in the CetZ1 polymers displayed no obvious changes in the liposome shape, whereas, for CetZ1.double mutant changes in the liposomes were evident. The deformation in liposomes and elongation in the liposome shape were seen due to the polymerization of CetZ1.double mutant (*Figure 4.3.C).*

For mutation designed to disrupt the GTPase activity of CetZ1 polymerization, CetZ1.E218A displayed changes in the liposome shape (*Figure 4.3.D)*. The liposome shape changed from

spherical to oblong with few indentation or negative curvatures seen at the periphery of the liposomes. The other mutant designed to affect the longitudinal interaction in the CetZ1 polymerization made in the GTP binding site, CetZ1.G108S did not display changes in the liposome shape (*Figure 4.3.E)*. The CetZ1.C-terminal tail mutant displayed few changes in the liposomes where few liposomes were elongated with concavities (*Figure 4.3.F)*.

4.3.3 Phase-contrast microscopy for lipid interaction studies of CetZ1

A key feature of tubulin superfamily proteins is their ability to interact with lipid membranes to modulate cell shape. Additionally, CetZ1 displayed peripheral localization in *in vivo* studies, suggesting that CetZ1 may have some interaction with the membrane. To mimic this *in vitro*, liposomes were formed from *H. volcanii* lipid membranes by sonication and mixed with 12 µM of CetZ1 polymerized in the presence of 2 mM GTP in polymerization buffer (PIPES buffer). The liposomes only control showed small particles of varying sizes (*Figure 4.4.a)*. When the liposomes were mixed with a control protein such as BSA, no observable changes in the liposome size or shape were seen (*Figure 4.4.a)*. This indicated that any changes seen upon incubation of the liposomes with CetZ1 are not non-specific changes due to the presence of a protein in general. As seen in *Figure 4.4.c*, a substantial number of changes in the liposome shape is evident when the liposomes are incubated with CetZ1 in presence of GTP. Occasionally we also found large liposomes that had concave depressions. The liposomes were no longer spherical shape but were altered most likely due to the force exerted by the CetZ1 on the liposomes.

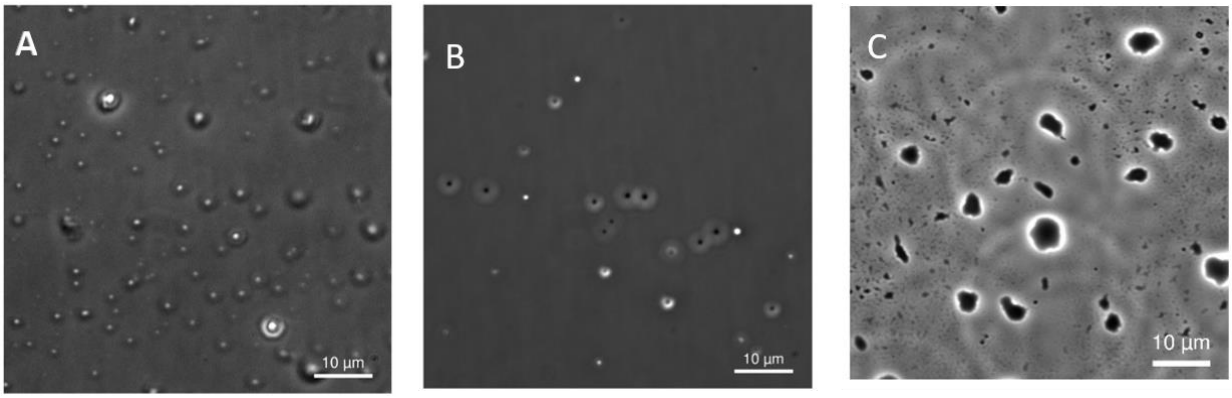

Figure 4.4: Changes in liposome shape in the presence of CetZ1 protein

Liposomes and CetZ1 interactions were assessed using phase and fluorescence microscopy. Phase microscopy was performed on all images using the auto exposure setting at 100X magnification. (a) Liposome only control (b) Liposomes incubated for 10 minutes with BSA control. (c) Liposomes incubated with wild-type CetZ1 for 10-15 min with polymerization in PIPES buffer and GTP.

4.3.4 Lipid interaction studies with CetZ1 mutants

The effect of point mutations on CetZ1 interaction with lipid membranes was explored next. The point mutants were polymerized in 800 mM PIPES buffer in the presence of GTP with the liposomes for 10-15 min and were then observed using phase contrast microscopy. The point mutants mapped to the side of the CetZ1 subunit, including the M-loop mutant, CetZ1 double mutant (R276E and K277E), and CetZ1.E188G, are believed to alter lateral interactions of CetZ1 protofilaments. These mutants were tested to determine if they have any interaction with the liposomes.

The CetZ1.M-loop mutant caused no obvious changes to liposome shape, as shown in *Figure 4.5.a*. This data suggests that, to efficiently associate with the membrane, CetZ1 requires the M-loop region to form polymers, which in turn interacts with lipid membranes.

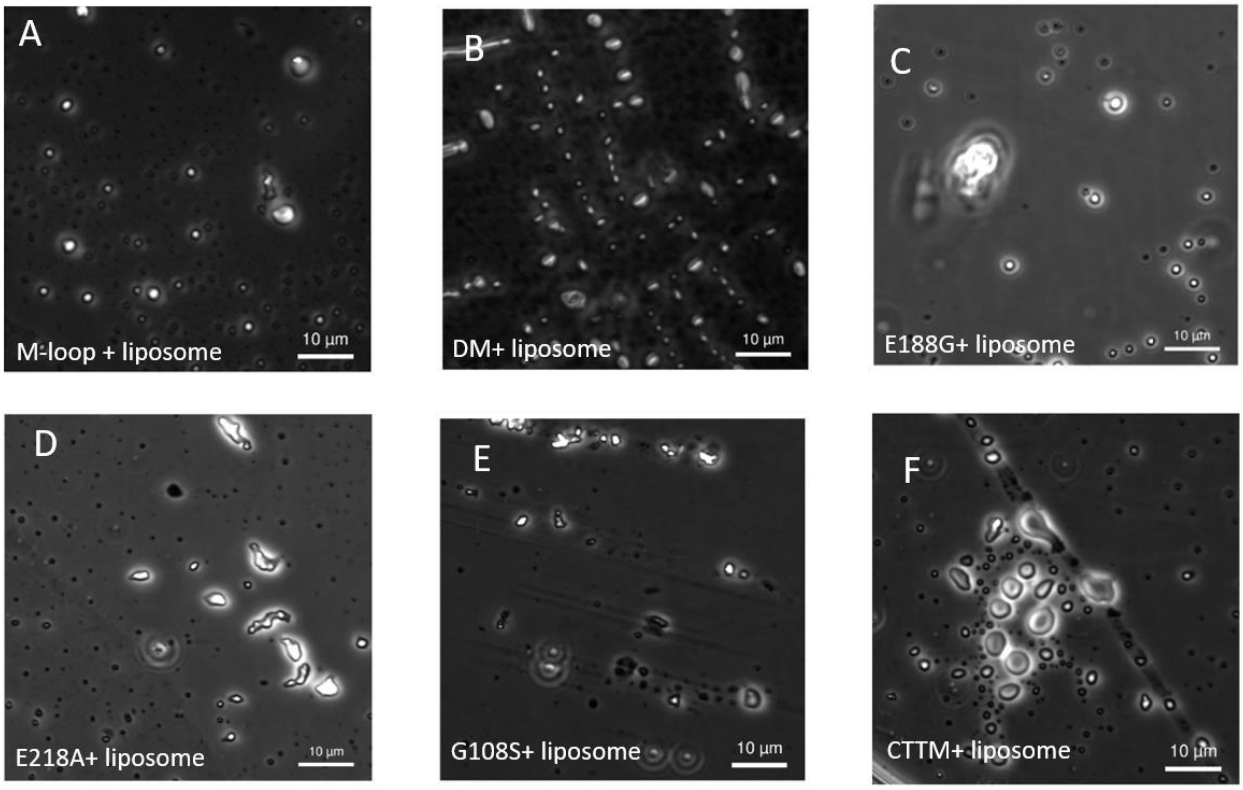

Figure 4.5: Effect of CetZ1 mutant on liposome shape

Liposomes were mixed with the mutant protein for 10-15min in PIPES buffer with GTP.

(A) CetZ1.M-loop mutant; (B) CetZ1.Double mutant; (C) CetZ1. E188G; (D) CetZ1. E218A; (E) CetZ1. G108S, (F) CetZ1 C-terminal tail mutant.

For the CetZ1.double mutant mixed with liposomes and GTP, most of the liposomes showed deformation in the liposome shape (*Figure 4.5.B*). The liposomes changed from spherical to altered (rod-like) shape.

The CetZ1.E188G mutation caused no obvious changes in the liposomes shape, though a few aggregated liposomes were seen, with clear areas of population with minimal change to the liposomes as seen in *Figure 4.5.C.*

CetZ1.E218A displayed significant changes in the liposome shape as seen in *Figure 4.5.D.* The liposomes changes shape from spherical to tubular like structures, with concave depressions inside the liposomes.

Another mutation that alters the GTP binding site of CetZ1, CetZ1.G108S, frequently showed changes in the liposome shape, but these changes were not as significant as that of CetZ1.E218A or wild-type CetZ1. As seen in *Figure 4.5.E* liposome became deformed in elongated shapes with depressions around the curvatures of the liposomes.

The mutation in the C-terminal tail of the CetZ1, was able to cause deformation in the liposomes, but only few liposomes showed this deformation where they changed to an elongated liposome . forming oblique shape in the liposomes (*Figure 4.5.F)*.

For quantitative analysis, the deformities were difficult to analyze due to small and heterogeneous size of the liposomes. It was observed that not the entire population of liposomes were quantifiable, as aggregation of liposomes in some places and smaller sizes made it difficult to analyze the entire slide. Additionally, the dye in some samples did not stain the liposomes properly, making it difficult to analyze the shape changes of the liposomes due to the CetZ1 proteins. Furthermore, because the structure of CetZ1 filaments was not visible with phase contrast microscopy, transmission electron microscopy was subsequently to directly observe CetZ1 polymer interaction with the liposomes.

4.3.5 Co-sedimentation of liposomes with CetZ1 and mutant proteins

Interaction between liposomes and CetZ1 was further investigated by co-sedimentation. For this assay, co-sedimentation was carried out using an ultracentrifuge at 55,000 rpm so that the lipid with the bounded protein would sediment in the presence of GTP. Liposomes with CetZ1 at a final concentration of 12 µM in polymerization buffer were polymerized in the presence of GTP. CetZ1 was found to be present in the pellet fraction. BSA instead of CetZ1 was used as a control in the reaction, and no interaction between the lipids and BSA was observed in the pelleted fractions. Additionally, only BSA and only CetZ1 without lipid fractions were used a control in the reaction (*Figure 4.6.a).*

(a)

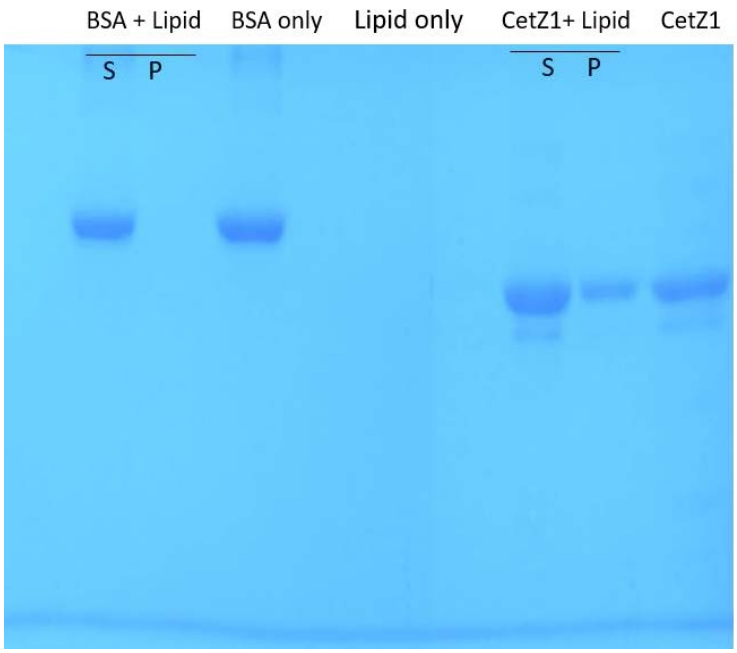

(b)

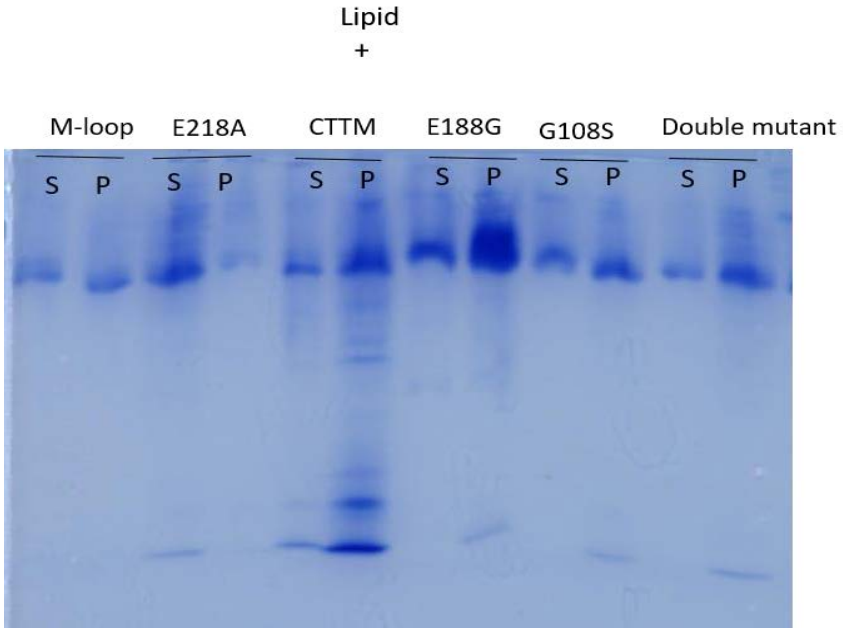

Figure 4.6: Co-sedimentation of liposomes with CetZ1 and mutant proteins.

(a) SDS-PAGE analysis revealed that at a concentration of 12 µM and in the presence of GTP, CetZ1 potentially interacts with liposomes. As a control BSA was co-sedimented with liposomes and no bands were observed in the pelleted fractions. BSA and CetZ1 only without protein and polymerization were also used as a control. S indicates supernatant fraction; P

indicates pellet fraction. (b) SDS-PAGE for mutant proteins co-sedimented with liposomes. (S) Supernatant, (P) pellet fractions from the experiments.

The same experiment was performed with the mutant proteins to see interaction between mutant CetZ1 and lipids. SDS-PAGE gel revealed that a high amount of mutant protein with lipids are found in the pelleted fractions (*Figure 4.6.b)*. However, the sedimentation assay, it is difficult to detect whether the proteins in the pelleted fractions are lipid bound or only polymerized proteins. Further investigation with cryo EM analysis is necessary.

Discussion

The study mainly provides preliminary evidence of CetZ1 protein interaction with the lipid membrane *in vitro*. In addition, the study suggests that CetZ1 can modulate the shape changes of liposomes in a nucleotide dependent manner. A variety of proteins can change the shape of lipid vesicles. For example, FtsZ forms tubulate liposomes when they interact with the liposomes *in vitro (Osawa et al., 2008, 2009).* They produce concave depressions and elongates the liposomes when added to the lipids. FtsZ has shown to form Z ring structures on liposomes, which are also able to exert constrictive force on the liposomes (Szwedziak et al., 2014). Dynamin forms small membrane tubule with helical structures wrapping around the membrane tubules (Sweitzer & Hinshaw, 1998). MreB, a bacterial actin homologue that functions in maintaining the cell shape, could also modulate the cell shape changes in liposomes (Garenne, Libchaber, & Noireaux, 2020).

CetZ1.E218A, the GTPase mutant showed patches of intense localization at the cell envelope. Moreover, the electron cryotomography sections of cells showed regions with an additional layer at the envelope produced by CetZ1.E218A. This indicates that effect of CetZ1 on cell structures directly remodels the cell envelope (Duggin et al., 2015). Additionally, the co-sedimentation assay performed with CetZ1 indicated that CetZ1 can directly bind to *H. volcanii* liposomes. However, the co-sedimentation can be unspecific, and does not enable us to distinguish between large polymers of CetZ1, and CetZ1 binding to lipids. Therefore, it was essential to monitor the ability of CetZ1 to modulate the shape of liposomes i*n vitro* by light microscopy an electron microscopy.

The multilamellar liposomes formed from *H.*volcanii were mostly spherical and aggregated in clumps. The size of *H. volcanii* liposomes were heterogeneous, even after sonication for 30 minutes. Hence, different lengths of sonication were used to obtain a homogenous population of liposomes, but this could not be achieved, but using extruder or microfluidics system may produce a homogenous size of liposomes but due to time constrain we could not use the alternative methods. We postulate that liposome deformation may result from the progression of polymerization, leading to formation of large assemblies near the membranes and thus changes in the shape. CetZ1 seems to bend the liposomes membranes by exerting forces on the membrane, thereby changing the liposome shape from spherical to oblique.

Subsequent CetZ1 polymerization upon associating with the membrane is a likely reason to introduce changes in membrane curvatures, and further exert a force for oblique liposome formation. However, the size of the liposomes, which is not easily controlled, can be an impediment for the light microscopy experiments, which showed less membrane deformation for the mutant CetZ1 proteins. Though certain mutants, like the E218A, showed notable deformation in the liposome membranes, how it specifically interacts with the membrane is yet to be fully elucidated. One of the possible reasons might be the filaments of CetZ1.E218A are slightly curved due to the mutation that affects the GTPase activity of the mutant. In FtsZ protofilaments it is seen that highly curved conformations are linked with the GTP hydrolysis (Erickson, 2009). For force generation, curved conformations are the most important since they require GTP hydrolysis for the bending of the membranes (Erickson, 1995).

Since no protein filaments or polymers were seen inside the liposomes it was difficult to identify the changes in the liposome shapes. Tagging the CetZ1 protein with a fluorescent protein will assist in better visualization of polymers of the protein or patches of the polymers on the inside of the liposomes. Therefore, making a membrane targeting CetZ1 construct with fluorescent proteins will help to observe the change in liposome shape by light microscopy.

The membrane deforming properties of the CetZ1 polymers were examined under the electron microscopy at lower magnification. While CetZ1 implicated changes in the liposome shape as frequently seen in the EM images. Mutants showed fewer influence on liposome shape. Mutant E218A and double mutant showed visible deformation in the liposome shape, while other mutants showed rare changes. Taken altogether, only wild-type CetZ1 and mutant E218A were classified as specific membrane deforming proteins as per the preliminary results seen in this study.

Due to time constraints, it was not possible to do more EM studies to quantify the effect of CetZ1 on the liposome shape. It will be essential to examine the ability of CetZ1 to modulate the liposome shape using cryoEM, fluorescent microscopy or dynamic light scattering in future in more detail. May be using correlative light electron microscopy with tagged CetZ1 and liposomes will help to elucidate how CetZ1 polymers interacts with the liposomes.

Finally, the *in vitro* studies conducted in chapter 3 and preliminary data from this study provides a foundation for studying the dynamic nature of CetZ1 polymers.

Chapter 5
General Discussion and Future Perspectives

The cytoskeleton plays an important role in modulating cell shape and is one of the key attributes that effects survival of microorganisms. Despite recent advancements in microscopy and biotechnology, we still have limited understanding of how these nanoscale molecular assemblies function and have an impact on fundamental biological processes on a micron-scale. Cells can change their morphology when under stress to adapt to their environment, and this ability to adapt plays a prime role in cell survival. While the control of cell shape and cytoskeletal components have been well studied in eukaryotes and bacteria, we have limited knowledge about the components and mechanisms of cell shape regulation in archaea. The recently discovered archaea-specific tubulin superfamily protein, CetZ1, transitions *H. volcanii* cells from plates to rods, which improves their swimming motility (Duggin et al., 2015). But further characterization is needed to understand how CetZ1 modulates these cell shape changes. The overall goal of this thesis was to improve our understanding of the i*n vitro* dynamics and molecular interactions of CetZ1.

To investigate the dynamics of CetZ1 in *H. volcanii*, regions of CetZ1 that have been predicted to be important for polymerisation and lateral interactions of polymers were considered. In each of these regions, several point mutations were made, and the resultant mutants were used to identify important structural features of CetZ1, and further understand the polymerisation of wild-type CetZ1 and its biological function. Finally, the potential of CetZ1 and its mutants to bind lipid bilayers was studied at the molecular level, to further understand their ability to remodel membranes and modulate shape. In doing so, this study has significantly contributed to our understanding of the roles of CetZ1 in the archaeal cytoskeleton and has provided interesting insights into the evolution of tubulin superfamily proteins.

5.1 *In vitro* assembly of CetZ1

In Chapter 3, several techniques that are commonly used to study assembly and activity of tubulin superfamily proteins were used, including light scattering, negative stain electron microscopy and sedimentation, in order to study CetZ1 polymerisation. The sedimentation of CetZ1 polymers allowed the quantification of the fraction of polymerized protein after a fixed reaction period and demonstrated that CetZ1 polymerization is GTP dependent and not GDP

dependent. The light scattering assay was then used to study the GTP-dependent polymerization of CetZ1, as well as its dynamic behaviour of polymerization and depolymerization in real-time. It also showed that CetZ1 displays a cooperative polymerization ability (De Silva, 2019). The GTP–dependent polymerization was further confirmed by transmission electron microscopy, where CetZ1 filaments were observed to be long and have the ability to bundle together in irregular clusters.

An investigation was conducted to identify the important regions of the CetZ1 structure for its function via structure guided site-directed mutagenesis and investigated some of their biochemical properties *in vitro*. Mutations were made to disrupt the possible longitudinal and lateral interactions in the CetZ1 polymer, and the consequences for polymerization behaviour and filament appearance by TEM were observed. The longitudinal interaction mutations were located in the T4-GTP binding loop (G108S) and T7-GTPase binding domain (E218A). The mutation in the GTP binding domain (G108S) showed a moderate polymerization capacity in the light scattering assay and could form some filaments as observed by TEM. Although these mutants show intense peripheral localization and could not transition the cell shape from plates to rods (De Silva, 2019), they did show basic filaments formation. This suggests that there is some intrinsic GTP binding ability in the mutants which is open to subunit-subunit affinity that promotes polymerization, albeit without the same capacity to function like wild-type CetZ1 filaments. The GTPase mutant, E218A, made in the synergy T7 loop, affected the polymerization and depolymerization ability of CetZ1, which resulted in smaller filament length, presumably due to the increased nucleation rate, which not only affects the polymerization, but depolymerization as well. These filaments were very stable over time, consistent with the lack of GTPase activity predicted in this mutant (Duggin et al., 2015).

We hypothesised that CetZ1 protofilaments probably interact laterally to form higher-order polymer structures that are necessary for CetZ1 function. Therefore, the residues in the C-terminal domain of CetZ1, which is positioned ideally for lateral association in other tubulin superfamily filament 3D structures, were studied for their importance in polymerization and filament assembly appearance by TEM. The M-loop mutant is a non-functional surface mutation in CetZ1 located at a similar position as that of microtubules' M-loop, which is important for the lateral interaction in microtubule (Sui & Downing, 2010). The diffused localisation and strongly defective polymerization of the CetZ1 M-loop mutant indicates its

importance in the overall polymerization of CetZ1 and possibly CetZ1 assembling into a higher order structure that is required for cell shape modulation. Other mutants in the C-terminal domain, which included CetZ1.E188G, CetZ1.double mutant and C-terminal tail mutant, displayed reduced level of polymerization in real time, but did form filaments which were shorter that wild-type filaments, and did not form the obvious clusters that wild-type CetZ1 did. Thus, the C-terminal domain is implicated in polymerization of CetZ1 and appears to have an impact on both longitudinal and lateral association between CetZ1 subunits. This was the first study to directly observe CetZ1 filament polymerization using an electron microscopy, and the results are consistent with the designation of this domain as the 'polymerization' domain of tubulin superfamily proteins (Duggin et al., 2015).

5.2 Interactions of CetZ1 with lipid membrane

Previous studies from our group have shown that CetZ1 localises adjacent to the cell envelope, and its GTPase mutant, CetZ1.E218A, also showed intense patches of localisation near the cell envelope (Duggin et al., 2015). Hence, it has been hypothesised that CetZ1 may be modulating cell shape via remodelling of the cell membrane, either directly or indirectly, alone or with other accessory proteins. Therefore, in this study, the possible interactions of CetZ1 with *H. volcanii* lipids was investigated. When CetZ1 was mixed with archaeal liposomes, CetZ1 caused shape changes in the liposomes as observed by light microscopy and TEM. Moreover, certain mutants such as CetZ1.E218A and CetZ1.double mutant distorted the liposome shape, suggesting that their polymerization ability of CetZ1 inflicts shape changes in liposomes. Moreover, mutants such as G108S, C-terminal tail mutant and E188G which did show polymerization ability *in vitro* but could not display shape changes in liposomes. Although these studies were preliminary, they were the first of their kind to be conducted on CetZ1 and are considered an important step towards improving our understanding of CetZ1 function in *H. volcanii*.

Future studies could investigate this hypothesis in further detail through the development and utilisation of biochemical methods combined with super resolution microscopy and cryoEM studies. These should also be conducted in parallel with i*n vivo* methods to detect interactions with lipids and other potential binding partners of CetZ1. Pull down assays may

also be useful in identifying interacting partners and accessory proteins similar to MAPs of microtubules.

Together, the work presented in Chapter 3 and 4 discusses the important structural regions of CetZ1, the dynamics of CetZ1 polymerisation and depolymerisation, and its ability to interact with lipid membranes. This work also confirms previously conducted *in vivo* studies, which hypothesized CetZ1 to be interacting with lipid membranes to modulate cell shape. Guided by the observation from these chapters, further research on functional properties and dynamics of CetZ1 polymer kinetics could provide further insights into the mechanism and function of CetZ1 polymerization, and its linkage to other cellular components and processes.

5.3 Concluding Remarks

The work described in this thesis investigated the polymerization ability of CetZ1 i*n vitro.* Based on the results, it can be concluded that CetZ1 forms GTP-dependent polymers. The GTP binding and GTPase domains are important for its proper polymerization ability, along with M-loop region being crucial for polymer formation. Furthermore, CetZ1 appears to interact with the lipid membrane, and modulate liposome shape changes *in vitro*. In future, cryoEM analysis of CetZ1 polymers, and the identification of potential CetZ1 interacting partners would provide further important insight into the function and mechanism of CetZ1 proteins. Although there still remains a lot unknown about CetZ1 function and mechanisms, this study has provided an important first look at the biochemistry and dynamics of CetZ1 polymerisation, and it creates an important link with previously conducted *in vivo* work. This is the first study to observe the dynamics of CetZs and is only one of very few studies to focus on archaeal cytoskeletal proteins. It is an important steppingstone to developing methodologies and fundamental knowledge about archaeal CetZs, a major part of the archaeal cytoskeleton. Moreover, studying archaeal cytoskeleton protein are expected to provide insight into the cytoskeleton evolution and help in understanding the fundamental principles of cytoskeleton function.

Appendix

Table 6.1: Summary of all observed in vivo and in vitro features of CetZ1 and mutant. +++++ indicates normal polymerization and lipid binding and – indicates no polymerization and lipid binding

	Mutation and Amino acid change	Location of mutation	In vivo study (De Silva 2019)		Polymerization ability (This study)	Avg.Filament length (This study)	Lipid binding (This study)
			Localization	Rod cell shape and motility			
Lateral interaction mutants	**M-loop LLSRL-SASRA**	S7-H9 C-terminal domain	Diffused localization	No rods Non-motile	_	75.51 ± 75.28 nm	_
	E188 Glutamic acid (E) change to Glycine(G)	H7 helix C-terminal domain	Patchy peripheral localization	Rods Motile	+++	33.41 ± 14.10 nm	_
	R276,K277 Arginine &Lysine (R,K) change to Glutamic acid(E)	H9 helix C-terminal domain	Intense filament like localization	No rods Non-motile	+++	44.55 ± 21.98 nm	++
	C-terminal tail LESLF-AESGG	C-terminal tail	Diffused peripheral localization	No rods Non-motile	+++	71.78 ± 30.28 nm	_
Longitudinal interaction mutants	**G108 Glycine(G) change to Serine(S)**	T4 loop N-terminal domain (GTP-binding site)	Intense peripheral localization	No rods Non-motile	+	56.70 ± 29.72 nm	_
	E218 Glutamic acid (E) change to Alanine(A)	T7 loop C-terminal domain (GTPase activation site)	Intense foci near cell membrane	Jagged shape cells less Motile	+++	30.68 ± 13.24 nm	++
	Wild type CetZ1	_	Dynamic, cell membrane localization	Rods Motile	+++++	144.8 ± 28.48	+++++

Supplementary Data

A. G108S

a)

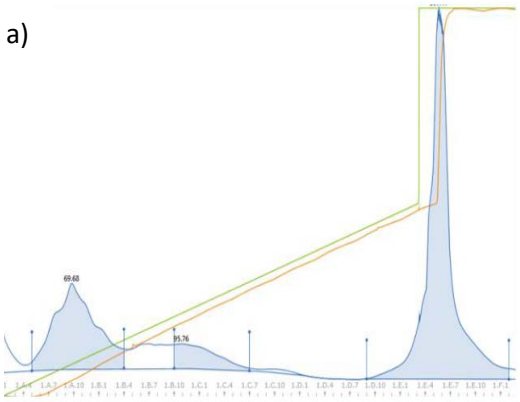

G108S

c)

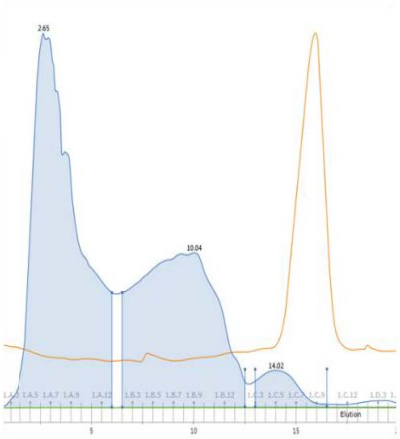

b)

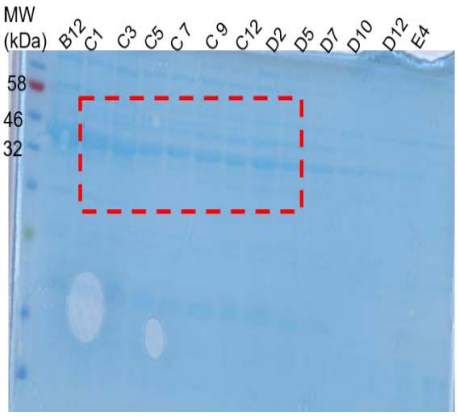

d)

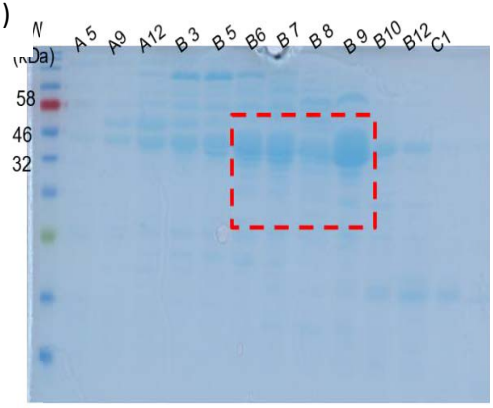

B. M-loop

a)

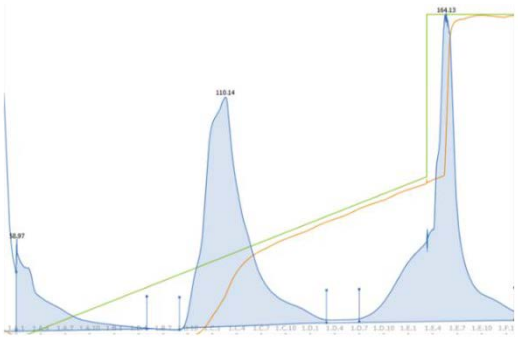

b)

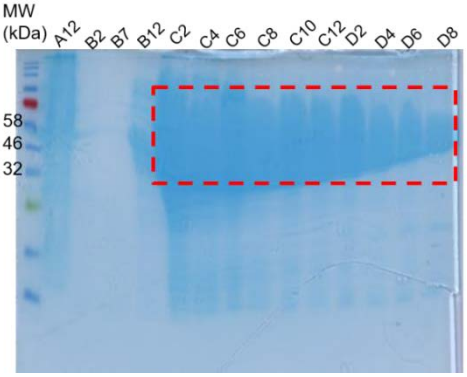

M-loop

c)

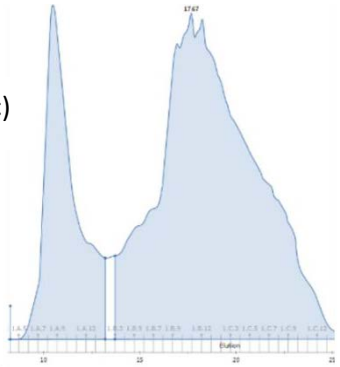

d)

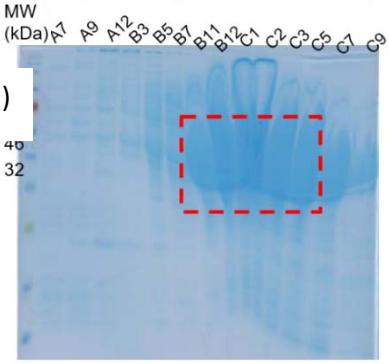

C. E188G

a)

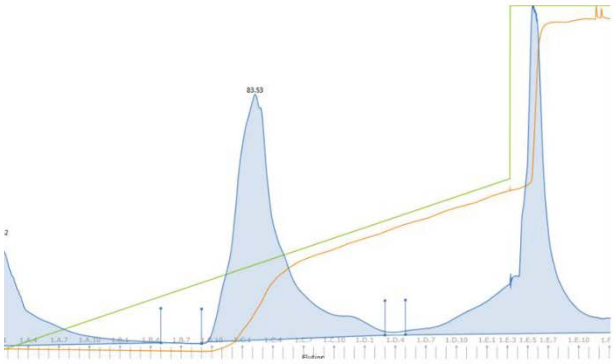

b)

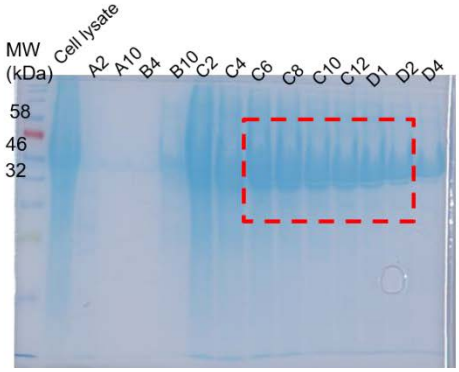

E188G

c)

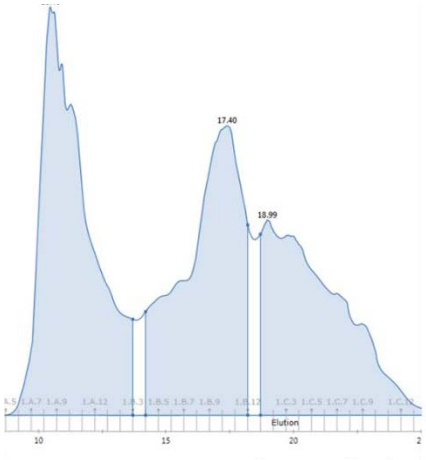

d)

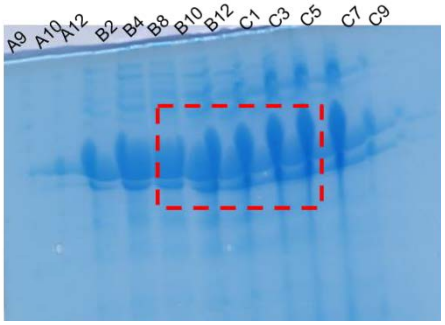

D. Double mutant

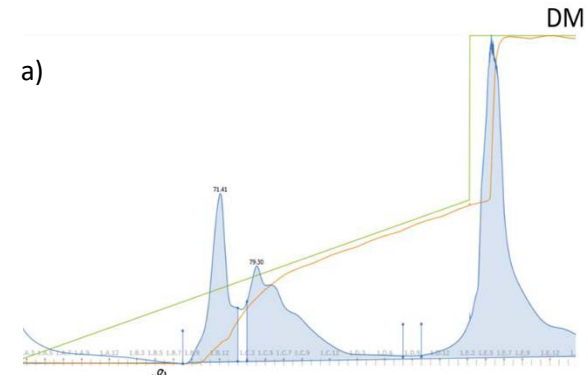

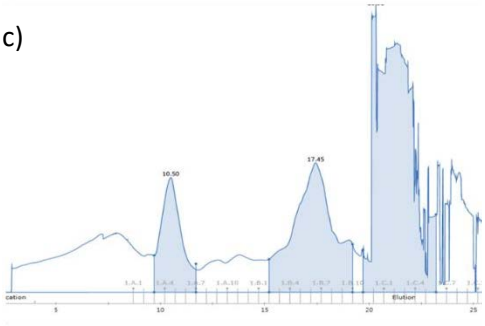

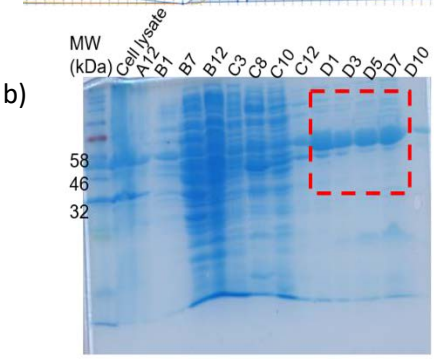

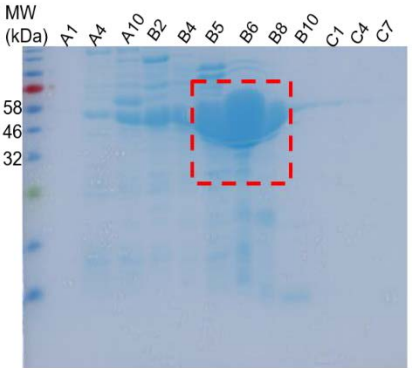

E. C-terminal tail mutant

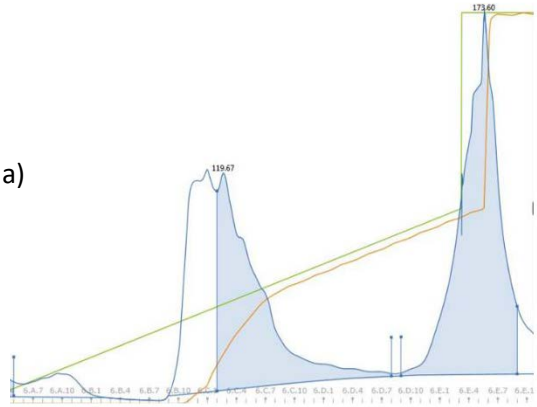

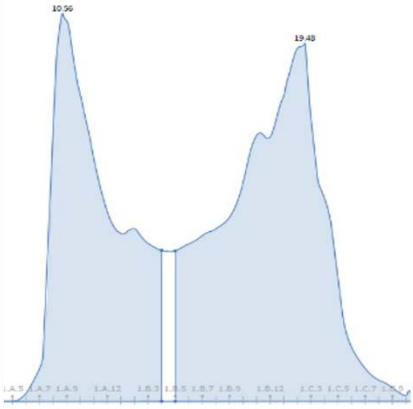

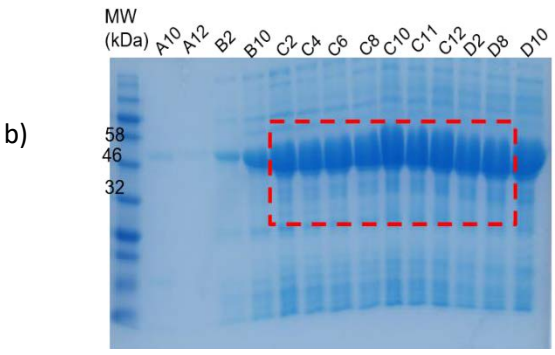

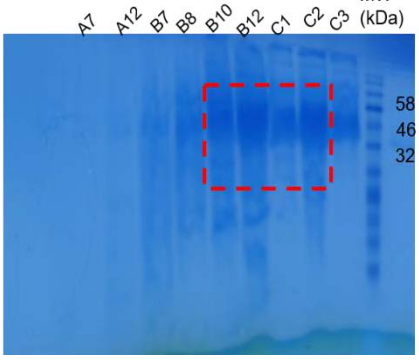

Supplementary Figure 1: Protein purification for CetZ1 mutants (G108S, M-loop, E188G, Double mutant and C-terminal tail mutant)

(a) Represent the chromatogram for the mutant ion exchange purification. The green colour line represents the KCl gradient and the orange colour line represent the conductivity (b) SDS-PAGE gel analysis of the collected fractions from the above chromatogram purification. Fractions shown by the red dotted box were pooled together for further purification. (c) Representation of the chromatogram of the mutant for gel filtration purification. (d) SDS-PAGE gel analysis of the collected fractions from the above chromatogram purification; (MW) is the molecular weight standard. Fractions were pooled and concentrated as shown by the red dotted box.

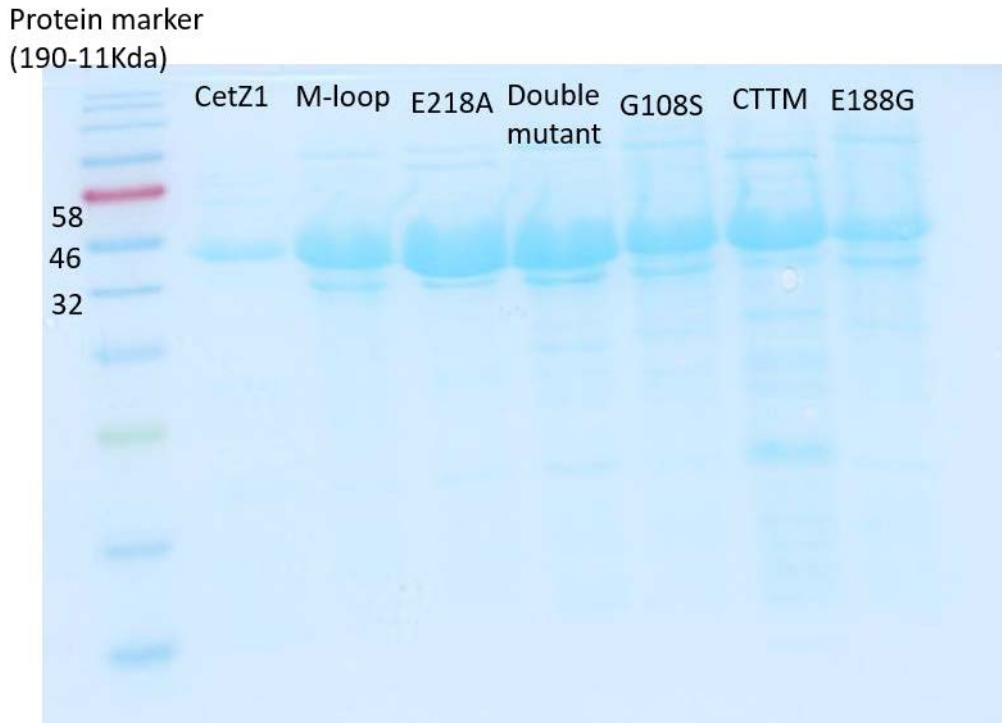

Supplementary Figure 2: SDS-PAGE image of purified proteins

SDS-PAGE gel image showing all the mutants and wild-type CetZ1 protein after purification.

References

Adams, D. W., & Errington, J. (2009). Bacterial cell division: assembly, maintenance and disassembly of the Z ring. *Nature Reviews Microbiology, 7*(9), 642.

Amos, L. A. (2001). Tubulin and microtubules. *eLS*, 1-12.

Amos, L. A., & Löwe, J. (1999). How Taxol® stabilises microtubule structure. *Chemistry & biology, 6*(3), R65-R69.

Amos, L. A., & Schlieper, D. (2005). Microtubules and maps. *Advances in protein chemistry, 71*, 257-298.

Anderson, D. E., Gueiros-Filho, F. J., & Erickson, H. P. (2004). Assembly dynamics of FtsZ rings in Bacillus subtilis and Escherichia coli and effects of FtsZ-regulating proteins. *Journal of bacteriology, 186*(17), 5775-5781.

Arjes, H. A., Lai, B., Emelue, E., Steinbach, A., & Levin, P. A. (2015). Mutations in the bacterial cell division protein FtsZ highlight the role of GTP binding and longitudinal subunit interactions in assembly and function. *BMC microbiology, 15*(1), 209.

Aylett, C. H., & Duggin, I. G. (2017). The tubulin superfamily in archaea. In *Prokaryotic Cytoskeletons* (pp. 393-417): Springer.

Baker, B. J., Comolli, L. R., Dick, G. J., Hauser, L. J., Hyatt, D., Dill, B. D., . . . Banfield, J. F. (2010). Enigmatic, ultrasmall, uncultivated Archaea. *Proceedings of the National Academy of Sciences, 107*(19), 8806-8811.

Bi, E., & Lutkenhaus, J. (1991). FtsZ ring structure associated with division in Escherichia coli. *Nature, 354*(6349), 161-164.

Bisson-Filho, A. W., Hsu, Y.-P., Squyres, G. R., Kuru, E., Wu, F., Jukes, C., . . . VanNieuwenhze, M. S. (2017). Treadmilling by FtsZ filaments drives peptidoglycan synthesis and bacterial cell division. *Science, 355*(6326), 739-743.

Bornens, M., Bailly, E., Gosti, F., & Keryer, G. (2012). The Centrosome: Recent Advances on Structure. *Progress in Molecular and Subcellular Biology, 11*, 86.

Bramhill, D., & Thompson, C. M. (1994). GTP-dependent polymerization of Escherichia coli FtsZ protein to form tubules. *Proceedings of the National Academy of Sciences, 91*(13), 5813-5817.

Brouhard, G. J., & Rice, L. M. (2018). Microtubule dynamics: an interplay of biochemistry and mechanics. *Nature reviews Molecular cell biology, 19*(7), 451-463.

Burns, D. G., Janssen, P. H., Itoh, T., Kamekura, M., Li, Z., Jensen, G., . . . Dyall-Smith, M. L. (2007). Haloquadratum walsbyi gen. nov., sp. nov., the square haloarchaeon of Walsby, isolated from saltern crystallizers in Australia and Spain. *International Journal of Systematic and Evolutionary Microbiology, 57*(2), 387-392.

Buske, P., & Levin, P. A. (2013). A flexible C-terminal linker is required for proper FtsZ assembly in vitro and cytokinetic ring formation in vivo. *Molecular microbiology, 89*(2), 249-263.

Buske, P. J., & Levin, P. A. (2012). Extreme C terminus of bacterial cytoskeletal protein FtsZ plays fundamental role in assembly independent of modulatory proteins. *Journal of Biological Chemistry, 287*(14), 10945-10957.

Carlier, M. F., & Pantaloni, D. (1981). Kinetic analysis of guanosine 5'-triphosphate hydrolysis associated with tubulin polymerization. *Biochemistry, 20*(7), 1918-1924.

Cavicchioli, R. (2011). Archaea—timeline of the third domain. *Nature Reviews Microbiology, 9*(1), 51-61.

Charbon, G., Cabeen, M. T., & Jacobs-Wagner, C. (2009). Bacterial intermediate filaments: in vivo assembly, organization, and dynamics of crescentin. *Genes & Development, 23*(9), 1131-1144.

De Silva, R. T. (2019). *CetZ1 in cell shape control of Haloarchaea: understanding the functional divergence of tubulin superfmaily proteins.* uts, uts.

Desai, A., & Mitchison, T. J. (1997). Microtubule polymerization dynamics. *Annual review of cell and developmental biology, 13*(1), 83-117.
Dhaked, H. P. S., Bhattacharya, A., Yadav, S., Dantu, S. C., Kumar, A., & Panda, D. (2016). Mutation of Arg191 in FtsZ impairs cytokinetic abscission of Bacillus subtilis cells. *Biochemistry, 55*(40), 5754-5763.
Dominguez, R., & Holmes, K. C. (2011). Actin structure and function.
Dougherty, C. A., Sage, C. R., Davis, A., & Farrell, K. W. (2001). Mutation in the β-tubulin signature motif suppresses microtubule GTPase activity and dynamics, and slows mitosis. *Biochemistry, 40*(51), 15725-15732.
Downing, K. H., & Nogales, E. (1998). Tubulin structure: insights into microtubule properties and functions. *Current opinion in structural biology, 8*(6), 785-791.
Drechsel, D. N., & Kirschner, M. W. (1994). The minimum GTP cap required to stabilize microtubules. *Current biology, 4*(12), 1053-1061.
Du, S., & Lutkenhaus, J. (2017). Assembly and activation of the Escherichia coli divisome. *Molecular microbiology, 105*(2), 177-187.
Duggin, I. G., Aylett, C. H., Walsh, J. C., Michie, K. A., Wang, Q., Turnbull, L., . . . Amos, L. A. (2015). CetZ tubulin-like proteins control archaeal cell shape. *Nature, 519*(7543), 362-365.
Dumon-Seignovert, L., Cariot, G., & Vuillard, L. (2004). The toxicity of recombinant proteins in Escherichia coli: a comparison of overexpression in BL21 (DE3), C41 (DE3), and C43 (DE3). *Protein expression and purification, 37*(1), 203-206.
Eme, L., Spang, A., Lombard, J., Stairs, C. W., & Ettema, T. J. (2017). Archaea and the origin of eukaryotes. *Nature Reviews Microbiology, 15*(12), 711.
Erickson, H. P. (1995). FtsZ, a prokaryotic homolog of tubulin? *Cell, 80*(3), 367-370.
Erickson, H. P. (2007). Evolution of the cytoskeleton. *Bioessays, 29*(7), 668-677.
Erickson, H. P. (2009). Modeling the physics of FtsZ assembly and force generation. *Proceedings of the National Academy of Sciences, 106*(23), 9238-9243.
Erickson, H. P., Anderson, D. E., & Osawa, M. (2010). FtsZ in bacterial cytokinesis: cytoskeleton and force generator all in one. *Microbiology and molecular biology reviews, 74*(4), 504-528.
Erickson, H. P., & O'Brien, E. T. (1992). Microtubule dynamic instability and GTP hydrolysis. *Annual review of biophysics and biomolecular structure, 21*(1), 145-166.
Esue, O., Cordero, M., Wirtz, D., & Tseng, Y. (2005). The assembly of MreB, a prokaryotic homolog of actin. *Journal of Biological Chemistry, 280*(4), 2628-2635.
Fuchs, E., & Weber, K. (1994). Intermediate filaments: structure, dynamics, function and disease. *Annual review of biochemistry, 63*(1), 345-382.
Gamba, P., Veening, J.-W., Saunders, N. J., Hamoen, L. W., & Daniel, R. A. (2009). Two-step assembly dynamics of the Bacillus subtilis divisome. *Journal of bacteriology, 191*(13), 4186-4194.
Gardner, K. A. A., Moore, D. A., & Erickson, H. P. (2013). The C-terminal linker of E scherichia coli FtsZ functions as an intrinsically disordered peptide. *Molecular microbiology, 89*(2), 264-275.
Garenne, D., Libchaber, A., & Noireaux, V. (2020). Membrane molecular crowding enhances MreB polymerization to shape synthetic cells from spheres to rods. *Proceedings of the National Academy of Sciences, 117*(4), 1902-1909.
Geyer, E. A., Burns, A., Lalonde, B. A., Ye, X., Piedra, F.-A., Huffaker, T. C., & Rice, L. M. (2015). A mutation uncouples the tubulin conformational and GTPase cycles, revealing allosteric control of microtubule dynamics. *Elife, 4*, e10113.
Gilson, P. R., & Beech, P. L. (2001). Cell division protein FtsZ: running rings around bacteria, chloroplasts and mitochondria. *Research in microbiology, 152*(1), 3-10.
Goehring, N. W., & Beckwith, J. (2005). Diverse paths to midcell: assembly of the bacterial cell division machinery. *Current biology, 15*(13), R514-R526.
González, J. M., Jiménez, M., Vélez, M., Mingorance, J., Andreu, J. M., Vicente, M., & Rivas, G. (2003). Essential cell division protein FtsZ assembles into one monomer-thick ribbons under

conditions resembling the crowded intracellular environment. *Journal of Biological Chemistry, 278*(39), 37664-37671.
Goodson, H. V., & Jonasson, E. M. (2018). Microtubules and microtubule-associated proteins. *Cold Spring Harbor perspectives in biology, 10*(6), a022608.
Gregoretti, I. (2007). *Modeling microtubule dynamic instability.* Citeseer,
Gribaldo, S., Poole, A. M., Daubin, V., Forterre, P., & Brochier-Armanet, C. (2010). The origin of eukaryotes and their relationship with the Archaea: are we at a phylogenomic impasse? *Nature Reviews Microbiology, 8*(10), 743-752.
Guan, F., Yu, J., Yu, J., Liu, Y., Li, Y., Feng, X.-H., . . . Ye, S. (2018). Lateral interactions between protofilaments of the bacterial tubulin homolog FtsZ are essential for cell division. *Elife, 7*, e35578.
Guy, L., Saw, J. H., & Ettema, T. J. (2014). The archaeal legacy of eukaryotes: a phylogenomic perspective. *Cold Spring Harbor perspectives in biology, 6*(10), a016022.
Hale, C. A., & de Boer, P. A. (1997). Direct binding of FtsZ to ZipA, an essential component of the septal ring structure that mediates cell division in E. coli. *Cell, 88*(2), 175-185.
Hale, C. A., & De Boer, P. A. (1999). Recruitment of zipa to the septal ring ofescherichia coli is dependent on ftsz and independent of ftsa. *Journal of bacteriology, 181*(1), 167-176.
Harry, E., Rodwell, J., & Wake, R. (1999). Co-ordinating DNA replication with cell division in bacteria: a link between the early stages of a round of replication and mid-cell Z ring assembly. *Molecular microbiology, 33*(1), 33-40.
Hartman, A. L., Norais, C., Badger, J. H., Delmas, S., Haldenby, S., Madupu, R., . . . Lowe, T. M. (2010). The complete genome sequence of Haloferax volcanii DS2, a model archaeon. *PloS one, 5*(3), e9605.
Heald, R., & Nogales, E. (2002). Microtubule dynamics. *Journal of cell science, 115*(1), 3-4.
Hill, T. L. (1985). Theoretical problems related to the attachment of microtubules to kinetochores. *Proceedings of the National Academy of Sciences, 82*(13), 4404-4408.
Imachi, H., Nobu, M. K., Nakahara, N., Morono, Y., Ogawara, M., Takaki, Y., . . . Ito, M. (2020). Isolation of an archaeon at the prokaryote–eukaryote interface. *Nature, 577*(7791), 519-525.
Kapitein, L. C., Schlager, M. A., Kuijpers, M., Wulf, P. S., van Spronsen, M., MacKintosh, F. C., & Hoogenraad, C. C. (2010). Mixed microtubules steer dynein-driven cargo transport into dendrites. *Current biology, 20*(4), 290-299.
Kaur, G., Garg, T., Rath, G., & Goyal, A. K. (2016). Archaeosomes: an excellent carrier for drug and cell delivery. *Drug delivery, 23*(7), 2497-2512.
Król, E., & Scheffers, D.-J. (2013). FtsZ polymerization assays: simple protocols and considerations. *JoVE (Journal of Visualized Experiments)*(81), e50844.
Land, A. D., Luo, Q., & Levin, P. A. (2014). Functional domain analysis of the cell division inhibitor EzrA. *PLoS One, 9*(7), e102616.
Lee, J.-C., Cha, J.-H., Zerbv, D. B., & Stewart, G. C. (2003). Heterospecific expression of the Bacillus subtilis cell shape determination genes mreBCD in Escherichia coli. *Current microbiology, 47*(2), 0146-0152.
Leibly, D. J., Nguyen, T. N., Kao, L. T., Hewitt, S. N., Barrett, L. K., & Van Voorhis, W. C. (2012). Stabilizing additives added during cell lysis aid in the solubilization of recombinant proteins. *PLoS One, 7*(12), e52482.
Leipe, D. D., Wolf, Y. I., Koonin, E. V., & Aravind, L. (2002). Classification and evolution of P-loop GTPases and related ATPases. *Journal of molecular biology, 317*(1), 41-72.
Li, DeRosier, Nicholson, Nogales, & Downing, K. (2002). Microtubule structure at 8 Å resolution. *Structure, 10*(10), 1317-1328.
Li, Z., Trimble, M. J., Brun, Y. V., & Jensen, G. J. (2007). The structure of FtsZ filaments in vivo suggests a force-generating role in cell division. *The EMBO journal, 26*(22), 4694-4708.

Liao, Y., Ithurbide, S., de Silva, R. T., Erdmann, S., & Duggin, I. G. (2018). Archaeal cell biology: diverse functions of tubulin-like cytoskeletal proteins at the cell envelope. *Emerging Topics in Life Sciences, 2*(4), 547-559.
Liao, Y., Ithurbide, S., Löwe, J., & Duggin, I. G. (2020). Two FtsZ proteins orchestrate archaeal cell division through distinct functions in ring assembly and constriction. *bioRxiv*.
Löwe, J., & Amos, L. A. (1998). Crystal structure of the bacterial cell-division protein FtsZ. *Nature, 391*(6663), 203-206.
Löwe, J., & Amos, L. A. (2009). Evolution of cytomotive filaments: the cytoskeleton from prokaryotes to eukaryotes. *The international journal of biochemistry & cell biology, 41*(2), 323-329.
Löwe, J., van den Ent, F., & Amos, L. A. (2004). Molecules of the bacterial cytoskeleton. *Annu. Rev. Biophys. Biomol. Struct., 33*, 177-198.
Lu, C., Reedy, M., & Erickson, H. P. (2000). Straight and curved conformations of FtsZ are regulated by GTP hydrolysis. *Journal of bacteriology, 182*(1), 164-170.
Lu, C., Stricker, J., & Erickson, H. P. (2001). Site-specific mutations of FtsZ-effects on GTPase and in vitro assembly. *BMC microbiology, 1*(1), 7.
Lutkenhaus, J. (2007). Assembly dynamics of the bacterial MinCDE system and spatial regulation of the Z ring. *Annu. Rev. Biochem., 76*, 539-562.
Makarova, K. S., & Koonin, E. V. (2010). Two new families of the FtsZ-tubulin protein superfamily implicated in membrane remodeling in diverse bacteria and archaea. *Biology Direct, 5*(1), 33.
Makarova, K. S., Yutin, N., Bell, S. D., & Koonin, E. V. (2010). Evolution of diverse cell division and vesicle formation systems in Archaea. *Nature Reviews Microbiology, 8*(10), 731-741.
Margolin, W., Wang, R., & Kumar, M. (1996). Isolation of an ftsZ homolog from the archaebacterium Halobacterium salinarium: implications for the evolution of FtsZ and tubulin. *Journal of bacteriology, 178*(5), 1320-1327.
Margolis, R. L., & Wilson, L. (1998). Microtubule treadmilling: what goes around comes around. *Bioessays, 20*(10), 830-836.
Maurer, S. P., Fourniol, F. J., Bohner, G., Moores, C. A., & Surrey, T. (2012). EBs recognize a nucleotide-dependent structural cap at growing microtubule ends. *Cell, 149*(2), 371-382.
McKean, P. G., Vaughan, S., & Gull, K. (2001). The extended tubulin superfamily. *Journal of cell science, 114*(15), 2723-2733.
Michie, K. A., & Löwe, J. (2006). Dynamic filaments of the bacterial cytoskeleton. *Annu. Rev. Biochem., 75*, 467-492.
Milam, S. L., Osawa, M., & Erickson, H. P. (2012). Negative-stain electron microscopy of inside-out FtsZ rings reconstituted on artificial membrane tubules show ribbons of protofilaments. *Biophysical journal, 103*(1), 59-68.
Mingorance, J., Rivas, G., Vélez, M., Gómez-Puertas, P., & Vicente, M. (2010). Strong FtsZ is with the force: mechanisms to constrict bacteria. *Trends in microbiology, 18*(8), 348-356.
Miraldi, E. R., Thomas, P. J., & Romberg, L. (2008). Allosteric models for cooperative polymerization of linear polymers. *Biophysical journal, 95*(5), 2470-2486.
Mitchison, T., & Kirschner, M. (1984). Dynamic instability of microtubule growth. *Nature, 312*(5991), 237-242.
Mitra, A., & Sept, D. (2008). Taxol allosterically alters the dynamics of the tubulin dimer and increases the flexibility of microtubules. *Biophysical journal, 95*(7), 3252-3258.
Miyata, H., & Hotani, H. (1992). Morphological changes in liposomes caused by polymerization of encapsulated actin and spontaneous formation of actin bundles. *Proceedings of the National Academy of Sciences, 89*(23), 11547-11551.
Monterroso, B., Reija, B., Jiménez, M., Zorrilla, S., & Rivas, G. (2016). Charged molecules modulate the volume exclusion effects exerted by crowders on FtsZ polymerization. *PLoS One, 11*(2), e0149060.

Mormile, M. R., Biesen, M. A., Gutierrez, M. C., Ventosa, A., Pavlovich, J. B., Onstott, T. C., & Fredrickson, J. K. (2003). Isolation of Halobacterium salinarum retrieved directly from halite brine inclusions. *Environmental Microbiology, 5*(11), 1094-1102.
Mukherjee, A., & Lutkenhaus, J. (1998). Dynamic assembly of FtsZ regulated by GTP hydrolysis. *The EMBO journal, 17*(2), 462-469.
Mukherjee, A., & Lutkenhaus, J. (1999). Analysis of FtsZ assembly by light scattering and determination of the role of divalent metal cations. *Journal of bacteriology, 181*(3), 823-832.
Müsch, A. (2004). Microtubule organization and function in epithelial cells. *Traffic, 5*(1), 1-9.
Nogales, E. (2001). Structural insights into microtubule function. *Annual review of biophysics and biomolecular structure, 30*(1), 397-420.
Nogales, E., Downing, K. H., Amos, L. A., & Löwe, J. (1998). Tubulin and FtsZ form a distinct family of GTPases. *Nature structural biology, 5*(6), 451-458.
Nogales, E., & Wang, H.-W. (2006). Structural mechanisms underlying nucleotide-dependent self-assembly of tubulin and its relatives. *Current opinion in structural biology, 16*(2), 221-229.
Nogales, E., Whittaker, M., Milligan, R. A., & Downing, K. H. (1999). High-resolution model of the microtubule. *Cell, 96*(1), 79-88.
Nunoura, T., Takaki, Y., Kakuta, J., Nishi, S., Sugahara, J., Kazama, H., . . . Atomi, H. (2011). Insights into the evolution of Archaea and eukaryotic protein modifier systems revealed by the genome of a novel archaeal group. *Nucleic acids research, 39*(8), 3204-3223.
O'Donnell, M., Langston, L., & Stillman, B. (2013). Principles and concepts of DNA replication in bacteria, archaea, and eukarya. *Cold Spring Harbor perspectives in biology, 5*(7), a010108.
Ohashi, T., Hale, C. A., de Boer, P. A., & Erickson, H. P. (2002). Structural evidence that the P/Q domain of ZipA is an unstructured, flexible tether between the membrane and the C-terminal FtsZ-binding domain. *Journal of bacteriology, 184*(15), 4313-4315.
Oliva, Cordell, C., & Löwe, J. (2004). Structural insights into FtsZ protofilament formation. *Nature structural & molecular biology, 11*(12), 1243-1250.
Oliva, M. A., & Andreu, J. M. (2001). Tubulin and FtsZ Superfamily of Protein Assembly Machines. *eLS*.
Oliva, M. A., Cordell, S. C., & Löwe, J. (2004). Structural insights into FtsZ protofilament formation. *Nature structural & molecular biology, 11*(12), 1243-1250.
Oren, A. (1999). The enigma of square and triangular halophilic Archaea. In *Enigmatic Microorganisms and Life in Extreme Environments* (pp. 337-355): Springer.
Osawa, M., Anderson, D. E., & Erickson, H. P. (2008). Reconstitution of contractile FtsZ rings in liposomes. *Science, 320*(5877), 792-794.
Osawa, M., Anderson, D. E., & Erickson, H. P. (2009). Curved FtsZ protofilaments generate bending forces on liposome membranes. *The EMBO journal, 28*(22), 3476-3484.
Pastoret, S., Fraipont, C., Den Blaauwen, T., Wolf, B., Aarsman, M. E., Piette, A., . . . Nguyen-Distèche, M. (2004). Functional analysis of the cell division protein FtsW of Escherichia coli. *Journal of bacteriology, 186*(24), 8370-8379.
Perdiz, D., Mackeh, R., Poüs, C., & Baillet, A. (2011). The ins and outs of tubulin acetylation: more than just a post-translational modification? *Cellular signalling, 23*(5), 763-771.
Petry, S., Groen, A. C., Ishihara, K., Mitchison, T. J., & Vale, R. D. (2013). Branching microtubule nucleation in Xenopus egg extracts mediated by augmin and TPX2. *Cell, 152*(4), 768-777.
Pichoff, S., & Lutkenhaus, J. (2002). Unique and overlapping roles for ZipA and FtsA in septal ring assembly in Escherichia coli. *The EMBO journal, 21*(4), 685-693.
Pichoff, S., & Lutkenhaus, J. (2005). Tethering the Z ring to the membrane through a conserved membrane targeting sequence in FtsA. *Molecular microbiology, 55*(6), 1722-1734.
Pilhofer, M. (2008). *Elucidation of the cell division mechanism and characterization of tubulins in the bacterial phylum Verrucomicrobia.* Technische Universität München,
Pinot, M., Chesnel, F., Kubiak, J., Arnal, I., Nedelec, F., & Gueroui, Z. (2009). Effects of confinement on the self-organization of microtubules and motors. *Current biology, 19*(11), 954-960.

Pontani, L.-L., Van der Gucht, J., Salbreux, G., Heuvingh, J., Joanny, J.-F., & Sykes, C. (2009). Reconstitution of an actin cortex inside a liposome. *Biophysical journal, 96*(1), 192-198.
Ramírez-Aportela, E., López-Blanco, J. R., Andreu, J. M., & Chacón, P. (2014). Understanding nucleotide-regulated FtsZ filament dynamics and the monomer assembly switch with large-scale atomistic simulations. *Biophysical journal, 107*(9), 2164-2176.
RayChaudhuri, D. (1999). ZipA is a MAP–Tau homolog and is essential for structural integrity of the cytokinetic FtsZ ring during bacterial cell division. *The EMBO journal, 18*(9), 2372-2383.
Regamey, A., Harry, E., & Wake, R. (2000). Mid-cell Z ring assembly in the absence of entry into the elongation phase of the round of replication in bacteria: co-ordinating chromosome replication with cell division. *Molecular microbiology, 38*(3), 423-434.
Rivas, G., & Minton, A. P. (2016). Macromolecular crowding in vitro, in vivo, and in between. *Trends in biochemical sciences, 41*(11), 970-981.
Robinson, J. L., Pyzyna, B., Atrasz, R. G., Henderson, C. A., Morrill, K. L., Burd, A. M., . . . Steele, S. M. (2005). Growth kinetics of extremely halophilic Archaea (family Halobacteriaceae) as revealed by Arrhenius plots. *Journal of bacteriology, 187*(3), 923-929.
Romberg, L., & Levin, P. A. (2003). Assembly dynamics of the bacterial cell division protein FtsZ: poised at the edge of stability. *Annual Reviews in Microbiology, 57*(1), 125-154.
Romberg, L., Simon, M., & Erickson, H. P. (2001). Polymerization of ftsz, a bacterial homolog of tubulin is assembly cooperative? *Journal of Biological Chemistry, 276*(15), 11743-11753.
Rothfield, L., Taghbalout, A., & Shih, Y.-L. (2005). Spatial control of bacterial division-site placement. *Nature Reviews Microbiology, 3*(12), 959-968.
Rowlett, V. W., & Margolin, W. (2015). The Min system and other nucleoid-independent regulators of Z ring positioning. *Frontiers in microbiology, 6*, 478.
Salje, J., van den Ent, F., de Boer, P., & Löwe, J. (2011). Direct membrane binding by bacterial actin MreB. *Molecular cell, 43*(3), 478-487.
Samson, R. Y., & Bell, S. D. (2011). Cell cycles and cell division in the archaea. *Current opinion in microbiology, 14*(3), 350-356.
Sanders, A. A., & Kaverina, I. (2015). Nucleation and dynamics of Golgi-derived microtubules. *Frontiers in neuroscience, 9*, 431.
Satir, P., & Christensen, S. T. (2007). Overview of structure and function of mammalian cilia. *Annu. Rev. Physiol., 69*, 377-400.
Scheffers, D.-J., & Driessen, A. J. (2001). The polymerization mechanism of the bacterial cell division protein FtsZ. *FEBS letters, 506*(1), 6-10.
Schlieper, D., Oliva, M. A., Andreu, J. M., & Löwe, J. (2005). Structure of bacterial tubulin BtubA/B: evidence for horizontal gene transfer. *Proceedings of the National Academy of Sciences, 102*(26), 9170-9175.
Shen, B., & Lutkenhaus, J. (2009). The conserved C-terminal tail of FtsZ is required for the septal localization and division inhibitory activity of MinCC/MinD. *Molecular microbiology, 72*(2), 410-424.
Siegrist, S. E., & Doe, C. Q. (2007). Microtubule-induced cortical cell polarity. *Genes & Development, 21*(5), 483-496.
Strauss, M. P., Liew, A. T., Turnbull, L., Whitchurch, C. B., Monahan, L. G., & Harry, E. J. (2012). 3D-SIM super resolution microscopy reveals a bead-like arrangement for FtsZ and the division machinery: implications for triggering cytokinesis. *PLoS biol, 10*(9), e1001389.
Stricker, J., Maddox, P., Salmon, E., & Erickson, H. P. (2002). Rapid assembly dynamics of the Escherichia coli FtsZ-ring demonstrated by fluorescence recovery after photobleaching. *Proceedings of the National Academy of Sciences, 99*(5), 3171-3175.
Sui, H., & Downing, K. H. (2010). Structural basis of interprotofilament interaction and lateral deformation of microtubules. *Structure, 18*(8), 1022-1031.
Sweitzer, S. M., & Hinshaw, J. E. (1998). Dynamin undergoes a GTP-dependent conformational change causing vesiculation. *Cell, 93*(6), 1021-1029.

Szwedziak, P., Wang, Q., Bharat, T. A., Tsim, M., & Löwe, J. (2014). Architecture of the ring formed by the tubulin homologue FtsZ in bacterial cell division. *Elife, 3*, e04601.

Ursinus, A., Van Den Ent, F., Brechtel, S., De Pedro, M., Höltje, J.-V., Löwe, J., & Vollmer, W. (2004). Murein (peptidoglycan) binding property of the essential cell division protein FtsN from Escherichia coli. *Journal of bacteriology, 186*(20), 6728-6737.

Vaughan, S., Wickstead, B., Gull, K., & Addinall, S. G. (2004). Molecular evolution of FtsZ protein sequences encoded within the genomes of archaea, bacteria, and eukaryota. *Journal of molecular evolution, 58*(1), 19-29.

Wagstaff, J., & Löwe, J. (2018). Prokaryotic cytoskeletons: protein filaments organizing small cells. *Nature Reviews Microbiology, 16*(4), 187.

Walker, R., Gliksman, N., & Salmon, E. (1990). Using video-enhanced differential interference contrast microscopy to analyze the assembly dynamics of individual microtubules in real time. *Optical Microscopy for Biology. B. Herman and K. Jacobson, editors. Wiley-Liss, New York*, 395-407.

Walker, R., O'brien, E., Pryer, N., Soboeiro, M., Voter, W., Erickson, H., & Salmon, E. (1988). Dynamic instability of individual microtubules analyzed by video light microscopy: rate constants and transition frequencies. *The Journal of cell biology, 107*(4), 1437-1448.

Wang, H.-W., & Nogales, E. (2005). Nucleotide-dependent bending flexibility of tubulin regulates microtubule assembly. *Nature, 435*(7044), 911-915.

Wang, W., Cantos-Fernandes, S., Lv, Y., Kuerban, H., Ahmad, S., Wang, C., & Gigant, B. (2017). Insight into microtubule disassembly by kinesin-13s from the structure of Kif2C bound to tubulin. *Nature communications, 8*(1), 1-11.

Ward Jr, J. E., & Lutkenhaus, J. (1985). Overproduction of FtsZ induces minicell formation in E. coli. *Cell, 42*(3), 941-949.

Waxman, P. G., Del Champo, A. A., Lowe, M. C., & Hamel, E. (1981). Induction of Polymerization of Purified Tubulin by Sulfonate Buffers: Marked Differences between 4-Morpholineethanesulfonate (Mes) and 1, 4-Piperazineethanesulfonate (Pipes). *European journal of biochemistry, 120*(1), 129-136.

Wickstead, B., & Gull, K. (2011). The evolution of the cytoskeleton. *Journal of Cell Biology, 194*(4), 513-525.

Wiese, C., & Zheng, Y. (2000). A new function for the γ-tubulin ring complex as a microtubule minus-end cap. *Nature cell biology, 2*(6), 358-364.

Woese, C. R., Kandler, O., & Wheelis, M. L. (1990). Towards a natural system of organisms: proposal for the domains Archaea, Bacteria, and Eucarya. *Proceedings of the National Academy of Sciences, 87*(12), 4576-4579.

Wu, L. J., & Errington, J. (2012). Nucleoid occlusion and bacterial cell division. *Nature Reviews Microbiology, 10*(1), 8-12.

Yu, X. C., & Margolin, W. (1997). Ca2+-mediated GTP-dependent dynamic assembly of bacterial cell division protein FtsZ into asters and polymer networks in vitro. *The EMBO journal, 16*(17), 5455-5463.

Yutin, N., & Koonin, E. V. (2012). Archaeal origin of tubulin. *Biology Direct, 7*(1), 10.

Zaremba-Niedzwiedzka, K., Caceres, E. F., Saw, J. H., Bäckström, D., Juzokaite, L., Vancaester, E., . . . Kjeldsen, K. U. (2017). Asgard archaea illuminate the origin of eukaryotic cellular complexity. *Nature, 541*(7637), 353-358.